NASA Technical Memorandum 78705

Aerodynamic Characteristics of a Counter-Rotating, Coaxial, Hingeless Rotor Helicopter Model With Auxiliary Propulsion

Arthur E. Phelps and Raymond E. Mineck

MAY 1978

NASA
National Aeronautics and Space Administration
Langley Research Center
Hampton, Virginia 23665

SUMMARY

A wind-tunnel investigation was conducted in the Langley V/STOL tunnel to determine the aerodynamic characteristics of a coaxial, counter-rotating helicopter model with auxiliary jet propulsion. The model was tested at advance ratios from 0 to 0.3 with and without auxiliary jet engine thrust. At each advance ratio and engine thrust, both the control power and the aircraft stability were measured.

The results indicate that there is a cross-coupling for collective pitch and longitudinal cyclic pitch inputs. The control power for these inputs increases with advance ratio. There is also a cross-coupling for differential collective pitch inputs. The airframe is longitudinally unstable, but the instability is less at the highest advance ratio tested. The airframe shows both positive effective dihedral and positive directional stability.

INTRODUCTION

Helicopter maximum flight speeds are limited by the ability of the rotor to maintain a lift balance on the retreating side of the rotor disk where retreating blade stall occurs. To maintain a lift balance, two co-axial counter-rotating rotors may be used with the advancing blade of each rotor providing most of the lift. In such an arrangement, the rotor system can be used primarily to provide lift and an auxiliary propulsion system may then be used to provide the propulsive force. One such helicopter, described in reference 1, uses jet engines for the auxiliary propulsion system. Research on jet VTOL configurations has shown that the jet exhaust can have a significant effect on the control power of the tail and the tail contribution to stability; a model of a coaxial counter-rotating helicopter with auxiliary propulsion was tested in the Langley V/STOL tunnel to determine the effect of jet thrust on stability and control. The model was tested at advance ratios from 0 to 0.3 with and without auxiliary jet engine thrust. The stability and control power of both the rotor and tail surfaces were determined at simulated 1.0 g level flight conditions.

SYMBOLS

The symbols used for the physical quantities defined in this paper are given in the International System of Units (S.I.) and parenthetically in the U.S. Customary Units. Conversion factors for the S.I. system are presented in reference 2. All measurements were made in the U.S. Customary Units.

The axis system used in the presentation of the data is illustrated in figure 1(a). The moment reference center was located 28.04 cm (11.04 in.) below the center of the upper rotor hub.

A rotor disk area, m^2 (ft^2)

A_{ls} rotor longitudinal cyclic pitch in the shaft axis system (see fig. 1(b))

B_{ls} rotor lateral cyclic pitch in the shaft axis system (see fig. 1(b))

C_D drag coefficient, $\frac{D}{\rho_\infty A V_T^2}$

$C_{D,r.o.}$ drag coefficient with the rotor removed, $\frac{D}{q_\infty A}$

C_H horizontal force coefficient, $\frac{H}{\rho_\infty A V_T^2}$

C_J net thrust coefficient of the auxiliary thrust jets, $\frac{T_J}{q_\infty A}$

C_L lift coefficient, $\frac{L}{\rho_\infty A V_T^2}$

$C_{L,r.o.}$ lift coefficient with the rotor removed, $\frac{L}{q_\infty A}$

C_l rolling-moment coefficient, $\frac{M_X}{\rho_\infty A V_T^2 R}$

$C_{l,r.o.}$ rolling-moment coefficient with the rotor removed, $\frac{M_X}{q_\infty A d}$

C_m pitching-moment coefficient, $\frac{M_Y}{\rho_\infty A V_T^2 R}$

$C_{m,r.o.}$ pitching-moment coefficient with the rotor removed, $\frac{M_Y}{q_\infty A d}$

C_n yawing-moment coefficient, $\frac{M_Z}{\rho_\infty A V_T^2 R}$

$C_{n,r.o.}$ yawing-moment coefficient with the rotor removed, $\frac{M_Z}{q_\infty A d}$

C_T rotor thrust coefficient, $\frac{T}{\rho_\infty A V_T^2}$

C_Y side-force coefficient, $\frac{F_Y}{\rho_\infty A V_T^2}$

$C_{Y,r.o.}$ side force coefficient with the rotor removed, $\frac{F_Y}{q_\infty A}$

D drag, N (lbf)

d rotor diameter, m (ft)

H horizontal force, N (lbf)

i_t horizontal tail incidence (positive trailing edge down), deg

L lift, N (lbf)

M_X rolling moment, N-m (lbf-in)

M_Y pitching moment, N-m (lbf-in)

M_Z yawing moment, N-m (lbf-in)

q_∞ free-stream dynamic pressure, Pa (lbf/ft^2)

R rotor radius, m (ft)

T rotor thrust, N (lbf)

T_J auxiliary jet engine net thrust, N (lbf)

V_∞ free-stream velocity, m/sec (ft/sec)

V_T tip speed, m/sec (ft/sec)

α angle of attack, deg

β angle of sideslip, deg

Γ rotor control phase angle (see fig. 1(b)), deg

δ_R rudder deflection (positive trailing edge left), deg

μ rotor advance ratio, $\frac{V_\infty \cos\alpha}{V_T}$

ρ_∞ free-stream density, kg/m^3 ($slugs/ft^3$)

$\overline{\theta}$ average rotor collective pitch angle at 0.75 R (see fig. 1(b)), deg

$\Delta\theta$ differential collective pitch angle (see fig. 1(b)), deg

ψ rotor blade azimuthal position (see fig. 1(b)), deg

Subscripts

A_{1s} partial derivative with respect to A_{1s}

B_{1s} partial derivative with respect to B_{1s}

i_t	partial derivative with respect to i_t
α	partial derivative with respect to α
β	partial derivative with respect to β
δ_R	partial derivative with respect to δ_R
$\Delta\theta$	partial derivative with respect to $\Delta\theta$
θ	partial derivative with respect to θ
μ	partial derivative with respect to μ
u	upper rotor
l	lower rotor

MODEL AND APPARATUS

The test program was conducted with a Froude-scaled model of an early version of the aircraft described in reference 1 and was equipped with auxiliary propulsion engines as shown in figures 2 and 3. In Froude scaling, the rotor blade physical properties are chosen such that the deflections due to gravity and airloads are geometrically scaled. The model tip speed is then reduced by the square root of model scale; compressibility effects are, therefore, not duplicated because of the reduction in Mach number.

The rotor system, control system, and rotor model were mounted on an aluminum structural assembly which was, in turn, mounted on a six-component strain-gage balance. The fuselage shell consisted of a number of molded fiberglass reinforced plastic sections attached to bulkheads on the main structural assembly. The horizontal and vertical tail assembly was attached to the fuselage tail cone and was equipped with actuators which allowed remote control of the tail incidence and rudder angle. The auxiliary propulsion engine simulators were mounted to the main structural assembly.

Power for the auxiliary propulsion engine simulators was provided through two airlines to two compressed air ejectors mounted in nacelles located beneath the rotor on the sides of the fuselage as shown in figure 2. The nozzle of each engine simulator was fitted with four wall static pressure orifices and nine total pressure tubes as shown in figure 2(b); the total pressure tubes were arranged so that they were alined along the geometric centerlines of three concentric equal-area rings. In addition, the two airlines were equipped with remotely controlled valves which allowed individual operation of each simulator from the tunnel control room.

The model rotor blades were constructed of fiberglass reinforced plastic applied to molded foam plastic cores. Table I provides a geometric description of the blades.

Rotor control was accomplished with an analog computer/controller utilizing a closed-loop, high-gain feedback system. The controller was used in conjunction with an on-line computer facility which provided real-time resolution of forces and moments about the aircraft "flight" center-of-gravity position. Two unique capabilities of the controller were the provision for in-flight variation of the swashplate phase angle Γ, and programmable, time-varying collective and cyclic control inputs which could be used to evaluate the rotor control power.

TEST AND CORRECTIONS

The tests were conducted in the Langley V/STOL tunnel which has a closed throat test section measuring 4.42 m (14.50 ft) by 6.63 m (21.75 ft). All testing at forward speeds was conducted in the closed throat test section at a rotor height of 1.07 diameters. Hover testing was conducted in the open throat test section at a height of 1.64 diameters. All testing was conducted at a rotor tip speed of 88 m/sec (288 ft/sec).

Each engine simulator was calibrated separately on the model. The engine thrust, measured on the balance, was calibrated against a reference exit dynamic pressure (the difference of the averaged exit total pressures and the exit static pressure). At zero net thrust ($C_J = 0$), the exit dynamic pressure was equal to the free-stream dynamic pressure. The exit dynamic pressure was biased by the free-stream dynamic pressure before being used in the calibration.

The model was tested at four advance ratios: 0.0, 0.1, 0.21, and 0.31. At each advance ratio, up to three auxiliary engine thrust levels were tested. These corresponded to scaled values of flight idle thrust, an intermediate or "trim" thrust, and maximum available thrust. At each advance ratio, the jet thrust from the two engines was balanced at a desired thrust level. The rotor controls and angle of attack were varied to provide zero moments and drag and trim lift. Once the trim control settings had been obtained, the controls were varied to obtain the rotor and tail control power at trim. The unique characteristics of the control system were used in the determination of the rotor control power. The rotor control was varied at a rate of 0.2 deg/sec for 10 seconds starting at 1° from the trim setting and moving through trim, and a continuous data record was obtained. The angle of attack, angle of sideslip, and forward speed were also varied to obtain the stability characteristics at trim.

It should be noted that when the rotor provides the propulsive force (low auxiliary engine thrust), the model is in a nose-down attitude. Similarly, when the auxiliary engines provide the propulsive force, the model is in a nose-up attitude. Therefore, the effects of auxiliary engine thrust level will include the effects of model attitude.

The strain-gage balance was calibrated with the two airlines in place to account for the additional stiffness due to the airlines. Each airline was then closed at the engine inlet and the airline pressurized. The loads, measured on the balance, due to the pressure in each airline were used to correct the data for airline pressure effects. The resultant balance accuracy was determined to

be 0.5 percent of the balance full-scale loads. The effect of the model motor cooling water hoses and transmission oil lubrication hoses were determined by loading the model with the hoses in place; this effect was also removed from the data. Also, all data have been corrected for wind-tunnel wall effects using the methods described in reference 3.

PRESENTATION OF RESULTS

The results of this wind-tunnel investigation have been presented in coefficient form. It should be noted that the rotor-off results are nondimensionalized by free-stream velocity squared (dynamic pressure) and the rotor-on results are nondimensionalized by the rotor tip-speed squared. If the rotor-off forces are multipled by $\mu^2/2$, they can then be compared directly with the rotor-on forces. Similarly, if the rotor-off moments are multipled by μ^2, they can be compared directly with the rotor-on moments.

Propulsive force may be provided by the auxiliary thrust jets and/or the rotor; therefore, there are numerous control combinations that would produce "1g" level flight. The control positions and test conditions for each parameter variation or run number are presented in the appendix. The results are presented as follows:

RESULTS AND DISCUSSION

Rotor Off

The longitudinal aerodynamic characteristics of the model with the rotor and tail removed are presented in figures 4(a) through 4(c) for various auxiliary engine thrust coefficients and three tunnel speeds. The data show that auxiliary engine thrust caused an increase in the lift-curve slope and actually contributed a small measure of stability to the C_m/C_L curve. The effect of the horizontal tail on the longitudinal aerodynamic characteristics is shown in figures 5(a) through 5(c) for a range of auxiliary engine thrust coefficients and for the same three tunnel speeds. A comparison of figures 4 and 5 indicates that the tail increased the airframe lift-curve slope significantly, and provided a substantial stability increment, as expected. The addition of auxiliary engine power moderately reduced the stability of the basic configuration and caused some small trim changes, as expected.

Figure 6 illustrates the effect of tail incidences on the longitudinal characteristics of the model for two thrust coefficients. The data of figure 6(a) indicate that the horizontal tail as tested was stalled when the tail angle of attack ($\alpha + i_t$ for the rotor off) was less than about $-10°$, but that there was good control power available from the tail for deflections below the stall angle. The significance of this characteristic will be more apparent later in the report in the discussion of rotor-on aerodynamics.

The lateral-directional characteristics of the model with the rotor removed are shown in figures 7 and 8 for the tail off and the tail on, respectively. The data show that auxiliary engine thrust generally had a small effect on the lateral characteristics, except at large angles of sideslip, where there was some reduction in the directional stability with the tail on at the lowest dynamic pressure ($q = 203$ Pa). The data of figure 8 indicate that the horizontal tail had a very large positive dihedral effect which was generally unaffected by thrust.

Rotor On

The rotor-on aerodynamic characteristics are presented in figures 9 through 17 as listed in the section dealing with the presentation of results, and are summarized as stability and control derivatives in figures 18 through 26. Since the fundamental aerodynamic characteristics of the model can be evaluated more easily in terms of derivatives than in the basic coefficient data form, this discussion will be limited to the summary plots of figures 18 through 26.

The control capabilities of the coaxial rotor as a function of advance ratio are presented in figures 18 through 21 for variation in the collective pitch $\bar{\theta}$, longitudinal cyclic pitch A_{1s}, lateral cyclic pitch B_{1s}, and differential collective pitch $\Delta\theta$, respectively. Data are presented for three auxiliary propulsion thrust levels: flight-idle, trim thrust, which was representative of the thrust required to trim the aircraft drag at the selected airspeed and flight attitude, and maximum thrust, which was representative of the maximum scaled thrust of a full-scale engine.

Figure 18 indicates that collective pitch variations affected both thrust coefficient C_T and pitching-moment coefficient C_m, and that there was very little coupling of the collective control power with the other four control components. In addition, the collective control power increased significantly with advance ratio, and the thrust-moment coupling remained essentially constant with increasing advance ratio. Auxiliary engine thrust appeared to have only a small effect at low advance ratio for all components, but there was an increase in the collective control power effect on rotor thrust at the high advance ratio.

Figure 19 presents the longitudinal cyclic control power $\partial/\partial A_{1s}$ as a function of airspeed, and shows the same coupling effect that was observed for the collective case. In fact, for the higher advance ratios, both collective pitch and longitudinal cyclic pitch provide about the same level of pitching-moment control power. The coupling of A_{1s} with C_T was less for the trim auxiliary thrust level than for the flight-idle thrust level. This reduced coupling might be explained by the lower angle of attack for the flight-idle case which resulted in a tip-path plane tilted forward with respect to the trim auxiliary thrust case, particularly for the high-speed condition. The control coupling observed in figures 18 and 19 appears to be due to direct rotor effects which arise from the complex longitudinal flow interactions of the two rotors, rather than rotor downwash effects on the airframe.

The lateral cyclic control power $\partial/\partial B_{1s}$ is shown in figure 20 for the same conditions as for the longitudinal cyclic control. The data show a modest increase in control power with airspeed, virtually no control coupling, and very small effects of auxiliary engine thrust.

One means of obtaining yaw control for a coaxial rotor of the type tested in this investigation is to operate the two rotors at different collective pitch settings so as to produce a torque imbalance. The results of using this technique are presented in figure 21 and show the differential collective control power $\partial/\partial\Delta\theta$ as a function of airspeed for hover and two advance ratios. The hover data indicate that there was some control power available for yaw at zero

airspeed, but that there was strong coupling with the rotor thrust coefficient. The technique used for obtaining differential collective was simply to displace the two rotor collective pitch values equal amounts from some mean or trim position; thus, it may be expected that considerable optimization could be performed. As forward speed was increased, the yaw control power remained essentially constant; the thrust coupling was somewhat reduced; and a very strong roll coupling developed. At the highest advance ratio tested, differential collective proved to be a far more effective device for roll control than it was for yaw control.

The control power of the horizontal tail $\partial/\partial i_t$ is presented in figure 22 as a function of advance ratio for two auxiliary engine thrust levels. The data show the tail to have virtually no control power for advance ratios below about 0.22, but there is a sharp increase in control power above $\mu = 0.22$. These data indicate that the horizontal tail was stalled below $\mu = 0.22$, evidently as a result of being immersed in the rotor wake at low air speeds. Increasing auxiliary engine power tended to reduce the control effectiveness of the horizontal tail, possibly because of the presence of a low static pressure region in the jet exhaust wake beneath the tail.

The control power of the rudder $\partial/\partial\delta_R$ is presented in figure 23 and shows the expected increase with increasing airspeed. Increasing auxiliary engine thrust caused a slight reduction in control power, as was the case with the horizontal tail.

The longitudinal stability characteristics of the model are shown in figure 24 as a function of advance ratio for two auxiliary engine thrust levels. The data show that the model as tested was longitudinally unstable throughout the range of advance ratios tested, but that the instability was significantly reduced at the highest advance ratio. There was a dramatic increase in the lift-curve slope at the higher advance ratios, possibly due to the unstalling of the horizontal tail at the higher speeds and to the increase in the rotor lift-curve slope with forward speed. Increasing auxiliary engine thrust tended to be destabilizing. It should be pointed out that, although the model was statically unstable, there was adequate control power to overcome the instability with a generous margin remaining for maneuvering control. Furthermore, it is suspected that the tail stall phenomena observed in the investigation was primarily due to the very low Reynolds number of the horizontal tail and may not occur under full-scale conditions.

The lateral-directional stability derivatives are shown in figure 25 as a function of advance ratio for two auxiliary engine thrust settings. In general, the data reveal a well-behaved configuration having positive directional stability and positive dihedral effect (negative C_{l_β}). A comparison of the data of figure 25 with the data of figures 7 and 8 indicate that approximately half of the dihedral effect of the complete configuration is attributable to the horizontal tail. As was true in the longitudinal case, auxiliary engine power tended to be destabilizing.

The speed stability of the model is shown in figure 26 as a function of advance ratio for two auxiliary engine thrust settings. The data show that the

model was "speed-stable" for the conditions tested except for the low auxiliary engine thrust case at high advance ratio, where a modest speed instability was encountered. Increasing auxiliary engine power increased the speed stability, and increasing speed was destabilizing.

SUMMARY OF RESULTS

The results of a wind-tunnel investigation of a model of a counterrotating coaxial helicopter with auxiliary propulsion may be summarized as follows:

1. Both collective pitch and longitudinal cyclic pitch control inputs exhibit a cross coupling effect on pitching moment and thrust. The control power increases with advance ratio.

2. Differential collective pitch control inputs exhibit cross coupling effects on rolling moment and thrust.

3. The rudder is effective at all the forward speeds that were tested. The horizontal tail was effective only at the highest speed tested.

4. The model is longitudinally unstable; however, the instability decreases at the highest forward speed.

5. The model shows both positive effective dihedral and positive directional stability.

REFERENCES

1. Ruddell, Andrew J.: Advancing Blade Concept (ABC^{TM}) Development - XH-59A Flight Tests. Am. Hel. Soc. J., vol. 22, Jan. 1977, pp. 13-23

2. Mechtly, E. A.: The International System of Units - Physical Constants and Conversion Factors (Second Revision). NASA SP-7012, 1973

3. Heyson, Harry H.: Use of Superposition in Digital Computers to Obtain Wind-Tunnel Interference Factors for Arbitrary Configurations With Particular Reference to V/STOL Models. NASA TR R-302, 1969

TABLE I. - DIMENSIONAL CHARACTERISTICS OF THE BLADES

Radial Station		Chord		Twist	Airfoil Thickness/Chord Ratio
cm	(in.)	cm	(in.)		
12.7	5.00	3.0	1.20	-	1.000
15.7	6.19	3.0	1.20	-	1.000
21.1	8.29	6.4	2.52	-	.480
25.7	10.13	9.1	3.60	5.00	.246
36.6	14.42	8.5	3.36	4.12	.204
40.6	16.00	8.3	3.28	3.80	.193
50.7	19.95	7.8	3.09	3.02	.165
61.6	24.25	7.3	2.86	2.17	.148
69.5	27.35	6.9	2.71	1.56	.131
76.7	30.20	6.6	2.59	1.00	.120
83.3	32.80	6.2	2.43	0	.120
89.4	35.20	5.9	2.32	-.93	.120
95.0	37.40	5.6	2.20	-1.78	.120
100.1	39.40	5.4	2.11	-2.56	.120
104.8	41.25	5.1	2.01	-3.27	.120
106.7	42.00	5.0	1.98	-3.56	.120

APPENDIX - SUMMARY OF ROTOR-ON TEST CONDITIONS

RUN	α	β	$\bar{\theta}$	$\Delta\theta$	A_{1S}	B_{1S}	Γ	l_t	δ_r	μ	C_J	q,psf	q,Pa
38	10.0	-.0	9.9	-.9	VARIED	.3	39.	-.3	-.06	.100	.41	1.00	47.87
39	10.0	-.0	9.9	-.9	-7.4	VARIED	39.	-.4	-.08	.100	.41	1.00	47.87
41	9.9	-.0	VARIED	-.9	-7.4	.3	39.	-.4	-.03	.101	.42	1.00	47.87
42	9.9	-.0	9.9	VARIED	-7.4	.3	39.	-.3	-.03	.101	.42	1.00	47.87
46	10.0	.0	9.1	-.9	-7.0	.5	39.	-5.3	VARIED	.100	.44	1.00	47.87
47	10.0	VARIED	9.1	-.9	-7.0	.5	39.	-5.4	.25	.100	.44	1.00	47.87
48	10.0	.0	9.1	-.9	-7.0	.5	39.	-5.4	.24	VARIED	.46	VARIED	
51	-1.2	.0	10.0	-.6	VARIED	.9	40.	-5.3	-.19	.208	.05	4.24	203.09
52	-1.2	.0	10.0	-.6	-6.8	VARIED	40.	-5.3	-.20	.209	.05	4.24	203.09
53	-1.2	.0	VARIED	-.5	-6.9	.8	40.	-5.3	-.11	.208	.05	4.24	203.09
54	-1.2	.0	10.0	VARIED	-6.8	.9	40.	-5.3	-.11	.209	.05	4.24	203.09
55	-1.2	.0	10.0	-.4	-6.8	.9	40.	-5.3	VARIED	.209	.05	4.24	203.09
56	-1.2	.0	10.1	-.7	-7.1	.8	40.	VARIED	-1.79	.209	.05	4.24	203.09
57	VARIED	.0	10.1	-.6	-7.0	.8	40.	-5.2	-1.76	.208	.05	4.25	203.35
58	-1.2	VARIED	10.0	-.6	-6.8	.9	40.	-5.2	-1.78	.209	.05	4.26	203.75
59	-1.2	.0	10.0	-.5	-6.8	.9	40.	-5.2	-1.77	VARIED	.05	VARIED	
61	-.6	.0	11.1	-2.2	VARIED	.2	39.	-5.2	.11	.103	.05	1.00	48.06
62	-.6	.0	11.1	-2.2	-5.9	VARIED	39.	-5.2	.11	.103	.05	1.00	48.06
63	-.6	.0	VARIED	-2.1	-5.9	.1	39.	-5.2	.13	.103	.05	1.00	48.06
64	-.6	.0	11.1	VARIED	-5.9	.2	39.	-5.2	.11	.103	.04	1.00	48.06
65	-.6	.0	11.1	-2.1	-5.9	.1	39.	VARIED	.11	.102	.04	1.00	47.67
66	-5.6	.0	11.1	-2.2	-5.9	.1	39.	VARIED	.09	.102	.04	1.00	47.67
67	4.4	-.0	11.1	-2.2	-5.9	.1	39.	VARIED	.11	.102	.04	1.00	47.67
68	-.6	.0	11.1	-2.2	-5.9	.1	39.	-5.1	VARIED	.102	.06	.99	47.27
69	-.6	VARIED	11.1	-2.1	-5.9	.1	39.	-5.1	-.00	.102	.06	.99	47.40
70	-.6	.0	11.1	-2.1	-5.9	.1	39.	-5.1	-.01	VARIED	.07	VARIED	
72	-.6	VARIED	11.7	-1.9	-7.1	.6	39.	-5.2	-.00	.102	1.12	1.00	47.67
73	-.6	-.0	11.8	-1.9	VARIED	.6	39.	-5.2	.01	.102	1.12	1.00	47.67
74	-.6	-.0	VARIED	-1.8	-7.1	.6	39.	-5.2	.01	.102	1.12	1.00	47.67
76	-8.8	.0	14.2	-.6	VARIED	.3	50.	5.4	1.82	.311	.[illegible]	9.50	454.82

APPENDIX - Concluded.

RUN	α	β	$\bar{\theta}$	$\Delta\theta$	A_{is}	B_{is}	Γ	i_t	δ_r	μ	C_j	q,psf	q,Pa
77	-8.0	.0	14.2	-.6	-8.5	VARIED	50.	5.4	3.81	.311	.00	9.50	454.82
78	-8.1	.0	VARIED	-.6	-8.5	.3	50.	5.4	3.81	.310	.00	9.50	454.82
79	-8.0	.0	14.2	-.6	-8.5	.3	50.	5.5	VARIED	.311	.00	9.49	454.56
80	-8.0	.0	14.2	-.6	-8.5	.3	50.	VARIED	3.80	.311	.00	9.50	454.82
81	-6.0	.0	14.2	-.5	-8.5	.3	50.	VARIED	3.81	.312	.00	9.50	454.82
82	-10.0	.0	14.2	-.6	-8.5	.3	50.	VARIED	3.79	.309	.00	9.50	454.82
83	-8.0	VARIED	14.1	-.7	-8.5	.3	50.	5.3	3.77	.311	.00	9.50	454.82
84	-8.0	.0	14.1	-.6	-8.5	.3	50.	5.3	3.78	VARIED	.00	VARIED	
86	5.1	-.0	6.6	-.3	VARIED	.8	40.	-4.9	5.69	.313	.05	9.50	454.82
87	5.0	-.0	6.7	-.4	-6.5	VARIED	40.	-4.9	5.69	.312	.05	9.50	454.82
88	5.0	-.0	VARIED	-.4	-6.5	.8	40.	-5.0	5.69	.313	.05	9.50	454.82
89	5.0	-.0	6.6	-.4	-6.6	.8	40.	-5.0	VARIED	.313	.05	9.51	455.22
90	5.0	-.0	6.6	-.5	-6.5	.8	40.	VARIED	5.45	.313	.05	9.51	455.22
91	-.1	.0	6.6	-.5	-6.5	.8	40.	VARIED	5.79	.314	.05	9.50	454.82
92	10.0	-.0	6.7	-.4	-6.5	.8	40.	VARIED	5.79	.308	.05	9.47	453.38
93	5.0	VARIED	6.7	-.4	-6.5	.8	40.	-4.9	5.80	.313	.05	9.51	455.22
94	5.0	.1	6.7	-.4	-6.5	.8	40.	-4.9	5.80	VARIED	.05	VARIED	
143	5.0	0.0	10.0	-.9	-7.3	.3	39.	VARIED	0.00	.101	.42	1.00	4.67
144	10.0	0.0	10.0	-.9	-7.3	.3	39.	VARIED	0.00	.101	.42	1.00	4.67
145	14.8	0.0	10.0	-.9	-7.3	.3	39.	VARIED	0.00	.101	.42	1.00	4.67
151	VARIED	0.0	11.1	-2.1	-5.5	.1	39.	-5.2	.10	.102	.04	1.00	4.67
152	VARIED	0.0	10.0	-.9	-7.3	.3	39.	-.2	0.00	.101	.42	1.00	4.67
161	VARIED	0.0	14.2	-.5	-8.5	.3	50.	5.3	3.80	.310	0.00	9.50	454.82
162	VARIED	0.0	6.7	-.5	-6.5	.8	40.	-5.2	5.44	.312	.05	9.49	454.47
228	0.0	0.0	15.8	-1.1	VARIED	.1	40.	0.0	0.00	0.000	0.00	0.00	0.00
229	0.0	0.0	15.9	0.0	0.0	VARIED	40.	0.0	0.00	0.000	0.00	0.00	0.00
230	0.0	0.0	VARIED	-1.0	0.0	-.2	40.	0.0	0.00	0.000	0.00	0.00	0.00
231	0.0	0.0	15.9	VARIED	0.0	-.2	40.	0.0	0.00	0.000	0.00	0.00	0.00

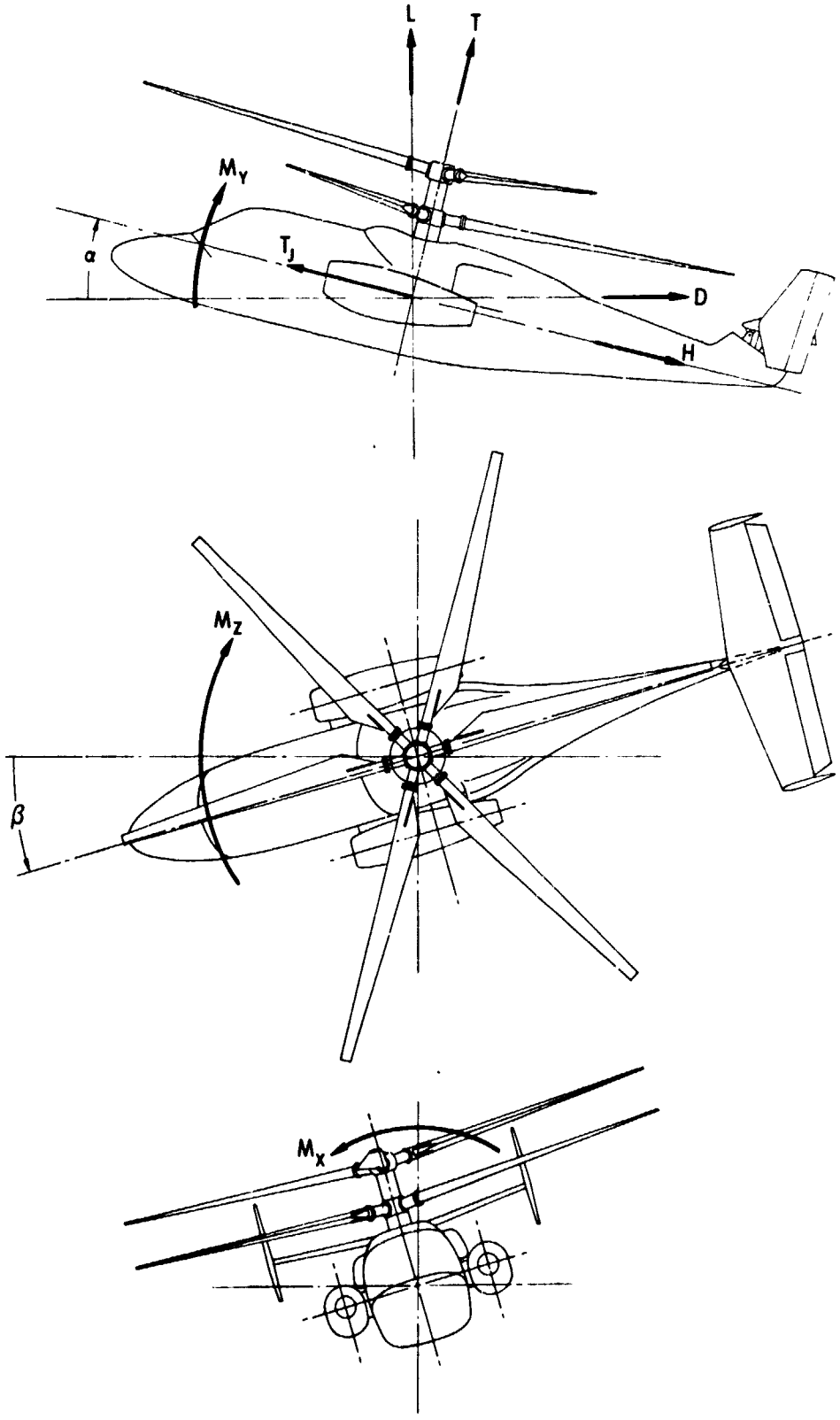

Figure 1. - Axis system used in presentation of data. Arrows denote directions of forces, moments, and angles.

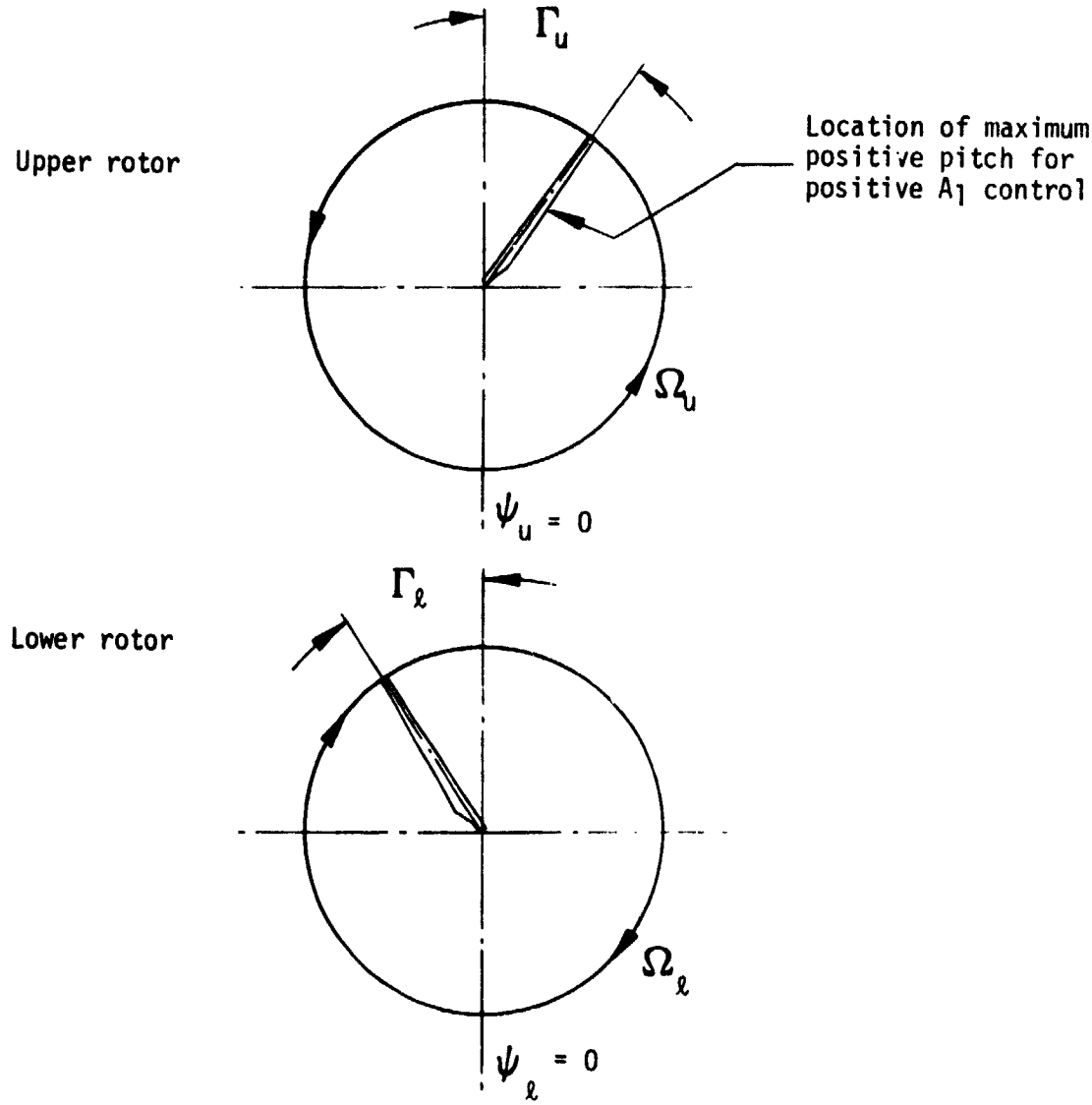

local blade pitch at 0.75R

$$\begin{cases} \theta_u = \theta_{o_u} - A_{1_u} \cos(\psi_u + \Gamma_u) - B_{1_u} \sin(\psi_u + \Gamma_u) \\ \theta_\ell = \theta_{o_\ell} - A_{1_\ell} \cos(\psi_\ell + \Gamma_\ell) - B_{1_\ell} \sin(\psi_\ell + \Gamma_\ell) \end{cases}$$

$$\overline{\theta} = \frac{\theta_{o_u} + \theta_{o_\ell}}{2} \qquad \Delta\theta = \theta_{o_u} \quad \theta_{o_\ell}$$

$$A_{1S} = \frac{A_{1_u} + A_{1_\ell}}{2}$$

$$B_{1S} = \frac{B_{1_u} + B_{1_\ell}}{2}$$

Figure 1. - Concluded.

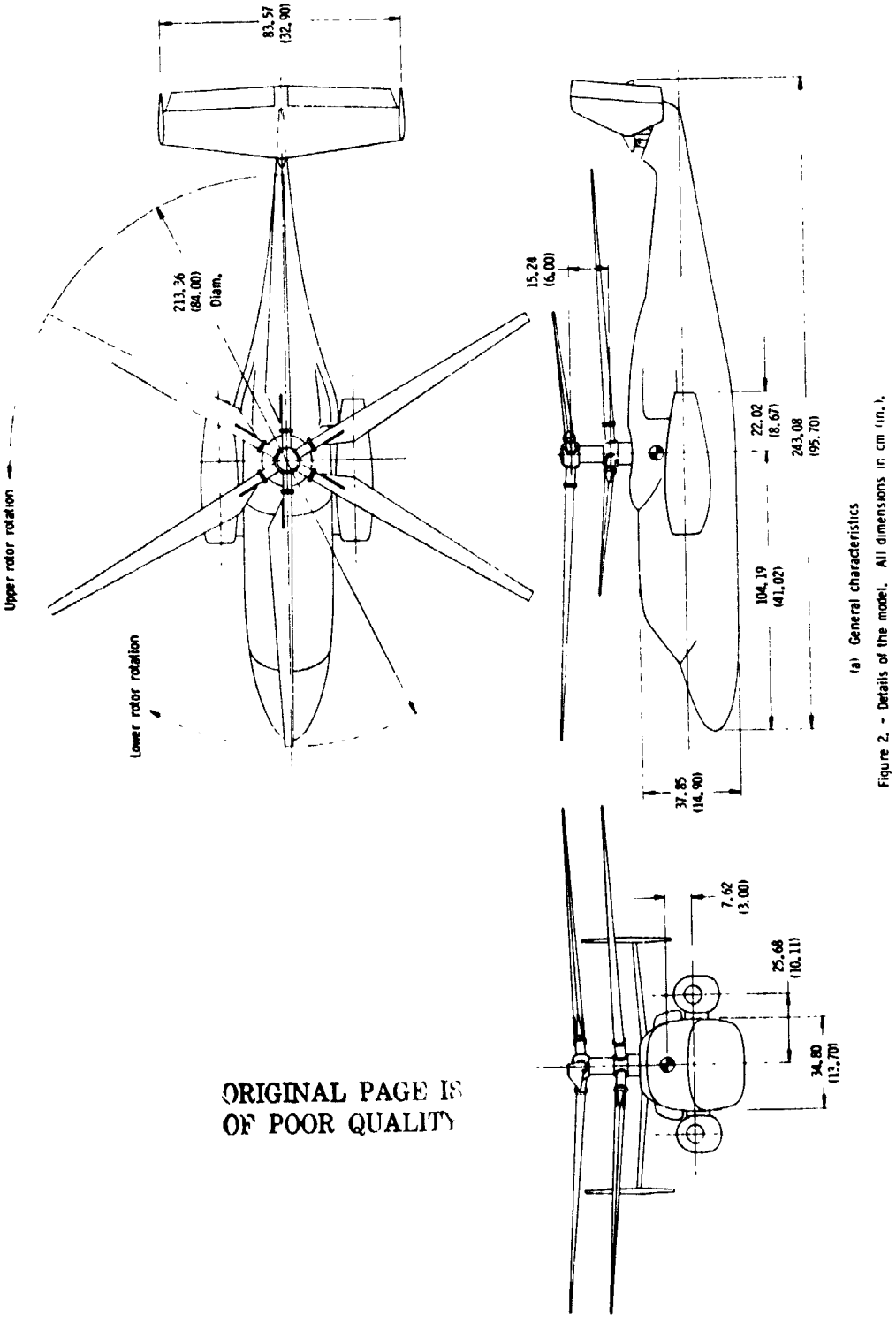

(a) General characteristics

Figure 2. - Details of the model. All dimensions in cm (in.).

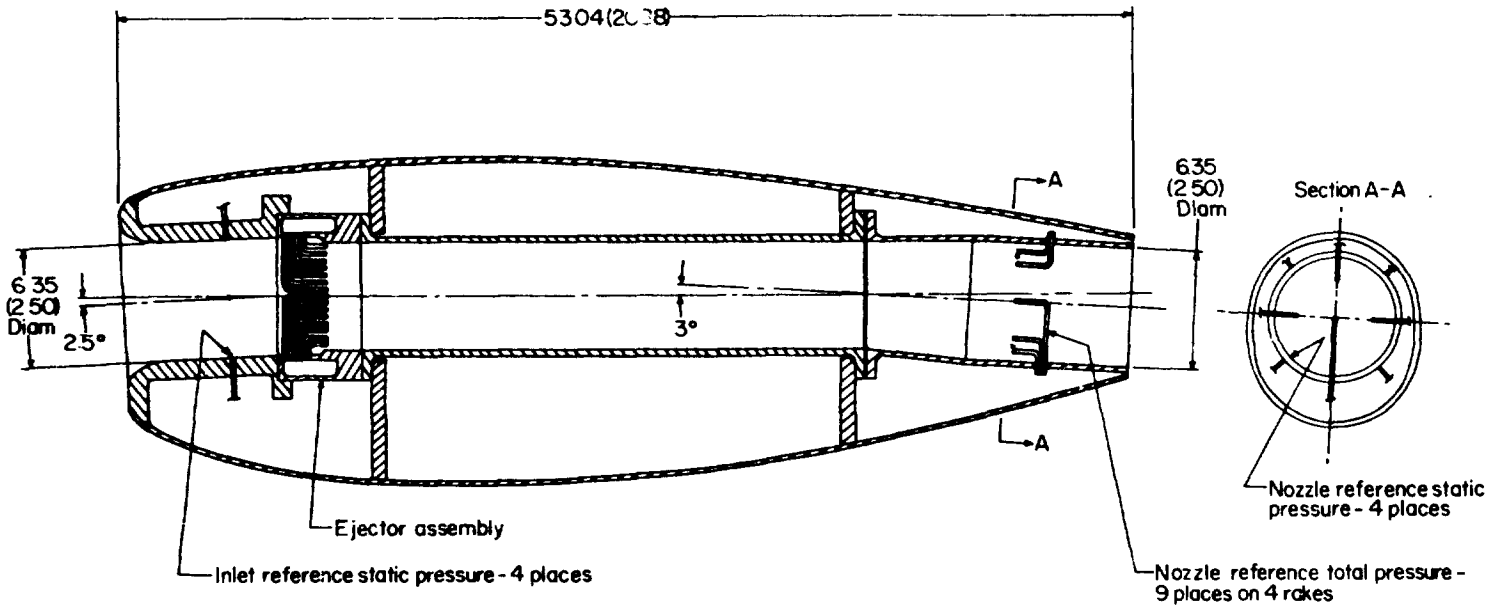

(b) Details of auxiliary engine simulators

Figure 2. - Concluded.

ORIGINAL PAGE IS
OF POOR QUALITY

Figure 3. - Model in V/STOL tunnel.

Figure 3. - Concluded.

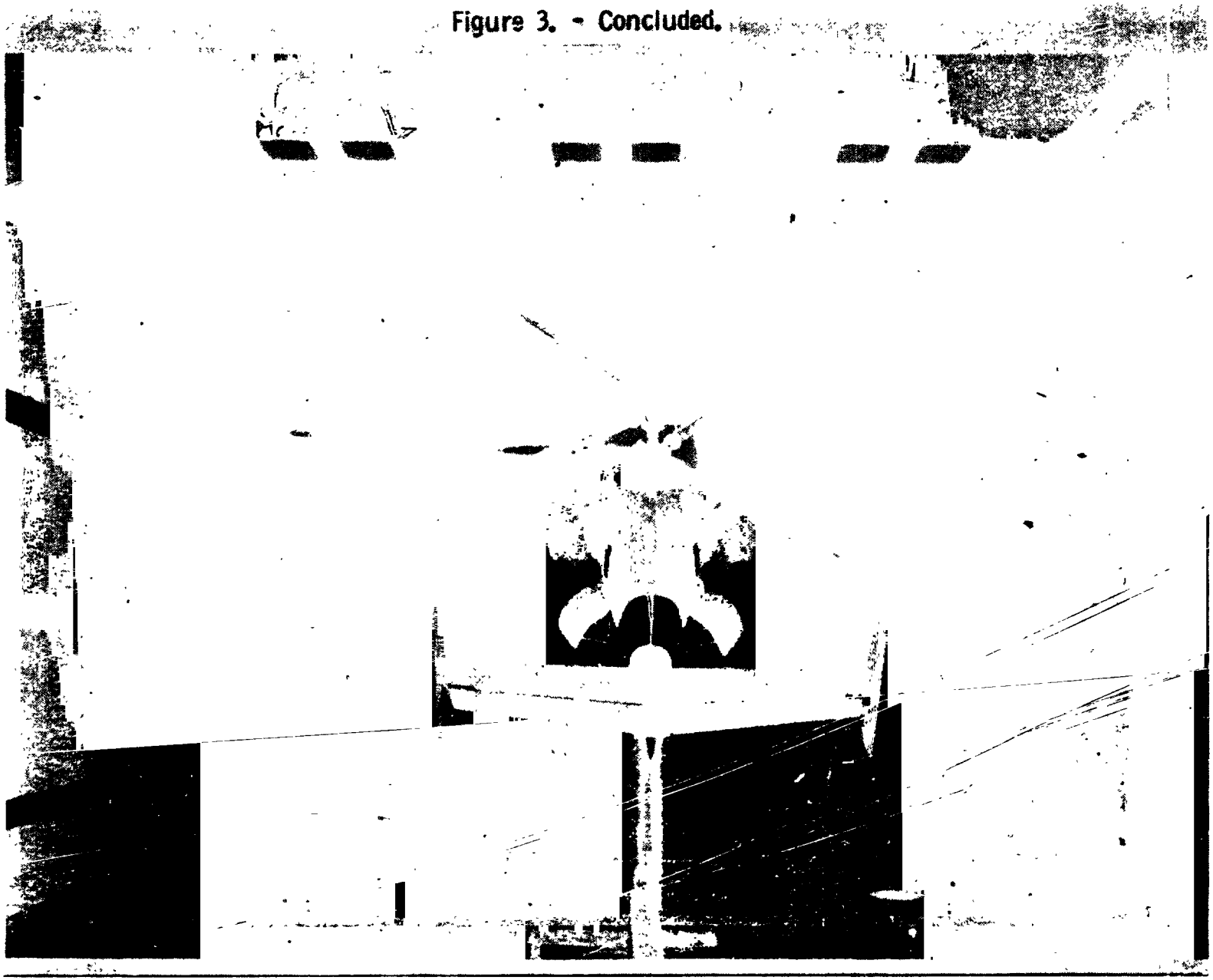

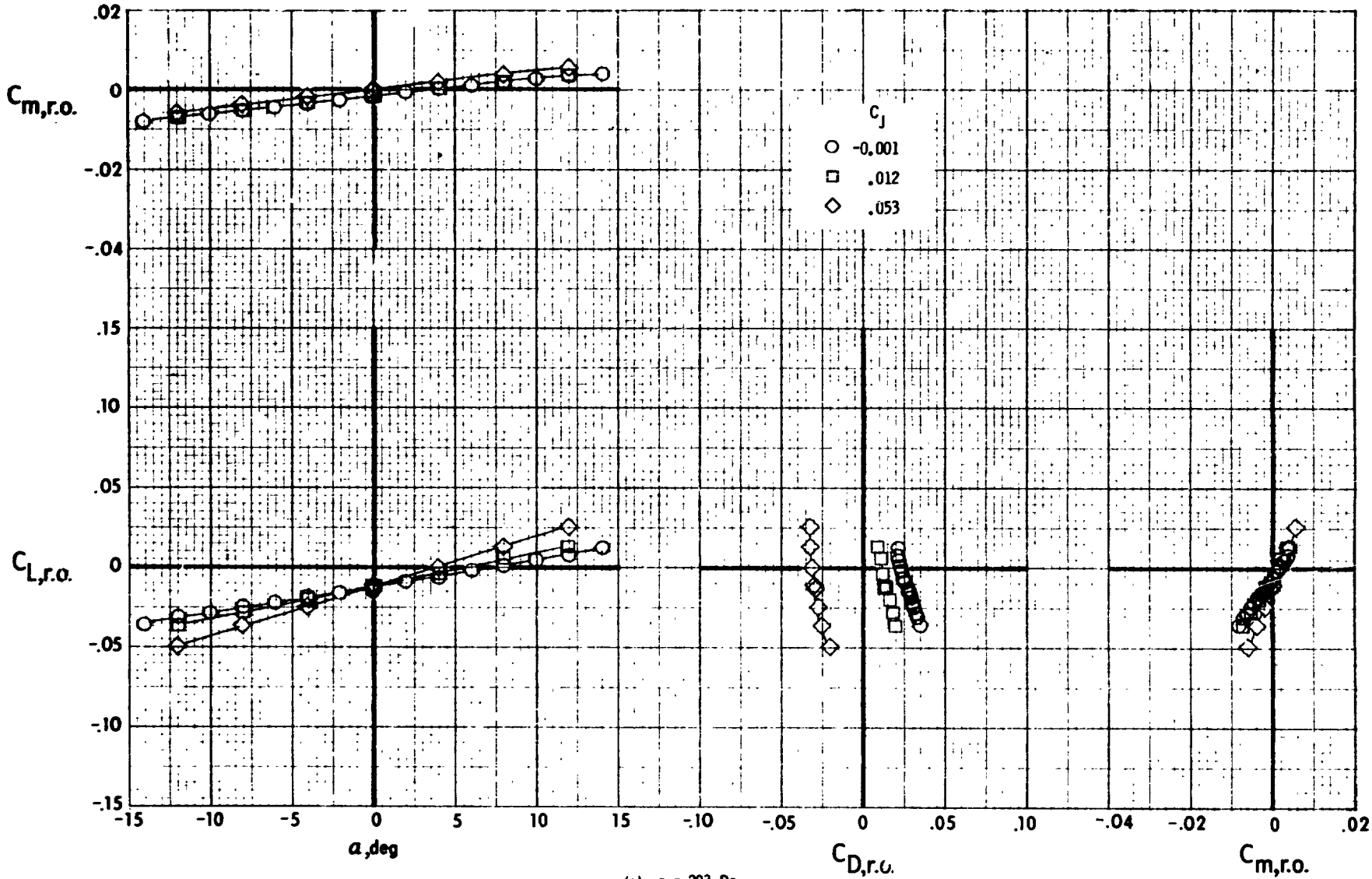

(a) q = 203 Pa

Figure 4. - Effect of auxiliary engine thrust on the longitudinal aerodynamic characteristics of the model with the rotor and tail removed.

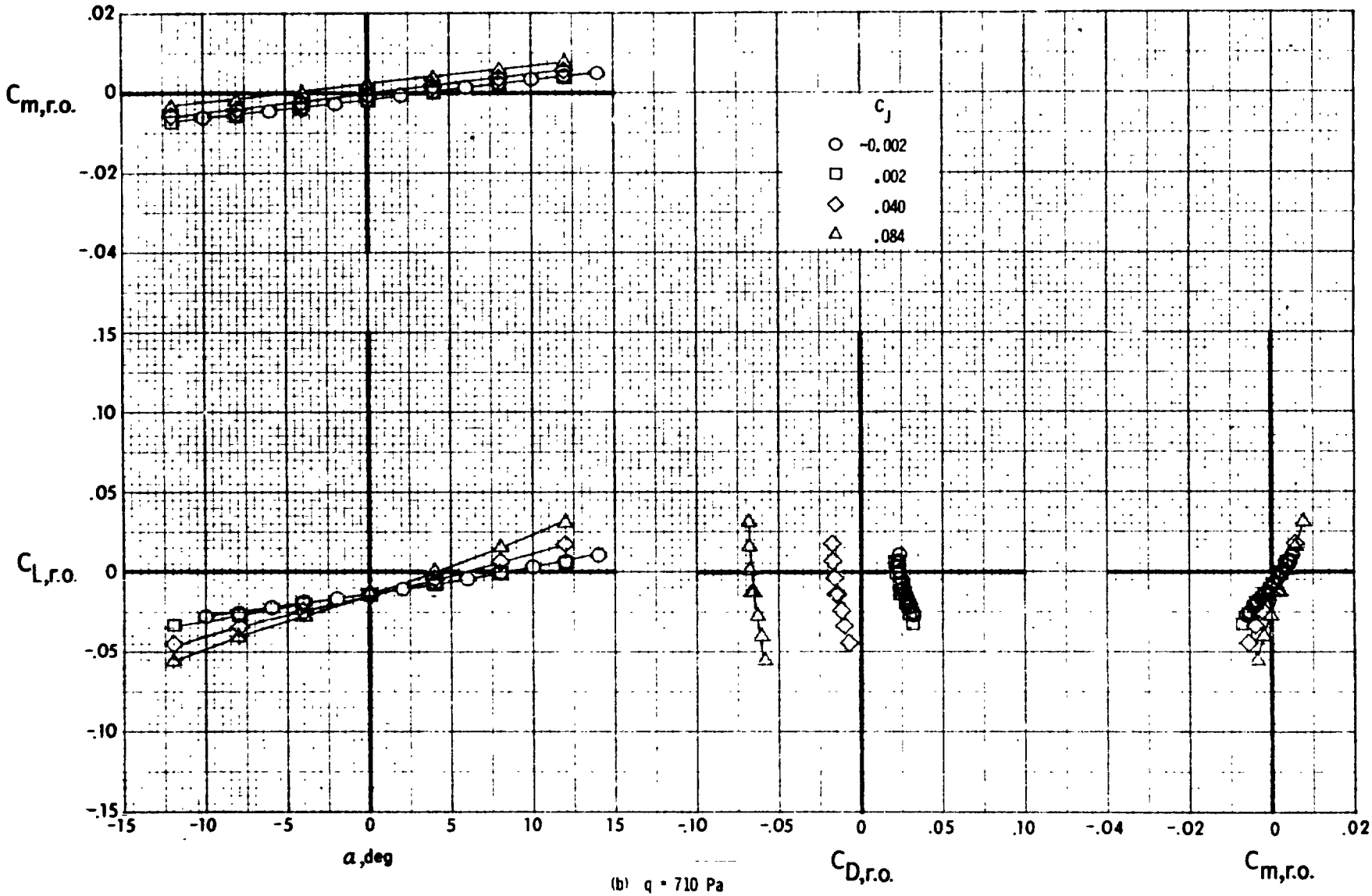

(b) q = 710 Pa

Figure 4. - Continued.

ORIGINAL PAGE IS
OF POOR QUALITY

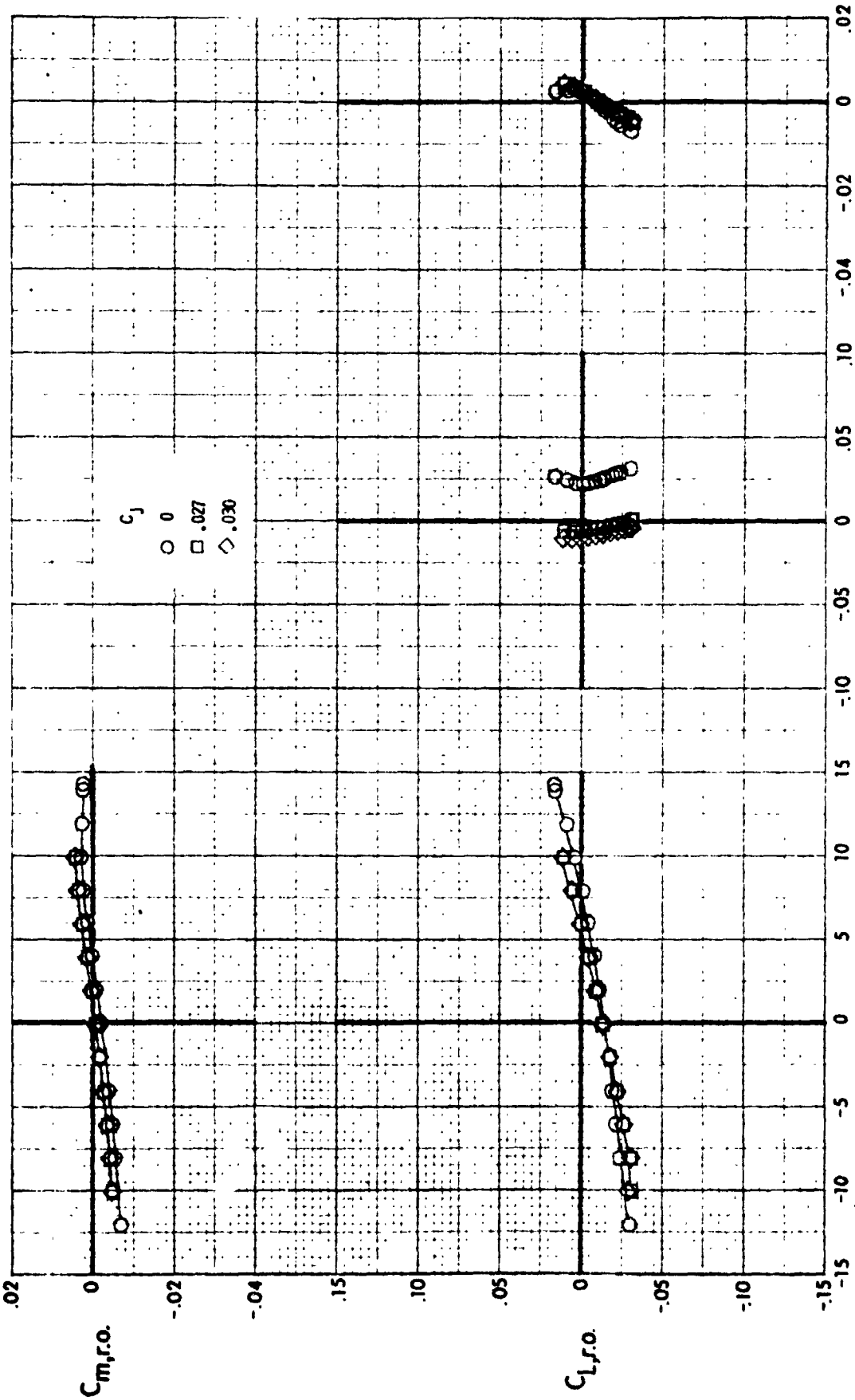

(c) q = 1974 Pa

Figure 4. - Concluded.

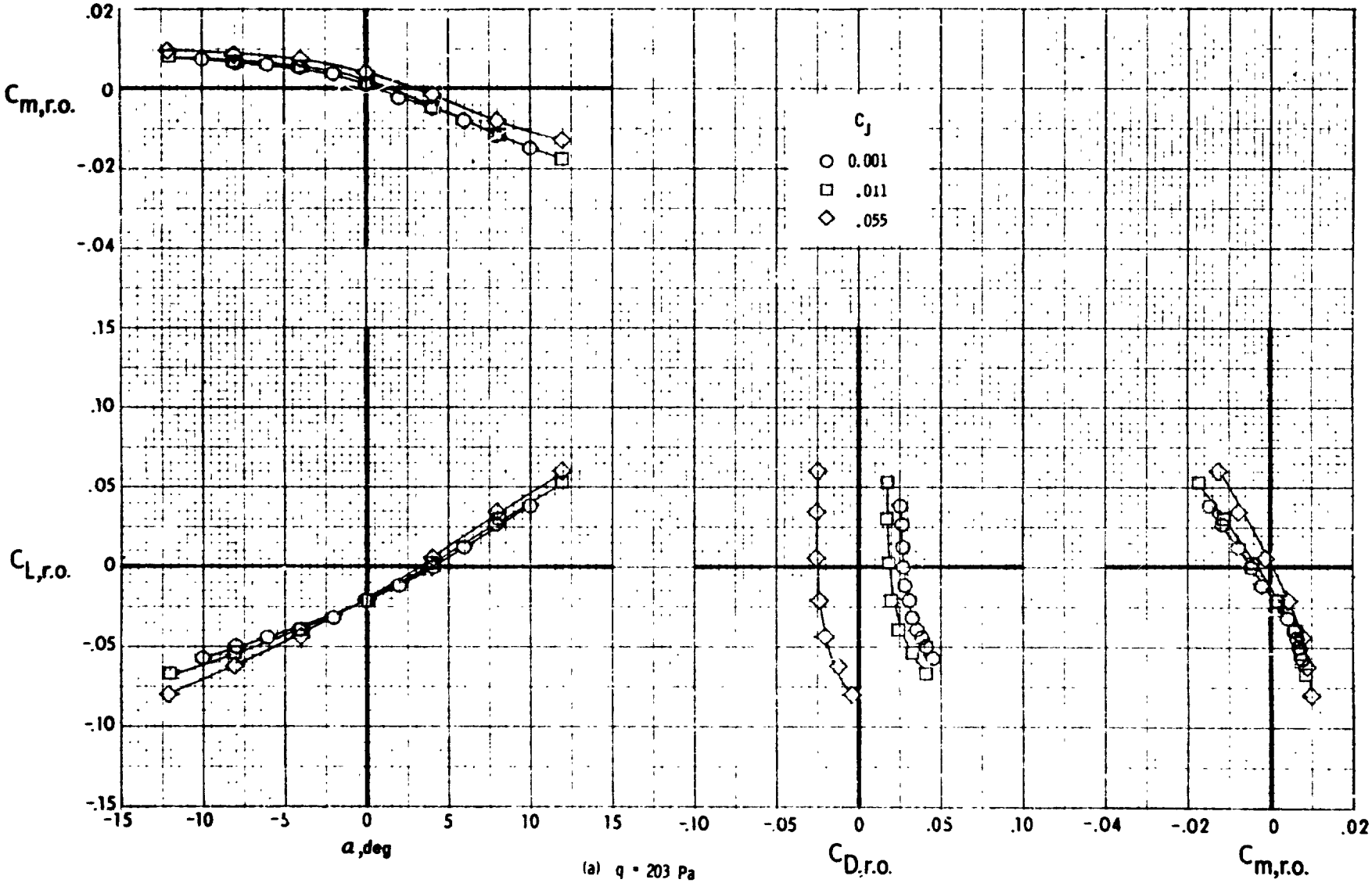

(a) $q = 203$ Pa

Figure 5. - Effect of auxiliary engine thrust on the longitudinal aerodynamic characteristics of the model with the rotor removed. $i_t = -5^0$, $\delta_R = 0^0$.

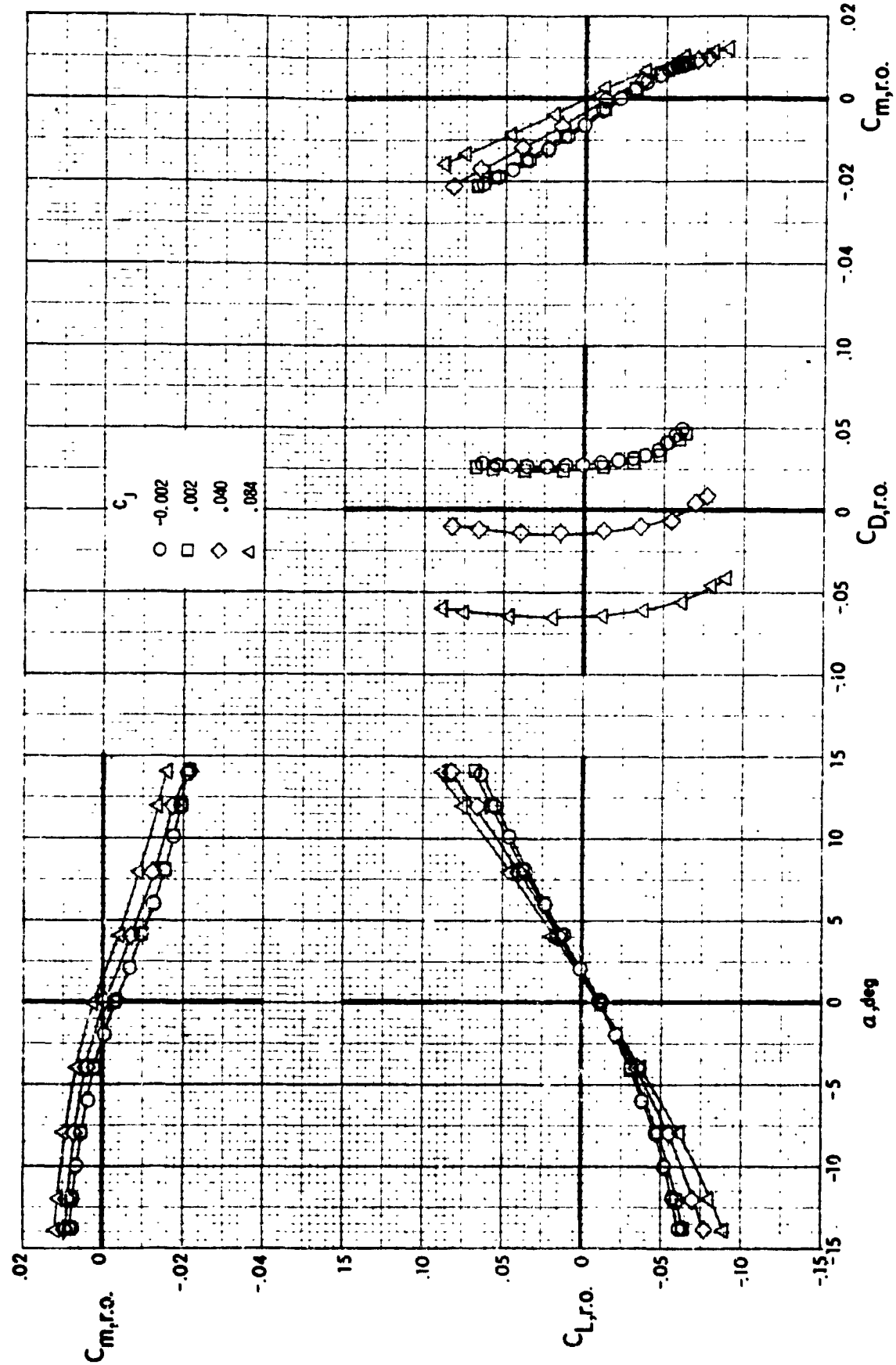

(b) q = 710 Pa

Figure 5. - Continued.

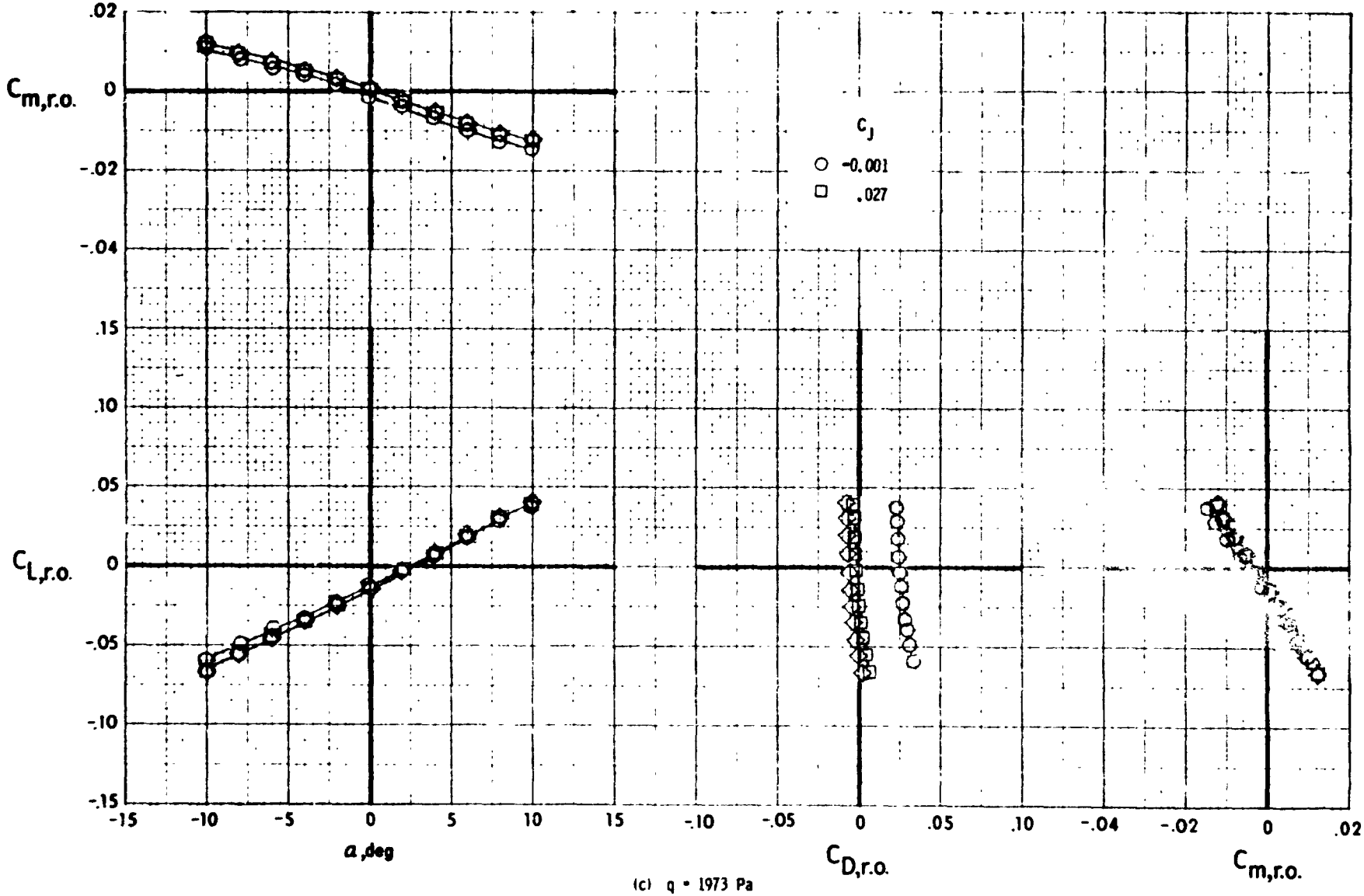

(c) q = 1973 Pa

Figure 5. - Concluded.

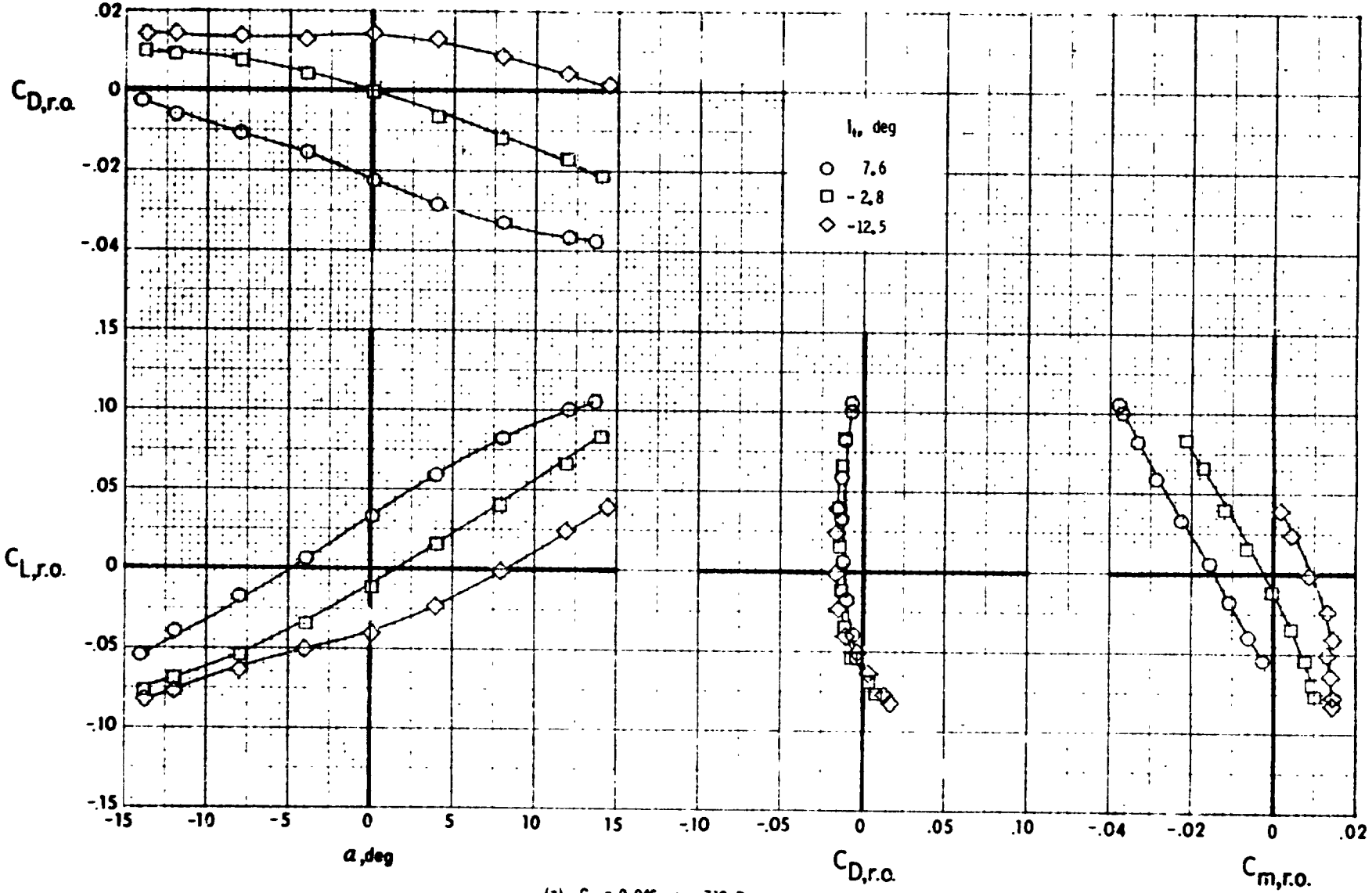

(a) $C_J = 0.040$, $q = 710$ Pa

Figure 6. - Effect of tail incidence on the longitudinal aerodynamic characteristics of the model with the rotor removed.

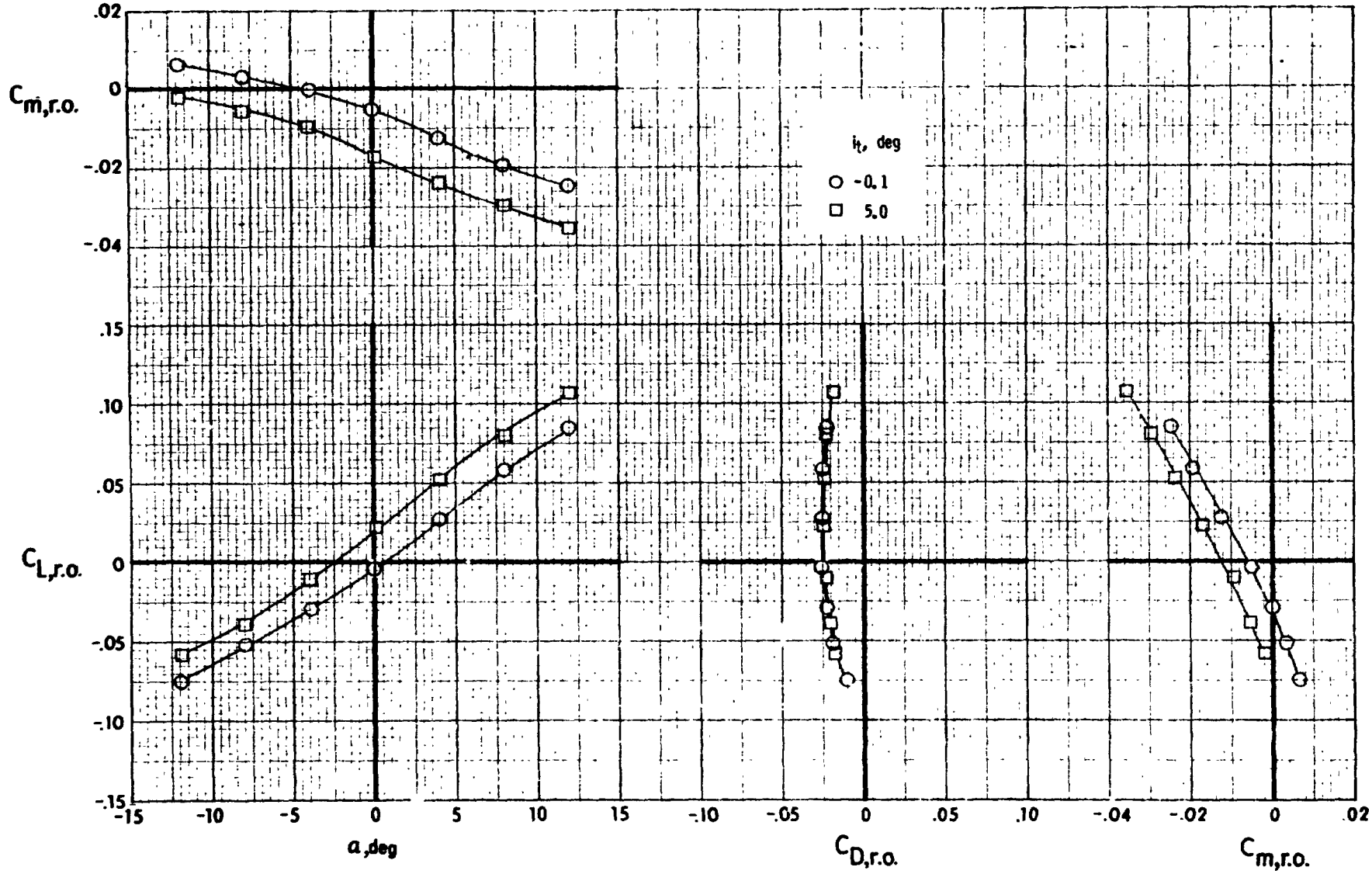

(b) C_j = 0.055, q = 203 Pa

Figure 6. - Concluded.

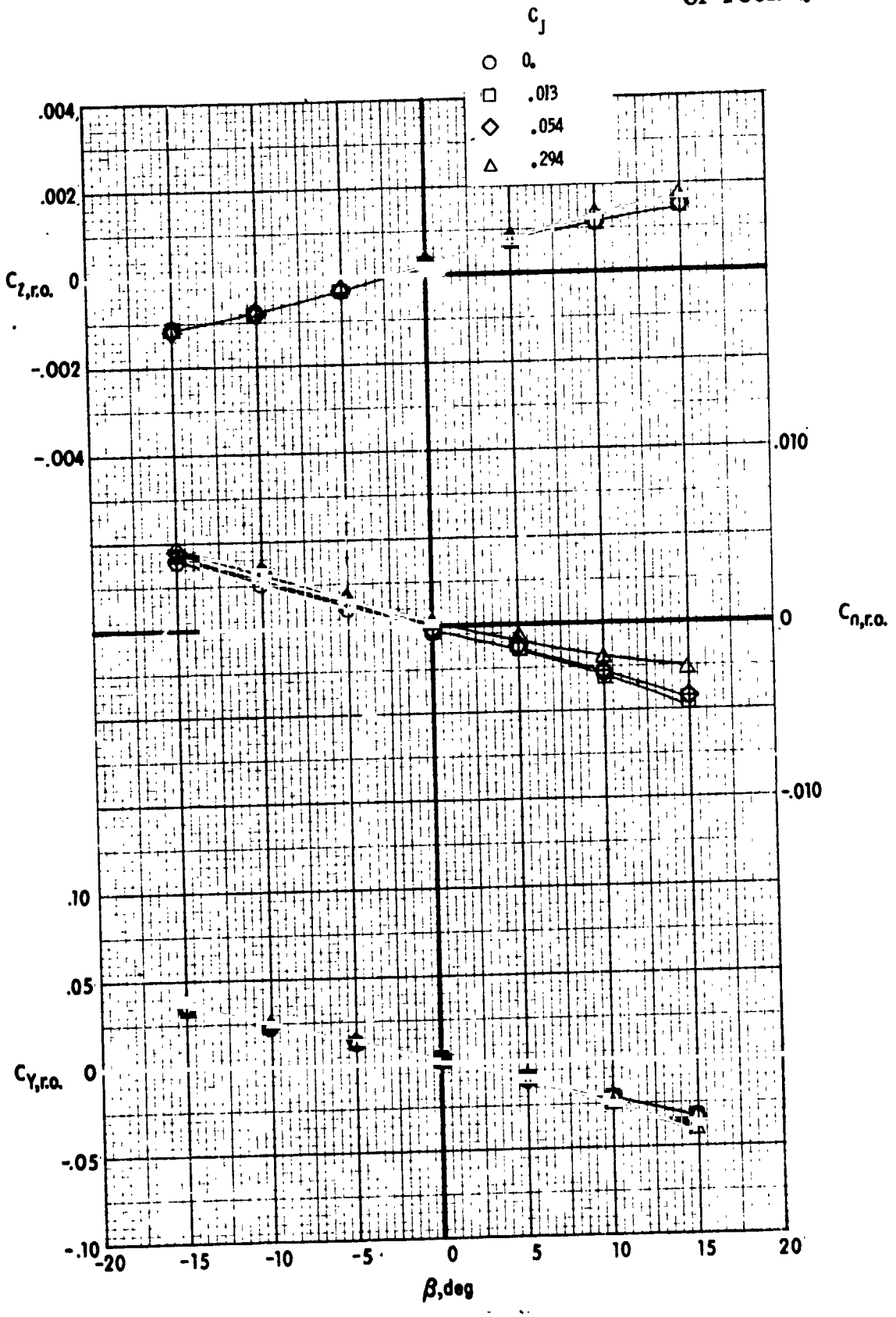

(a) q = 201 Pa

Figure 7. - Effect of auxiliary engine thrust level on the lateral aerodynamic characteristics of the model with the rotor and tail removed.

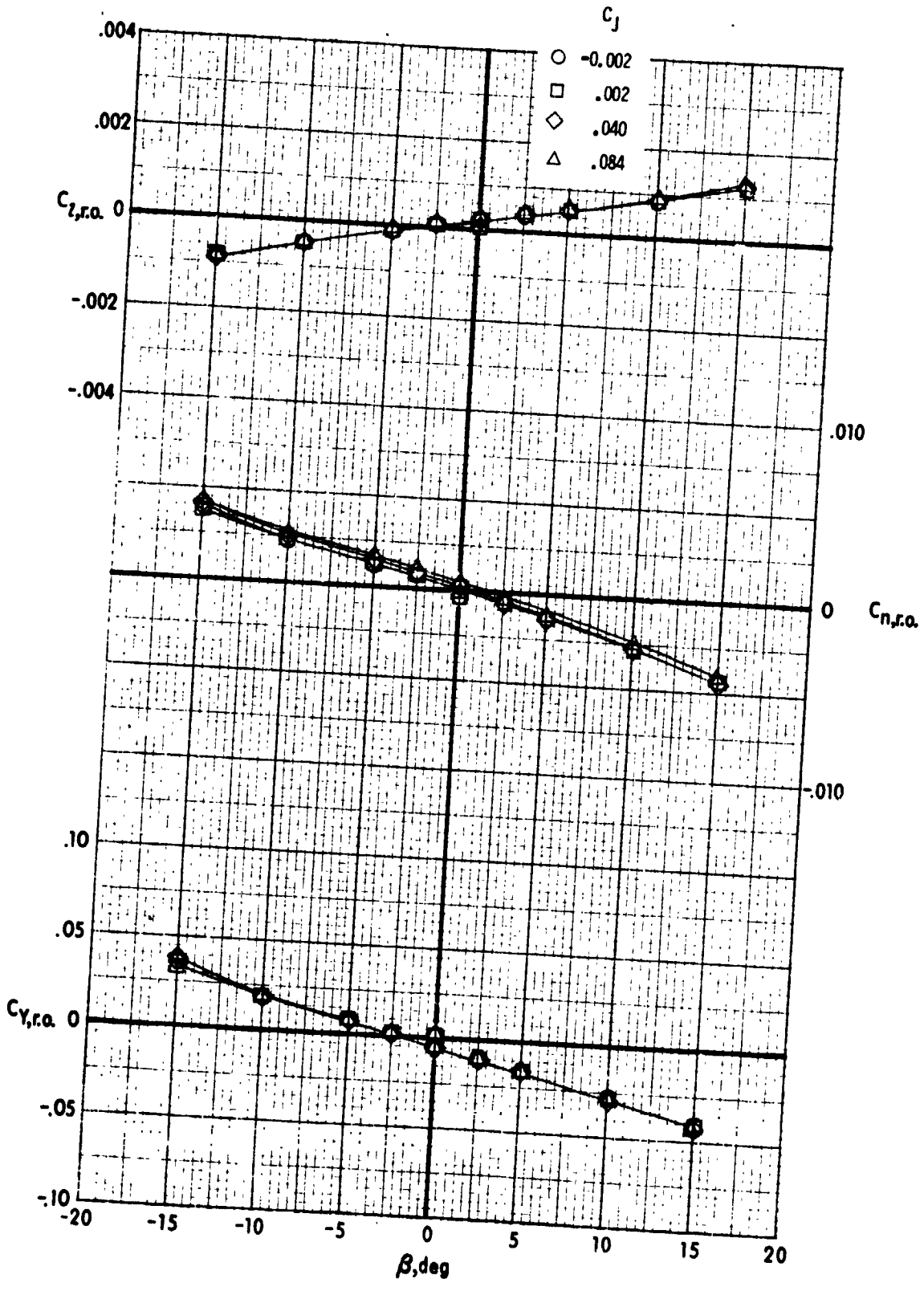

(b) q = 710 Pa

Figure 7. - Continued.

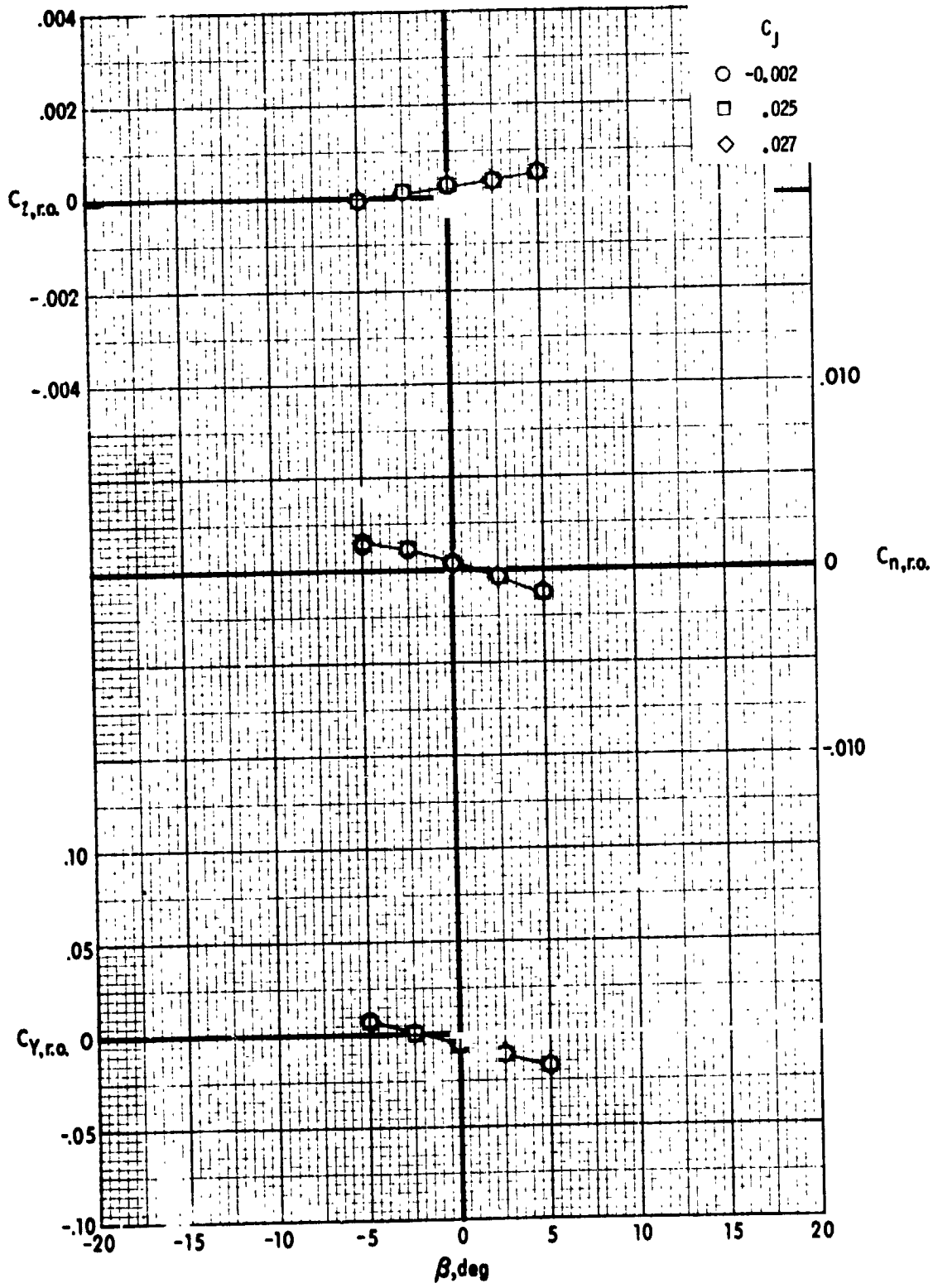

(c) q = 1973 Pa

Figure 7. - Concluded.

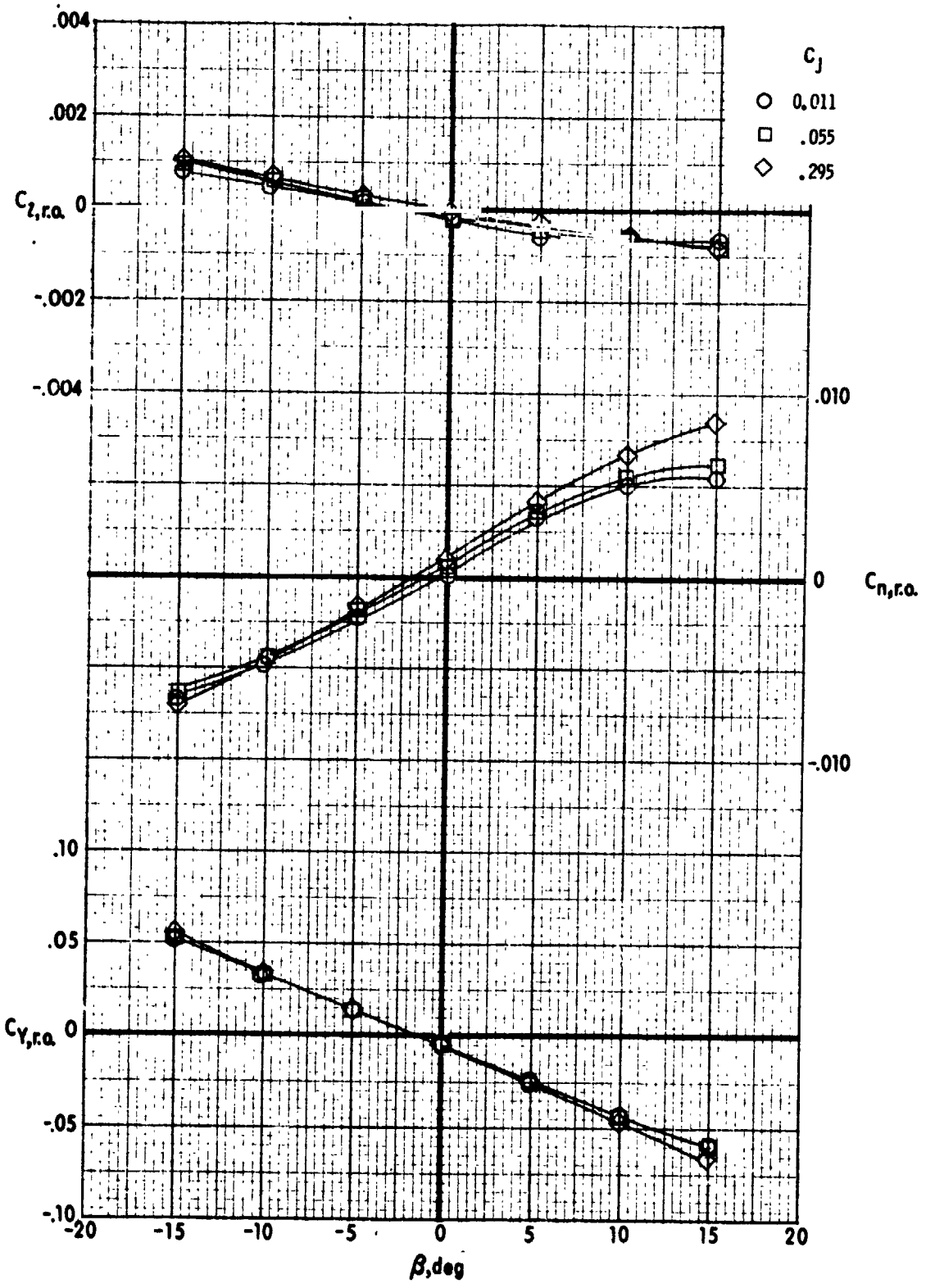

(a) q = 203 Pa

Figure 8. - Effect of auxiliary engine thrust level on the lateral aerodynamic characteristics of the model with the rotor removed.

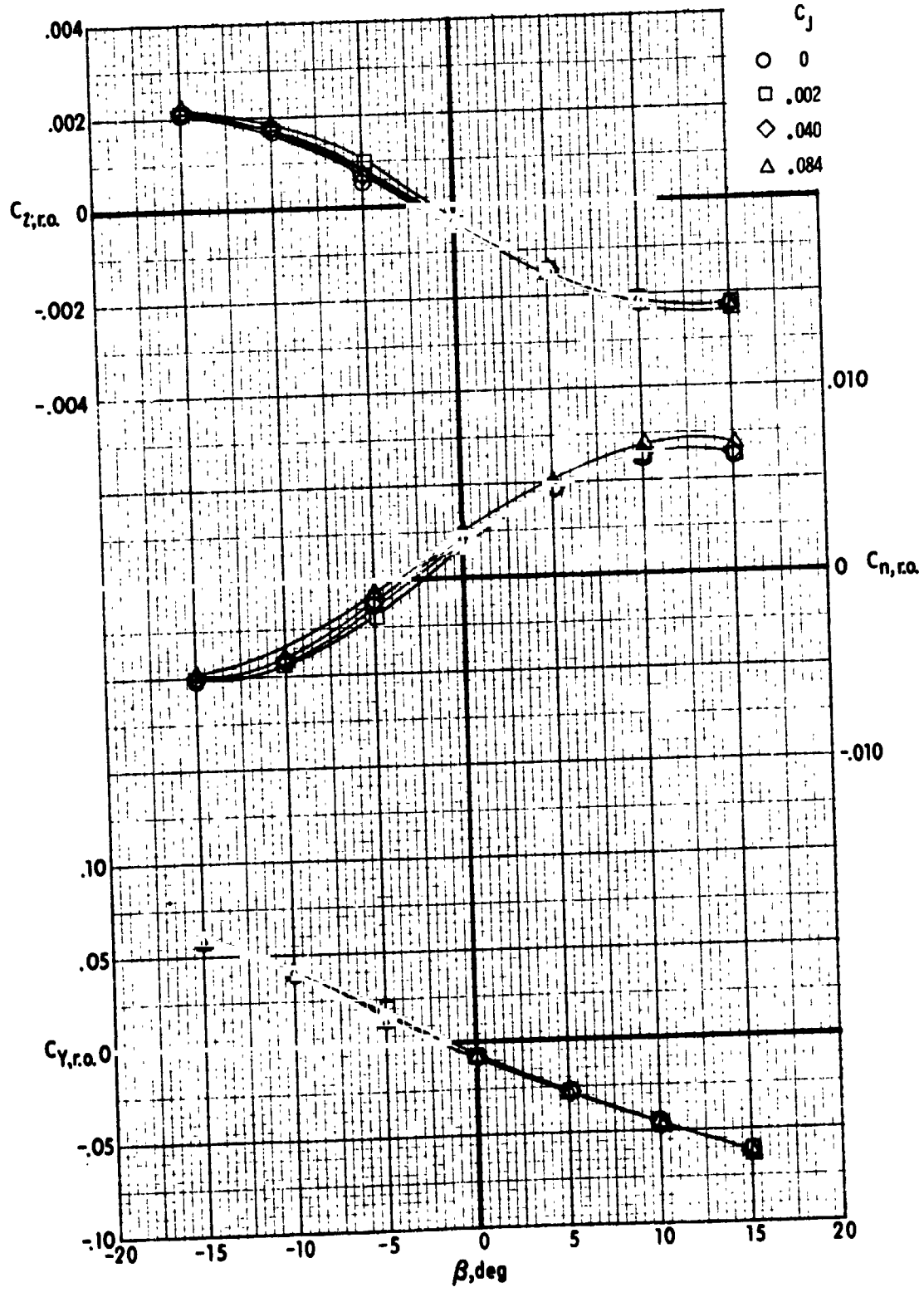

(b) q = 710 Pa

Figure 8. - Continued.

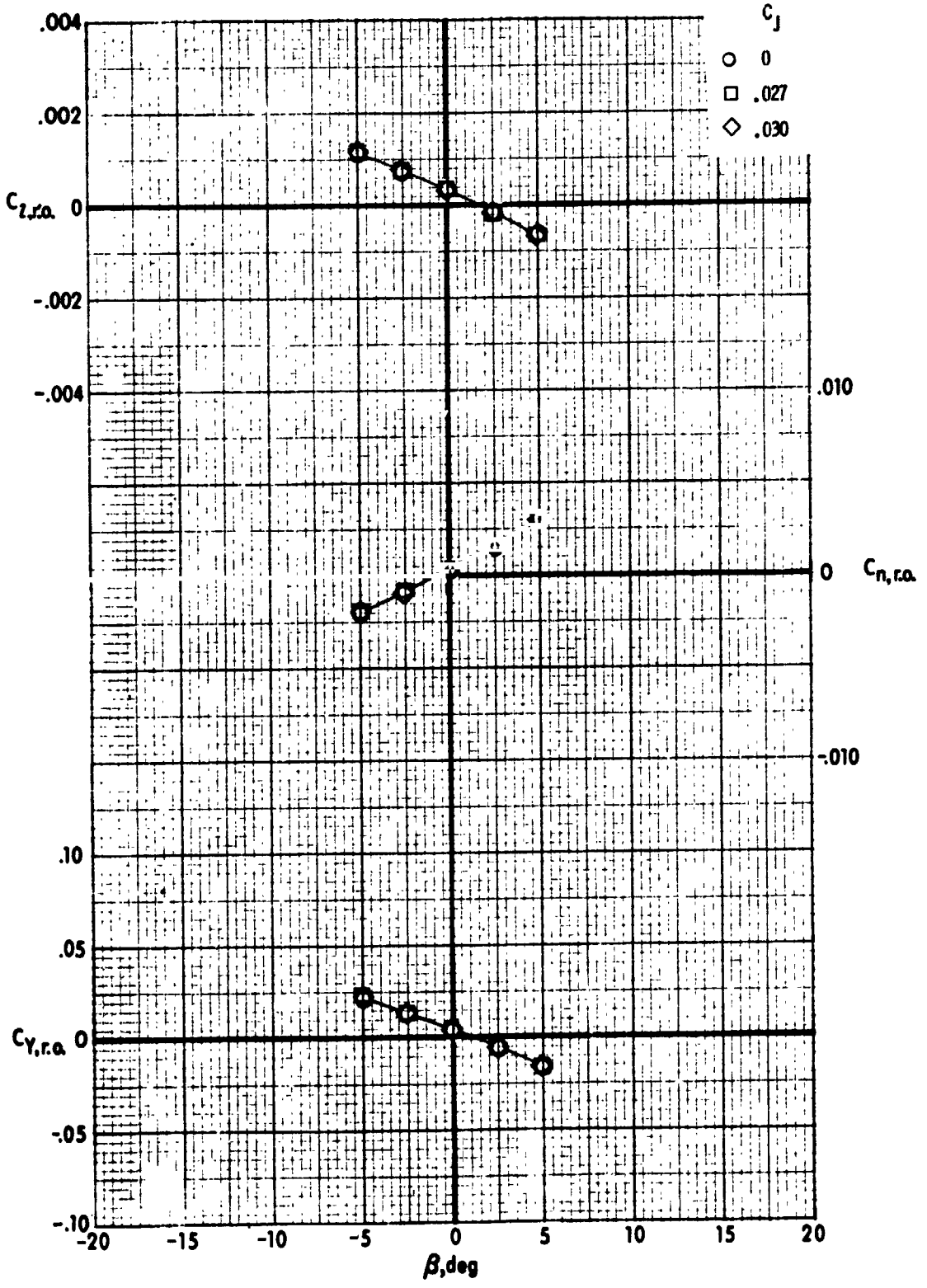

(c) q = 1973 Pa

Figure 8. - Concluded.

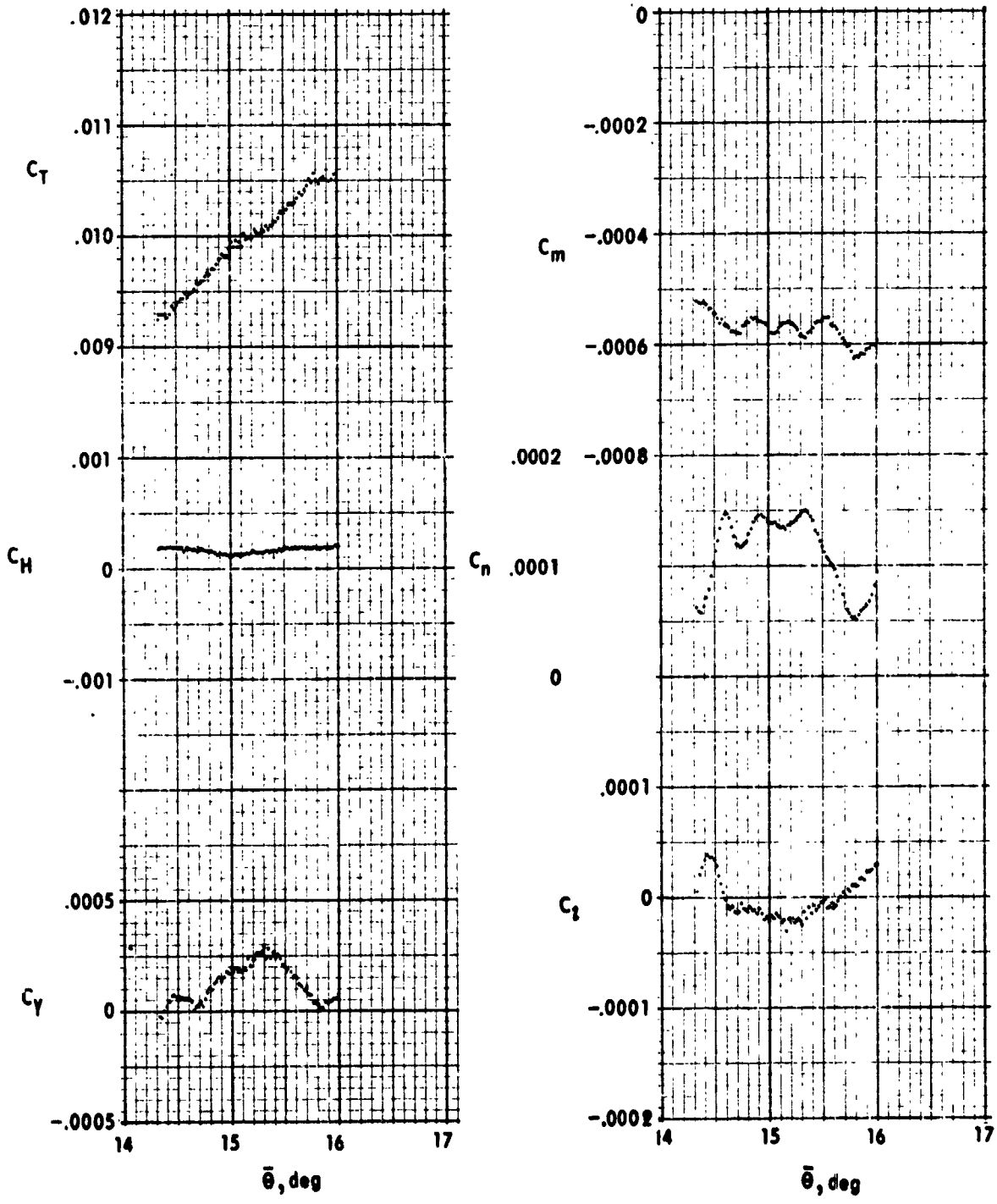

(a) $\mu \approx 0$, no thrust, run 230

Figure 9. - Variation of the airframe forces and moments with rotor collective pitch.

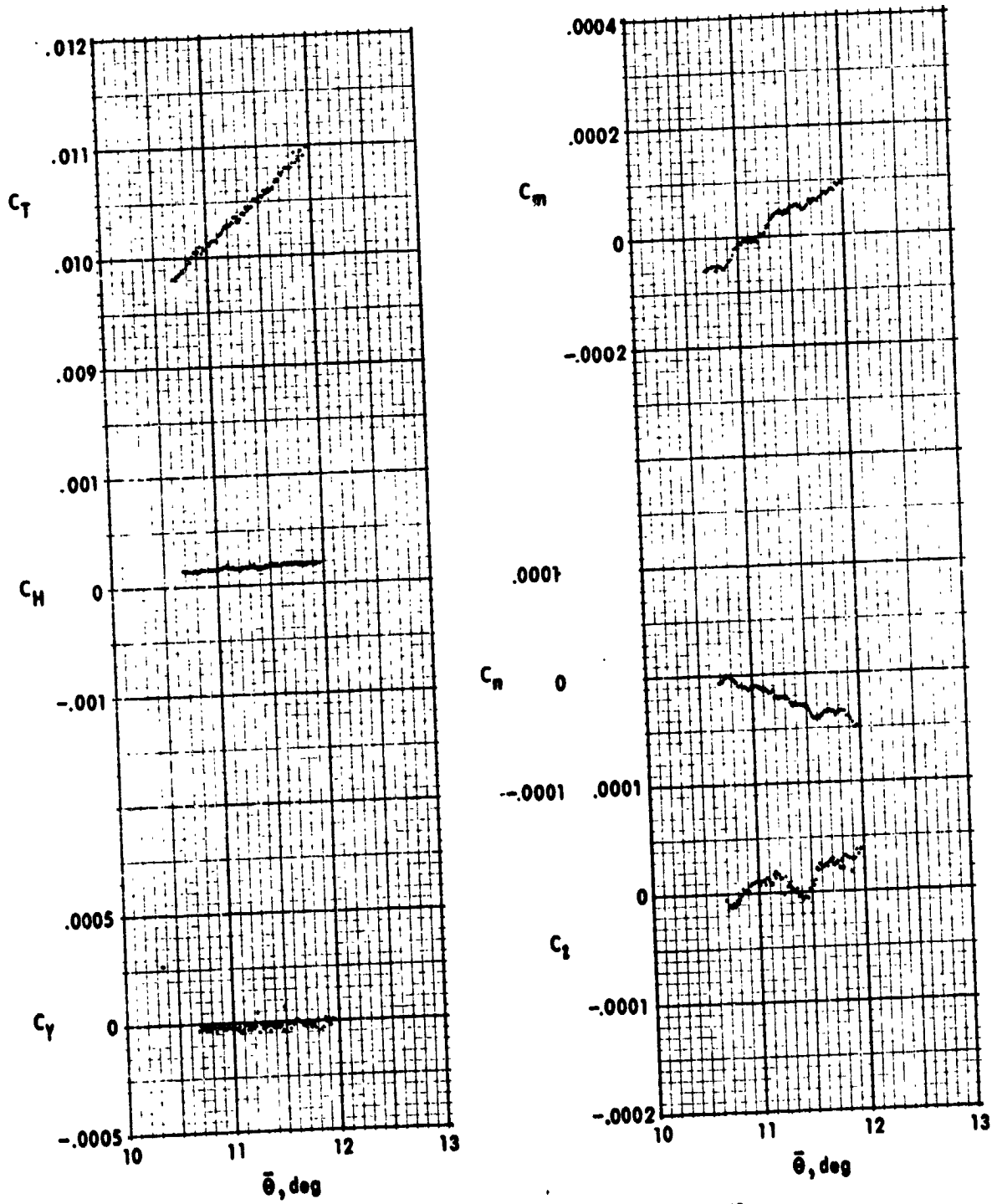

(b) $\mu \approx 0.1$, flight idle thrust, run 63

Figure 9. - Continued.

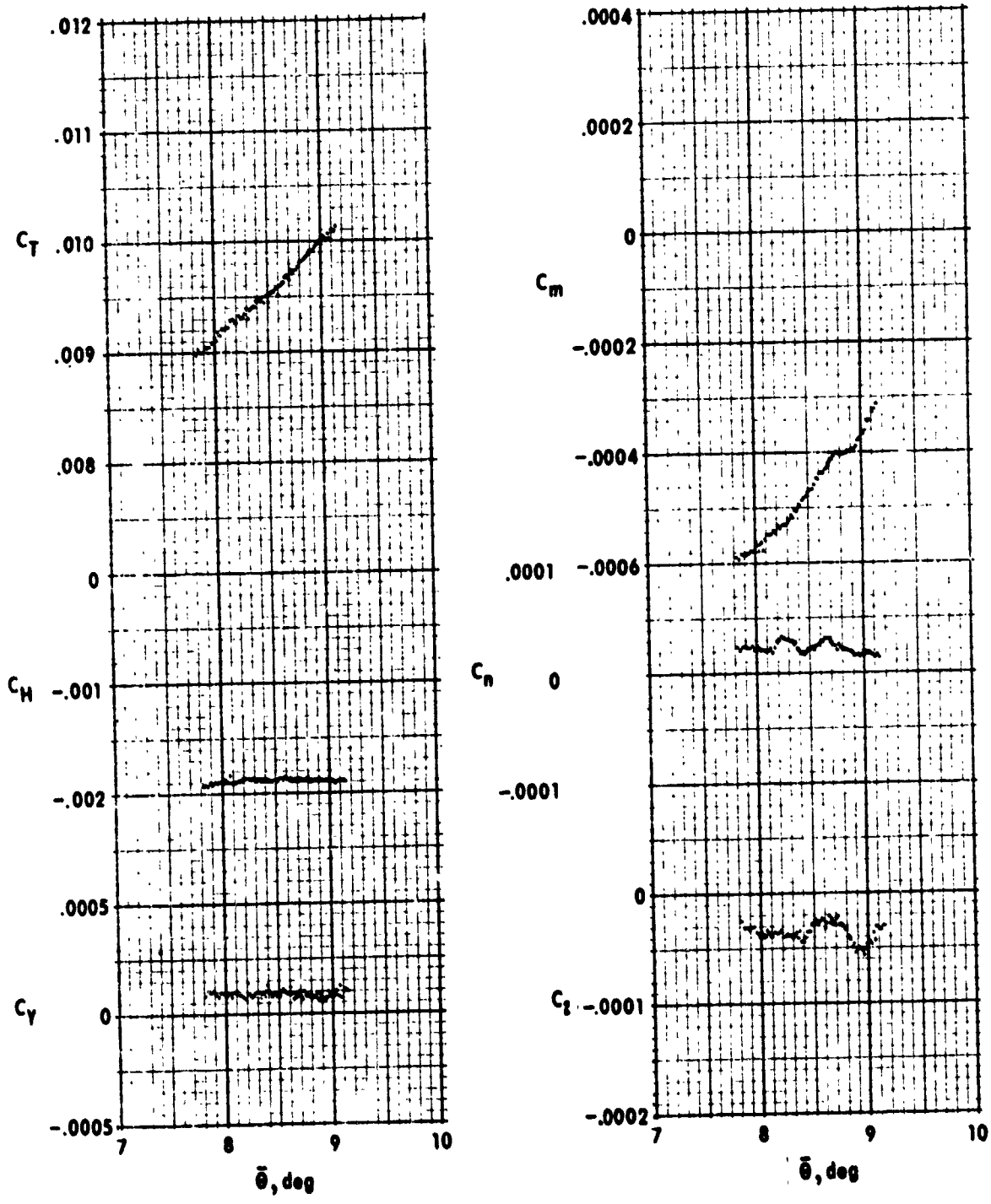

(c) $\mu \approx 0.1$, trim thrust, run 41

Figure 9. - Continued.

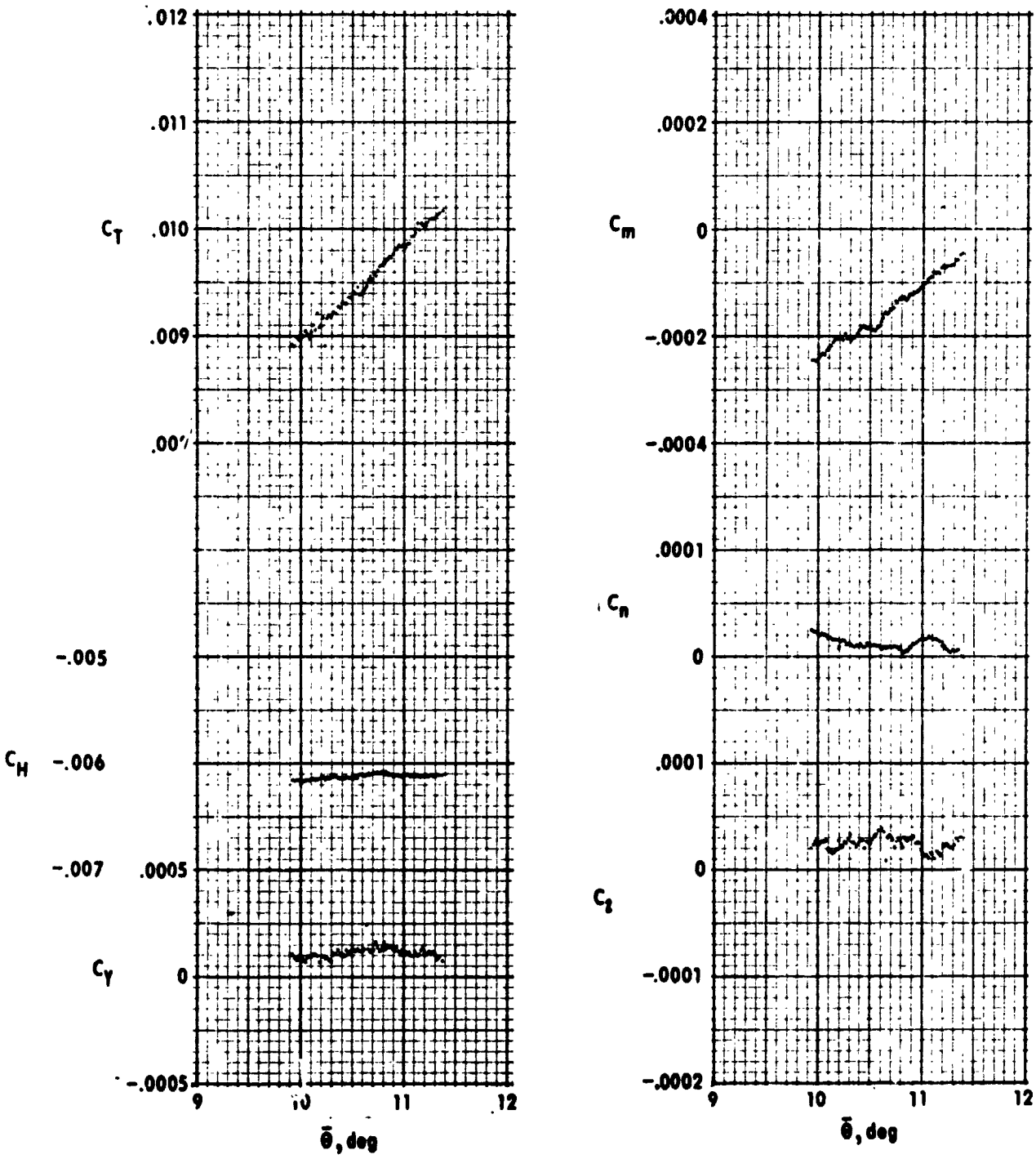

(d) $\mu \approx 0.1$, maximum thrust, run 74

Figure 9. - Continued.

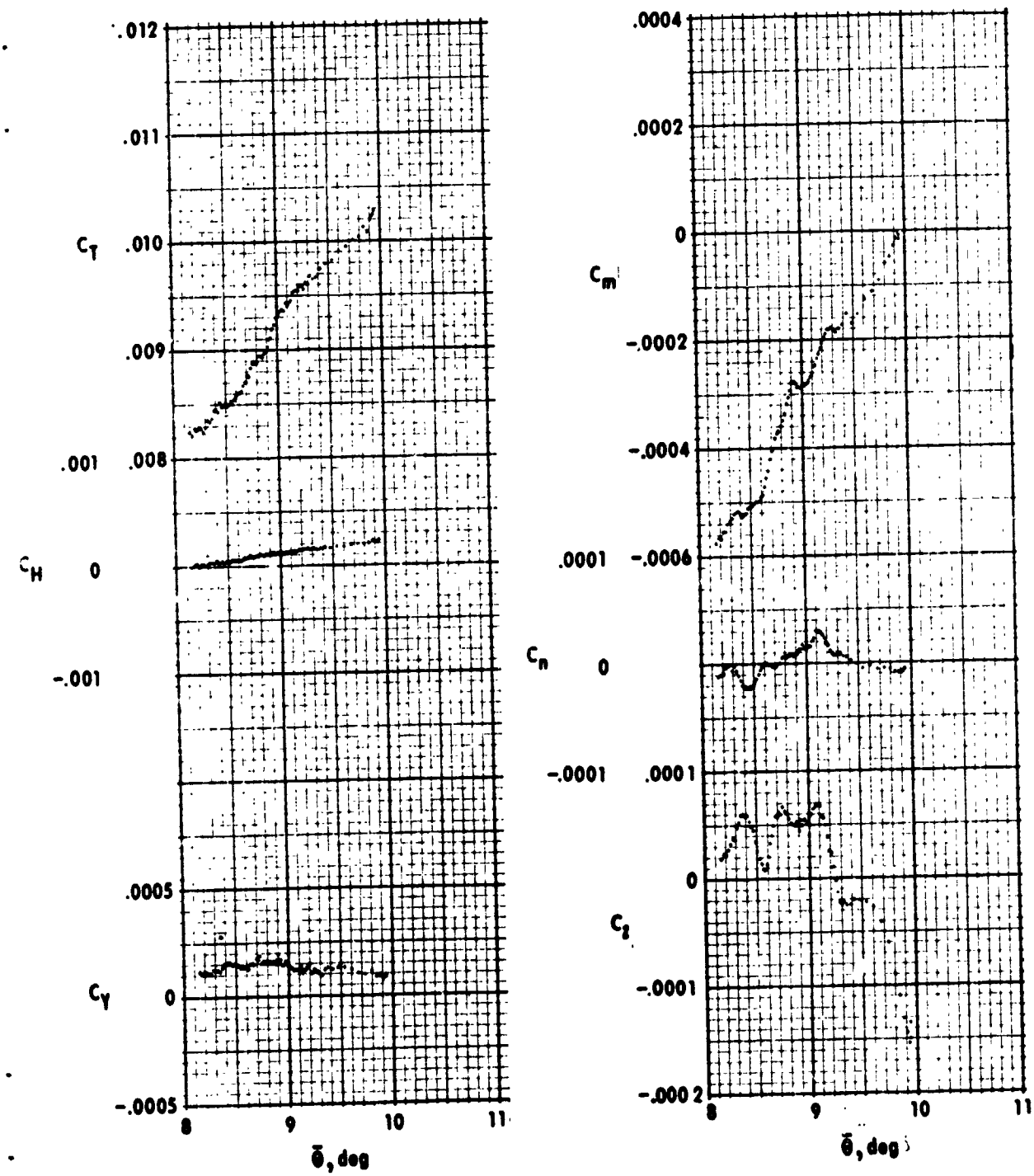

(e) $\mu \approx 0.2$, trim thrust, run 53

Figure 9. - Continued.

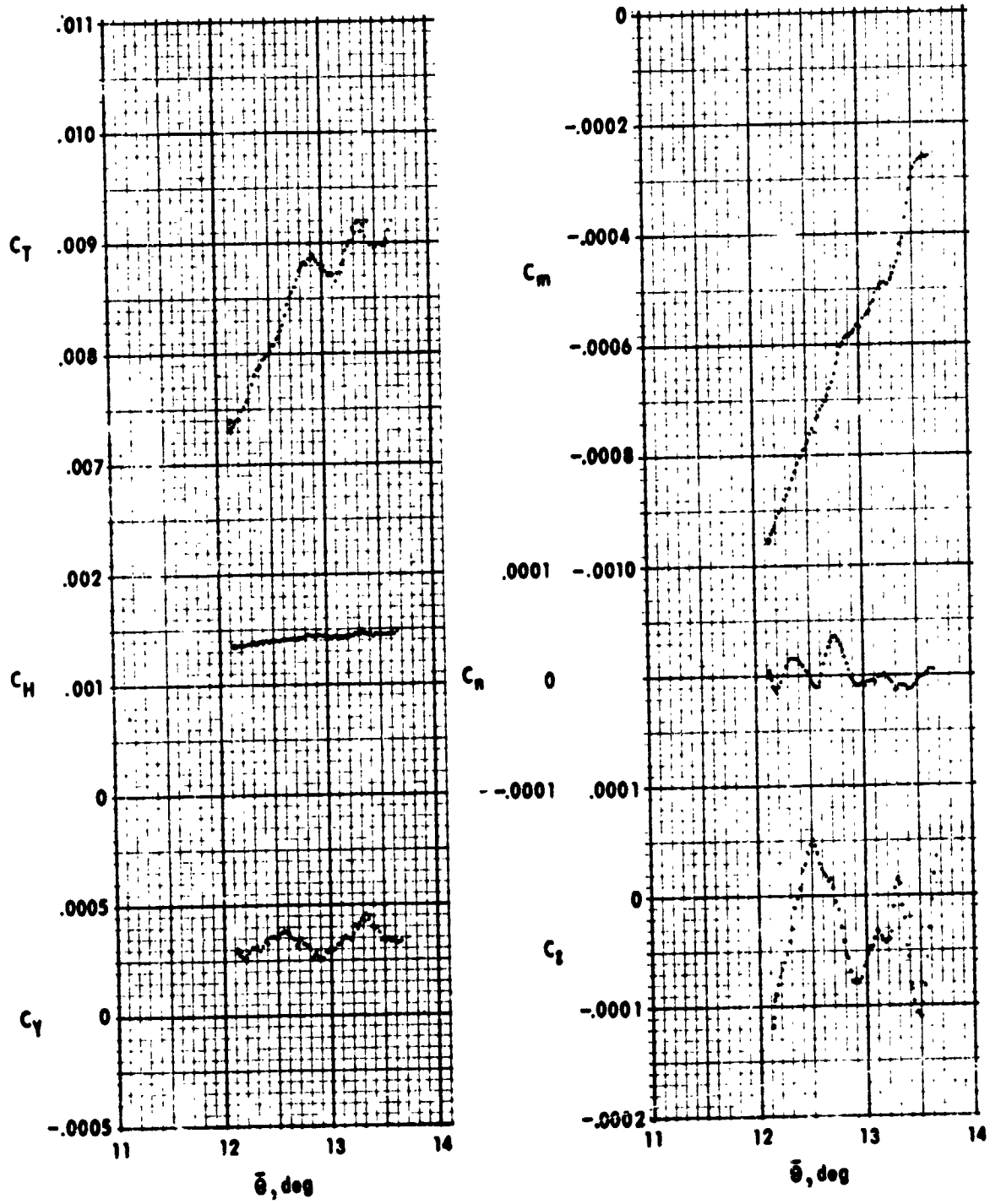

(f) $\mu \approx 0.3$, flight idle thrust, 78

Figure 9. - Continued.

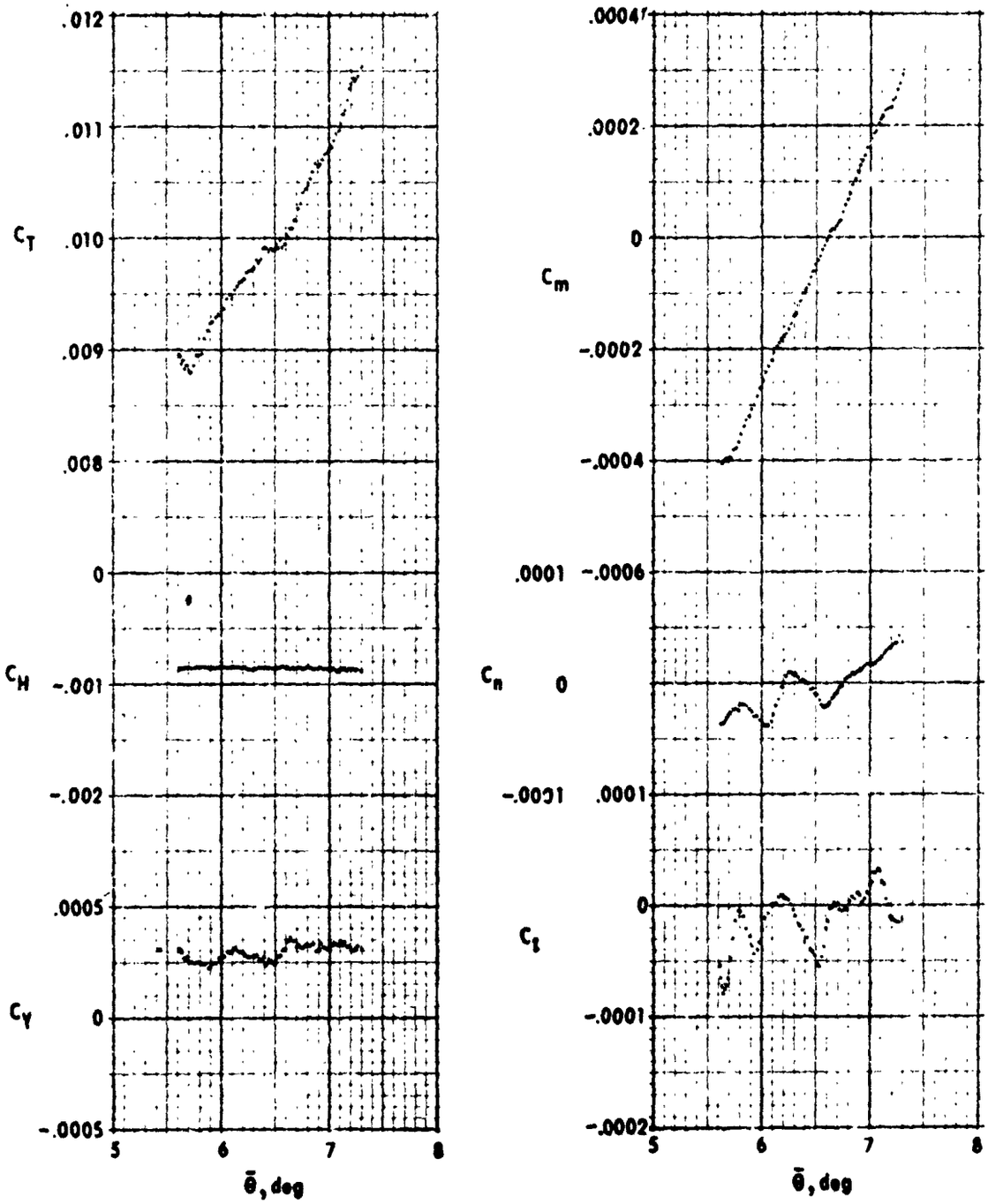

(c) $\mu \approx 0.3$, trim thrust, run 88

Figure 9. - Concluded.

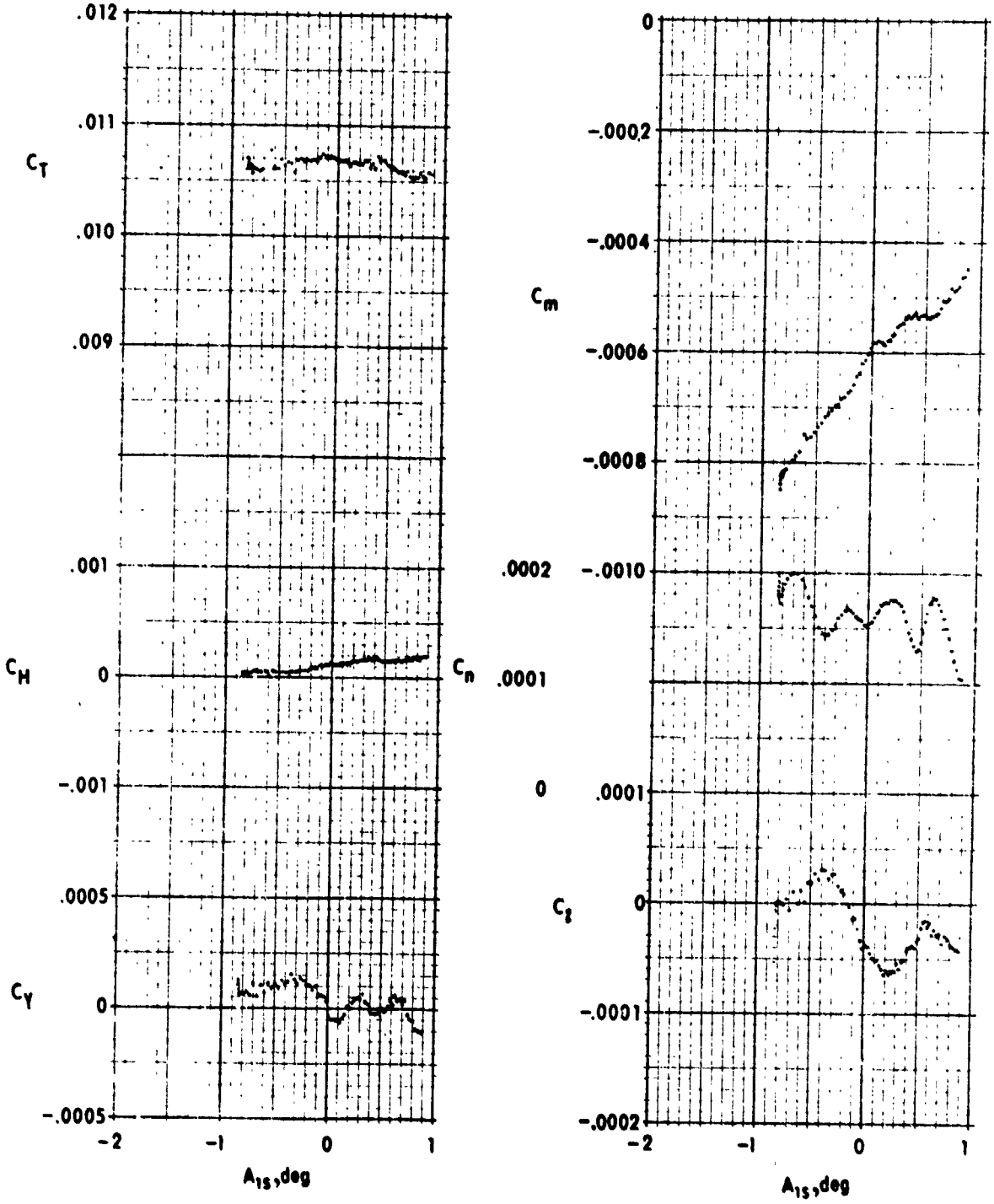

(a) $\mu \approx 0$, no thrust, run 228

Figure 10. - Variation of airframe forces and moments with rotor cyclic pitch.

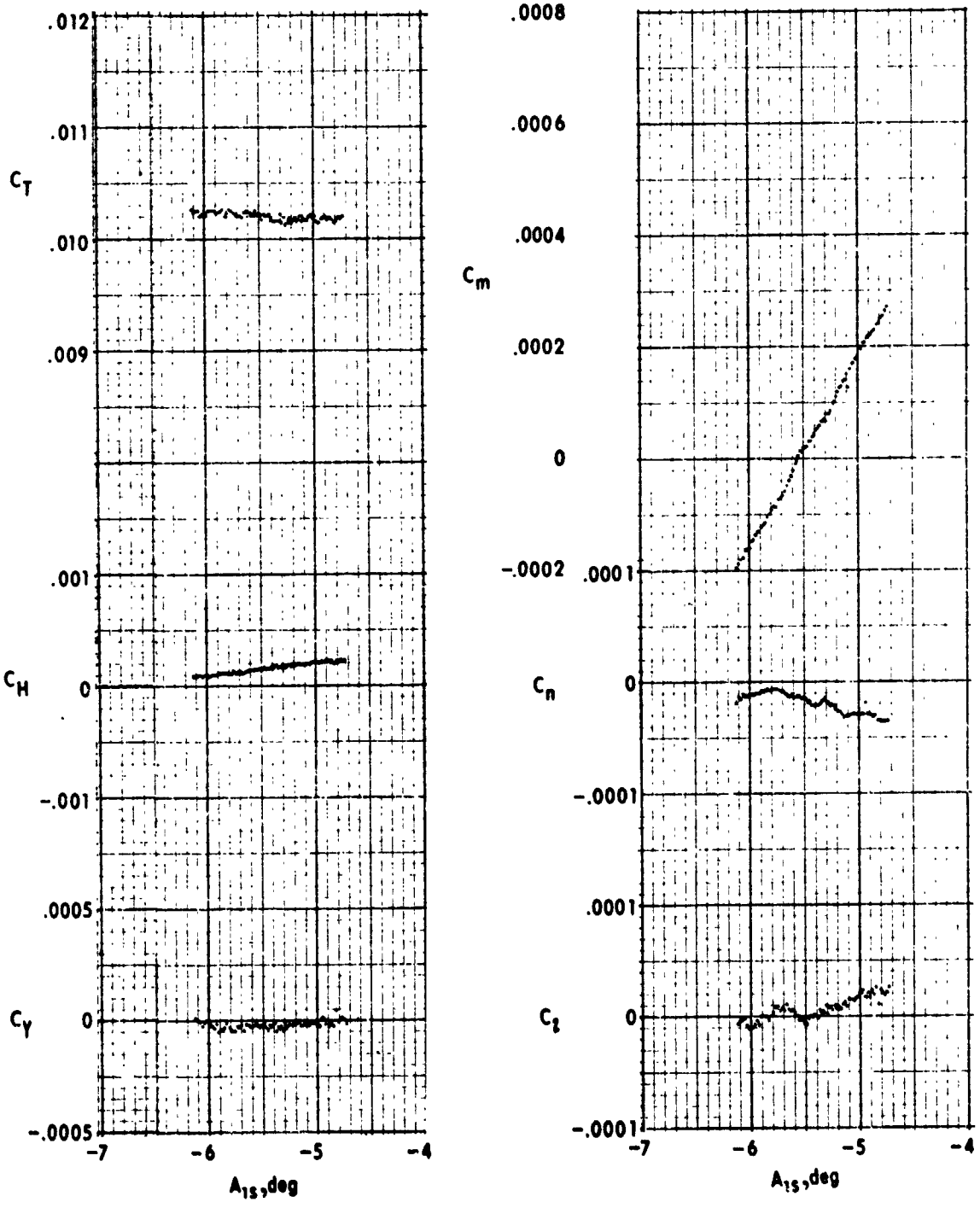

(b) $\mu \approx 0.1$, flight idle thrust, run 61.

Figure 10. - Continued.

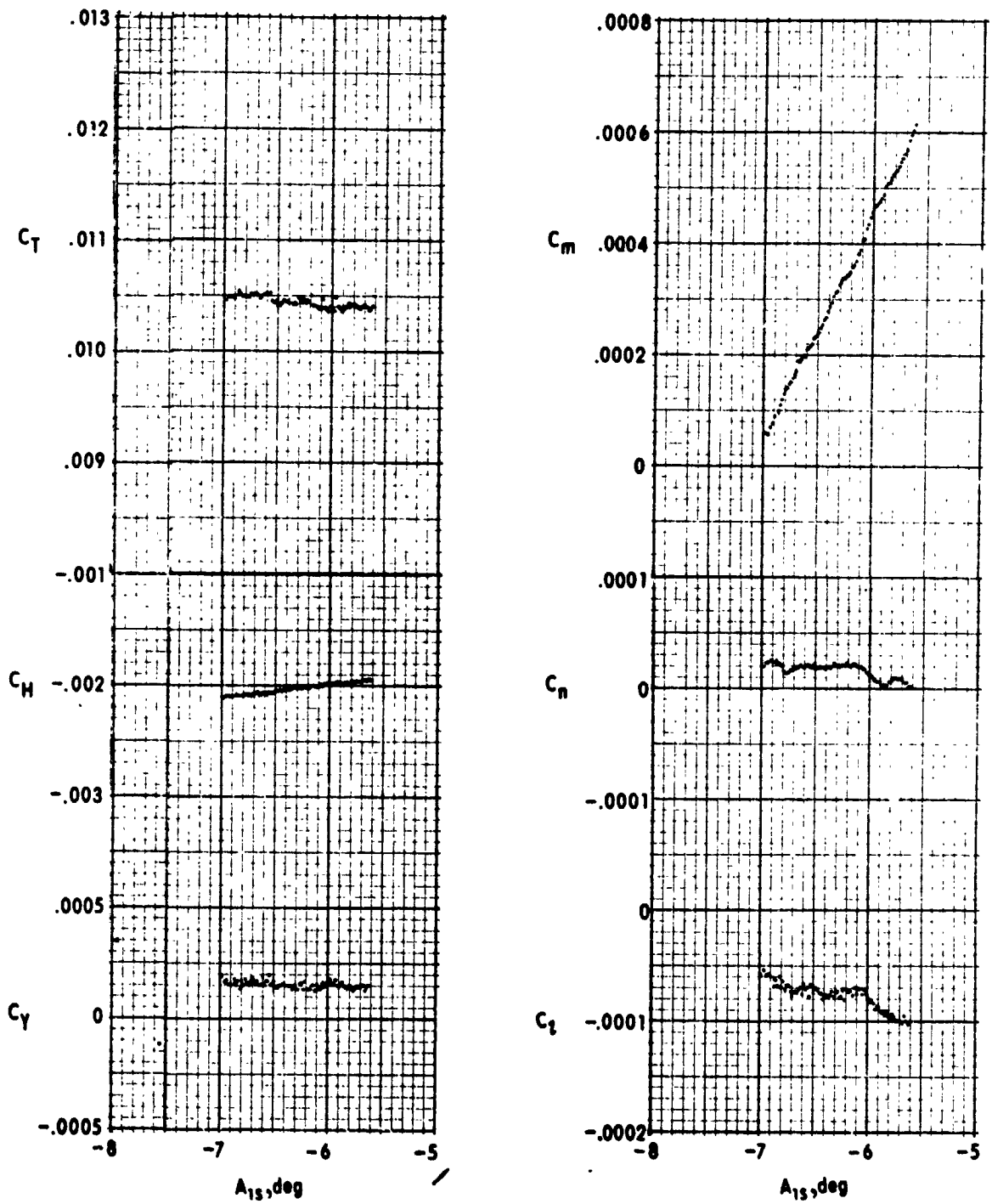

(c) $\mu \approx 0.1$, trim thrust, run 38

Figure 10. - Continued.

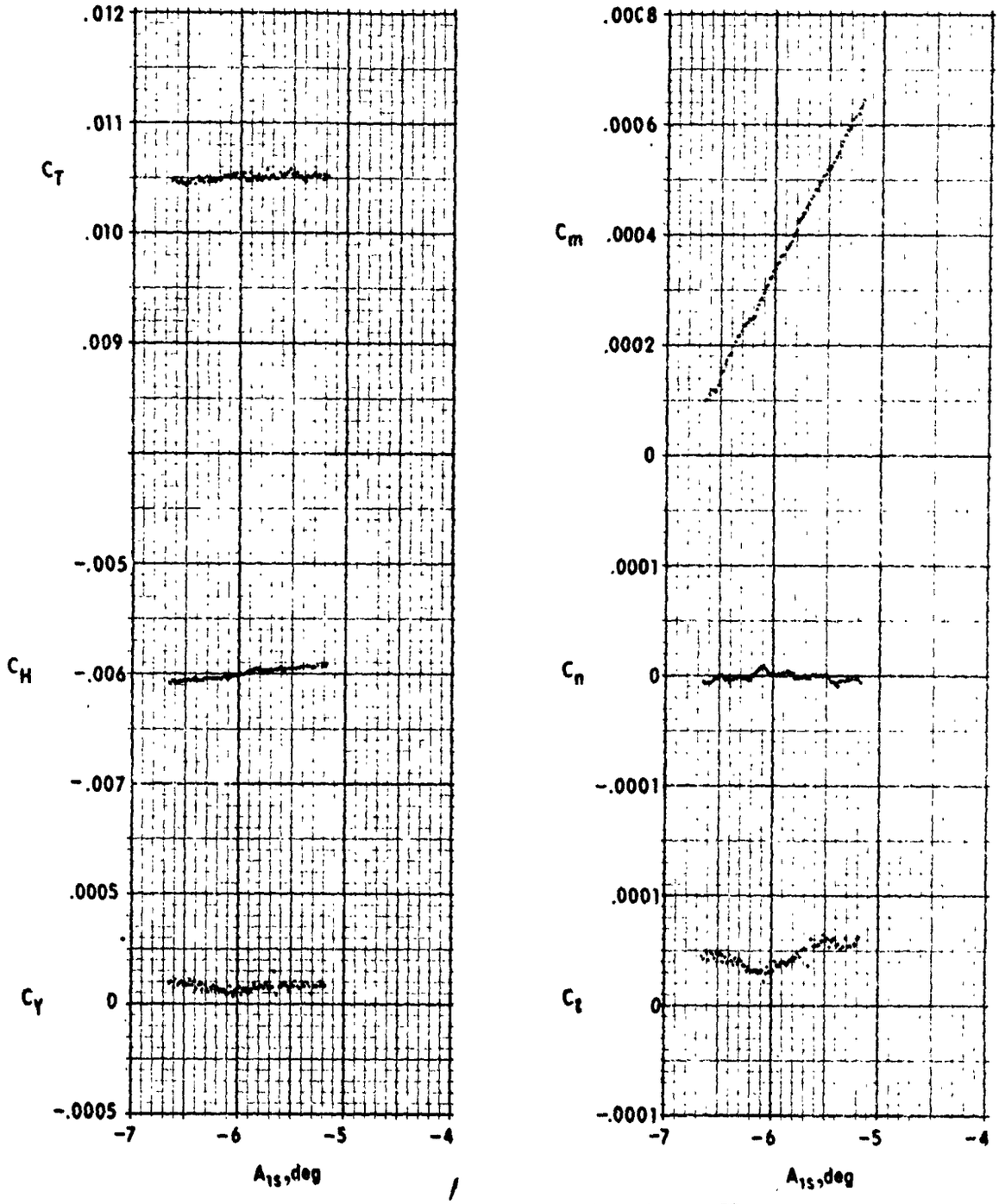

(d) $\mu \approx 0.1$, maximum thrust, run 73

Figure 10. - Continued.

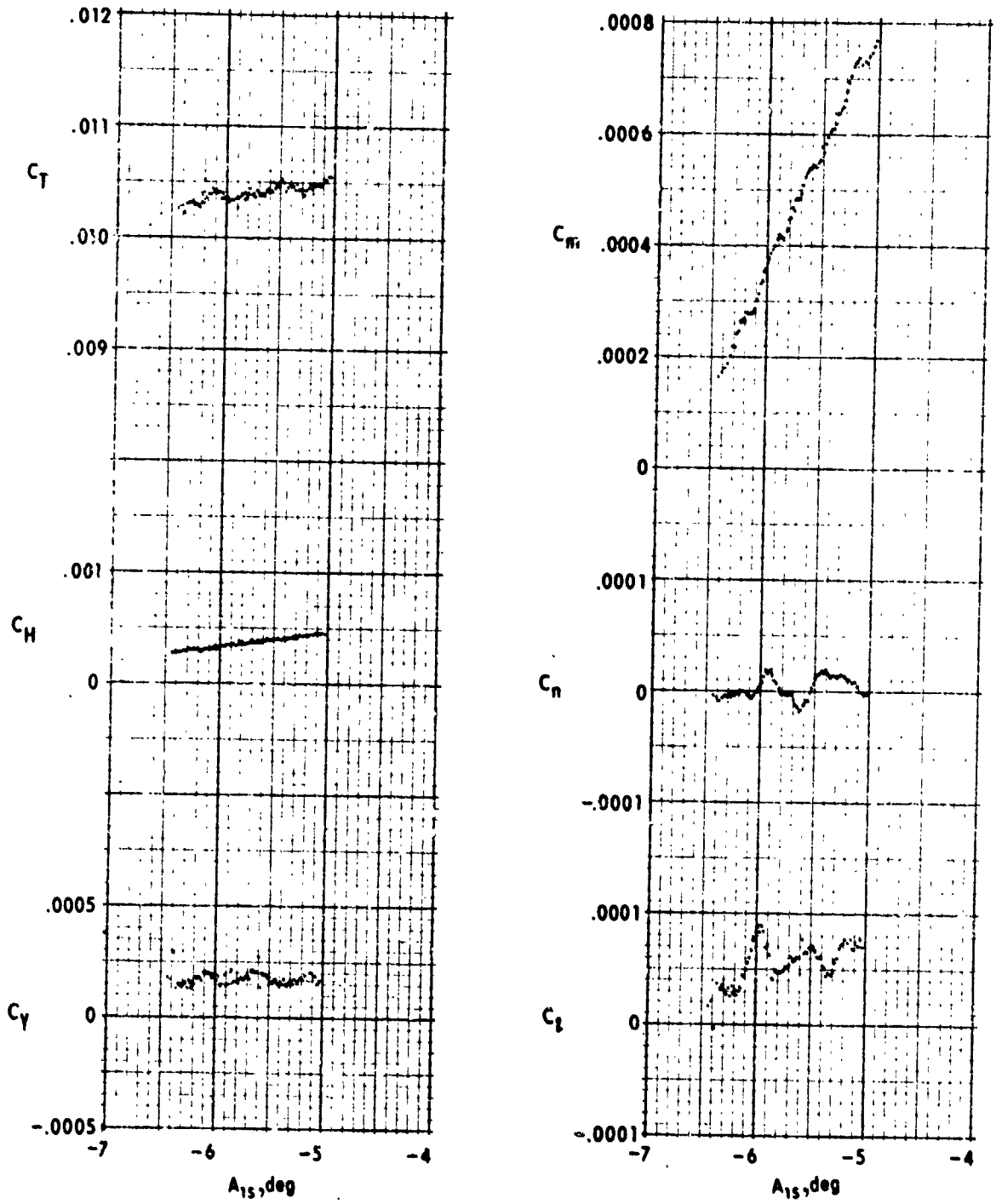

(e) $\mu \approx 0.2$, trim thrust, run 51

Figure 10. - Continued.

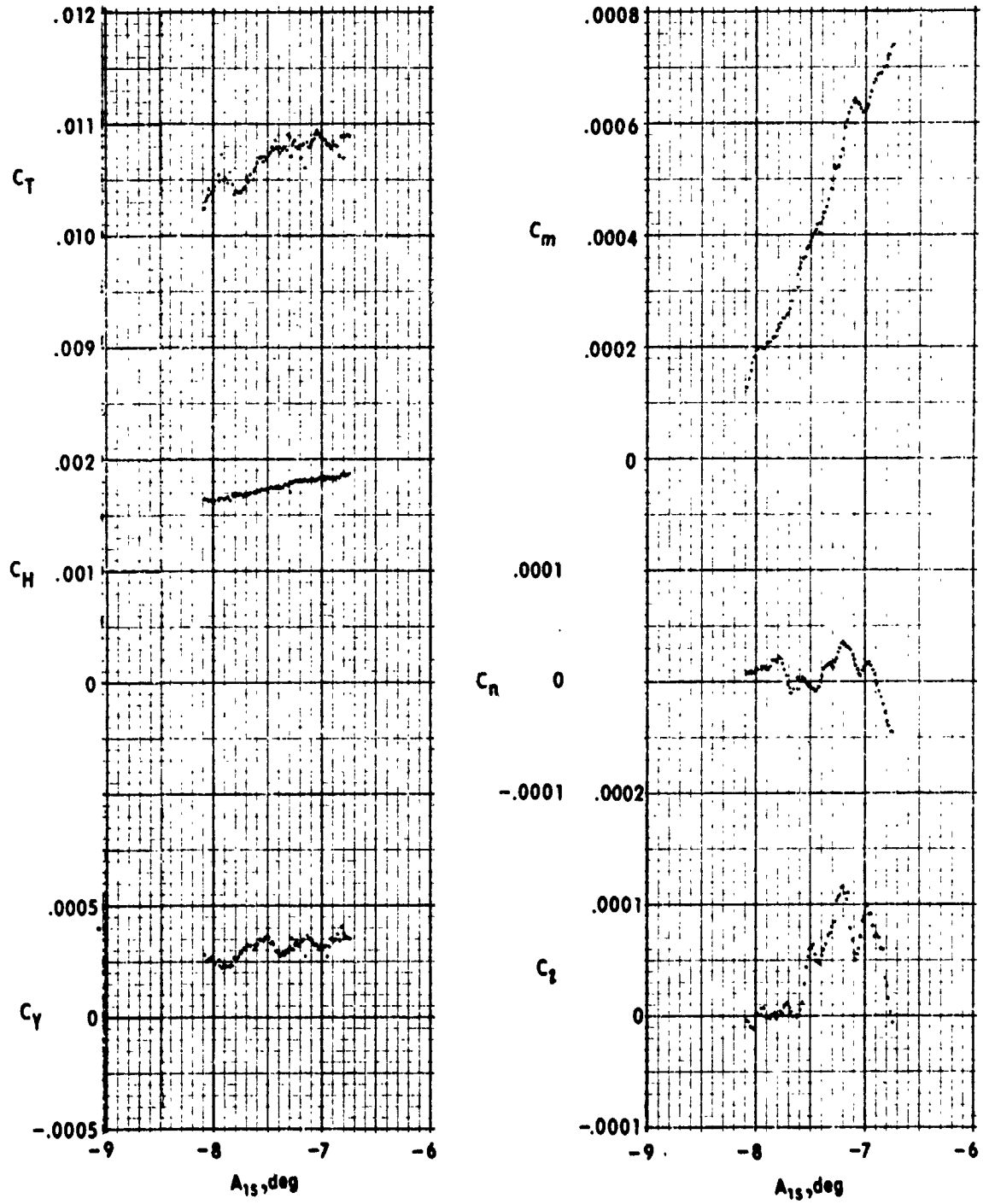

(f) $\mu \approx 0.3$, flight idle thrust, run 76

Figure 10. - Continued.

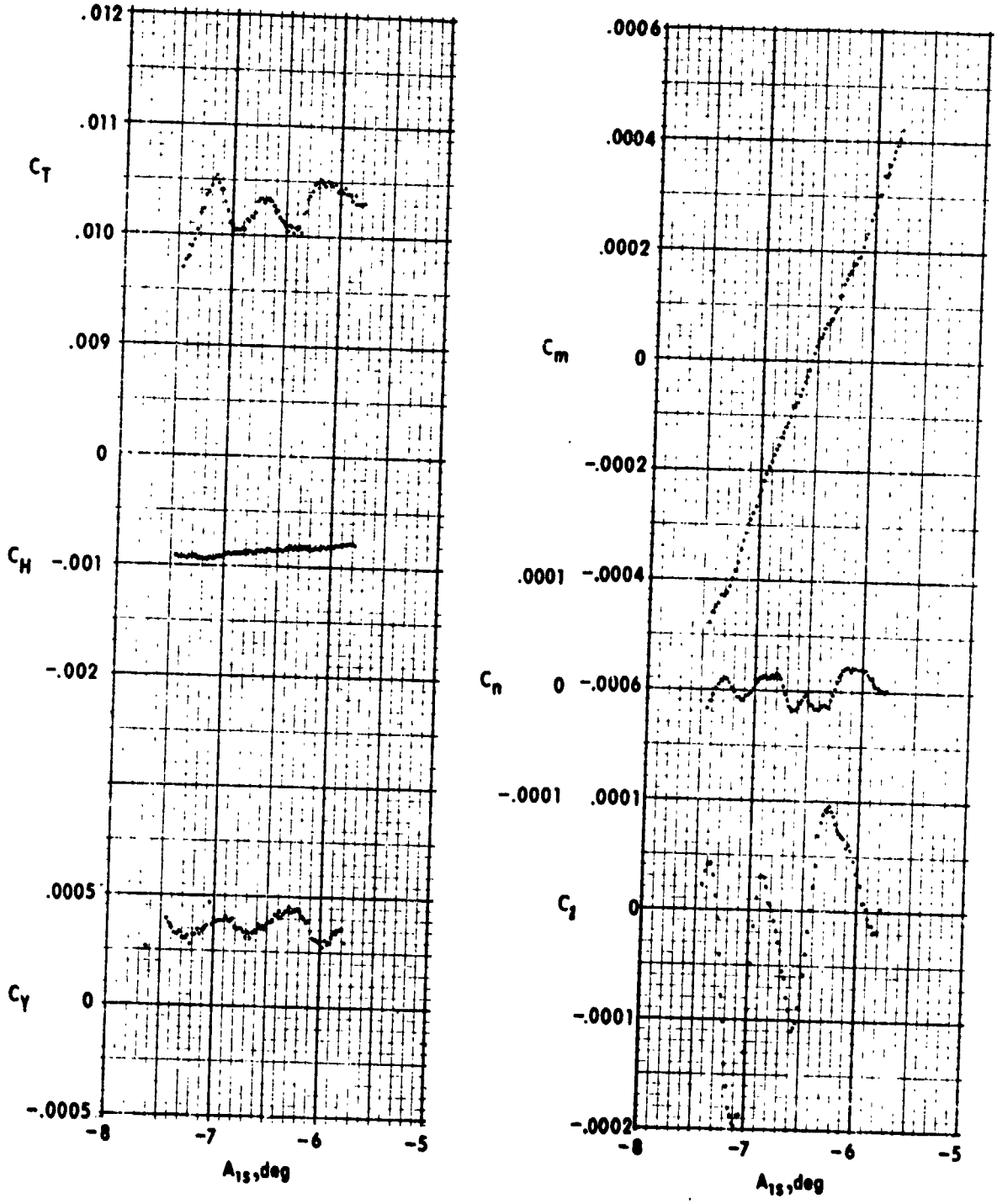

(g) $\mu \approx 0.3$, trim thrust, run 86

Figure 10. - Concluded.

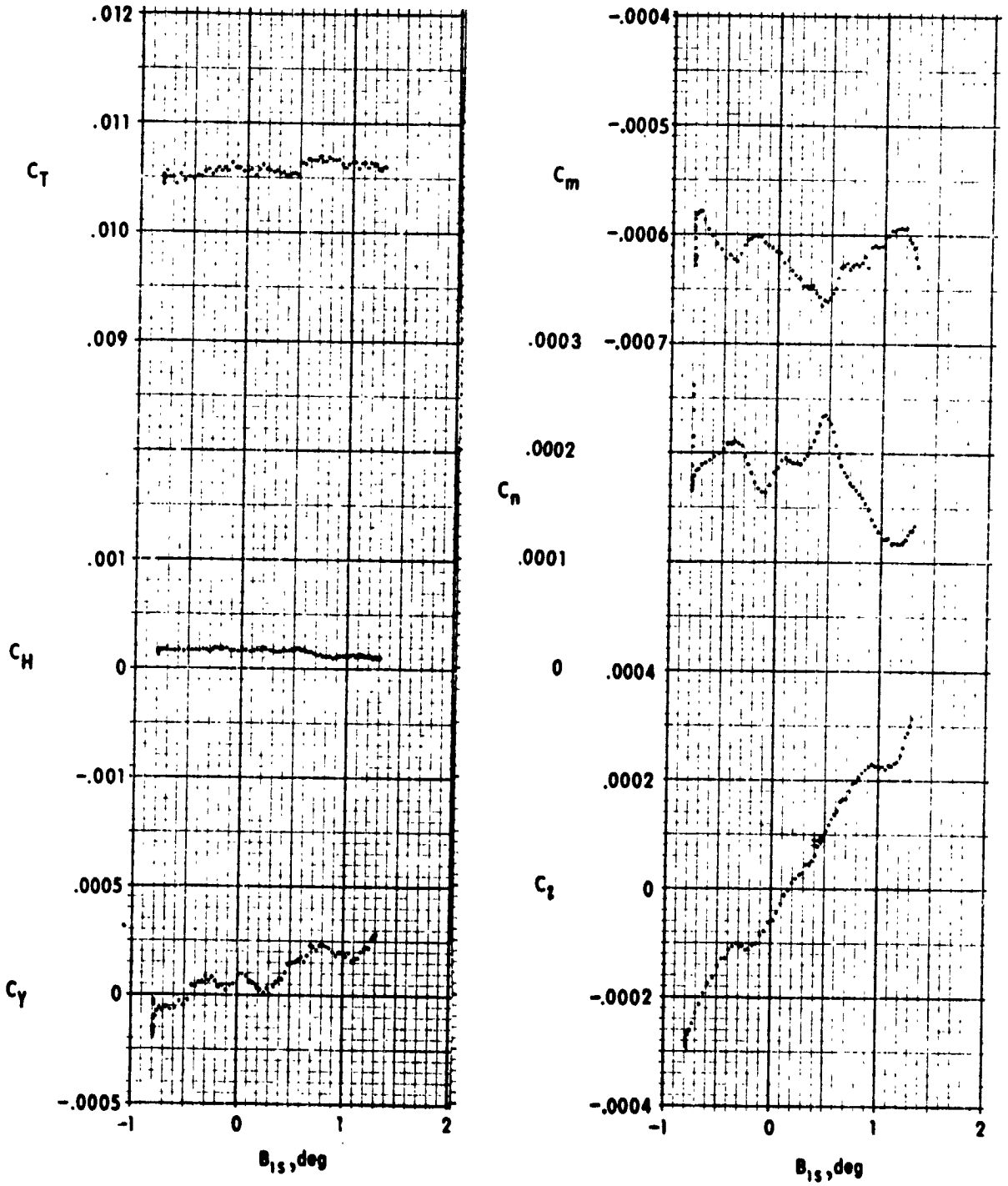

(a) $\mu \approx 0$, no thrust, run 229

Figure 11. - Variation of airframe forces and moments with rotor lateral cyclic pitch.

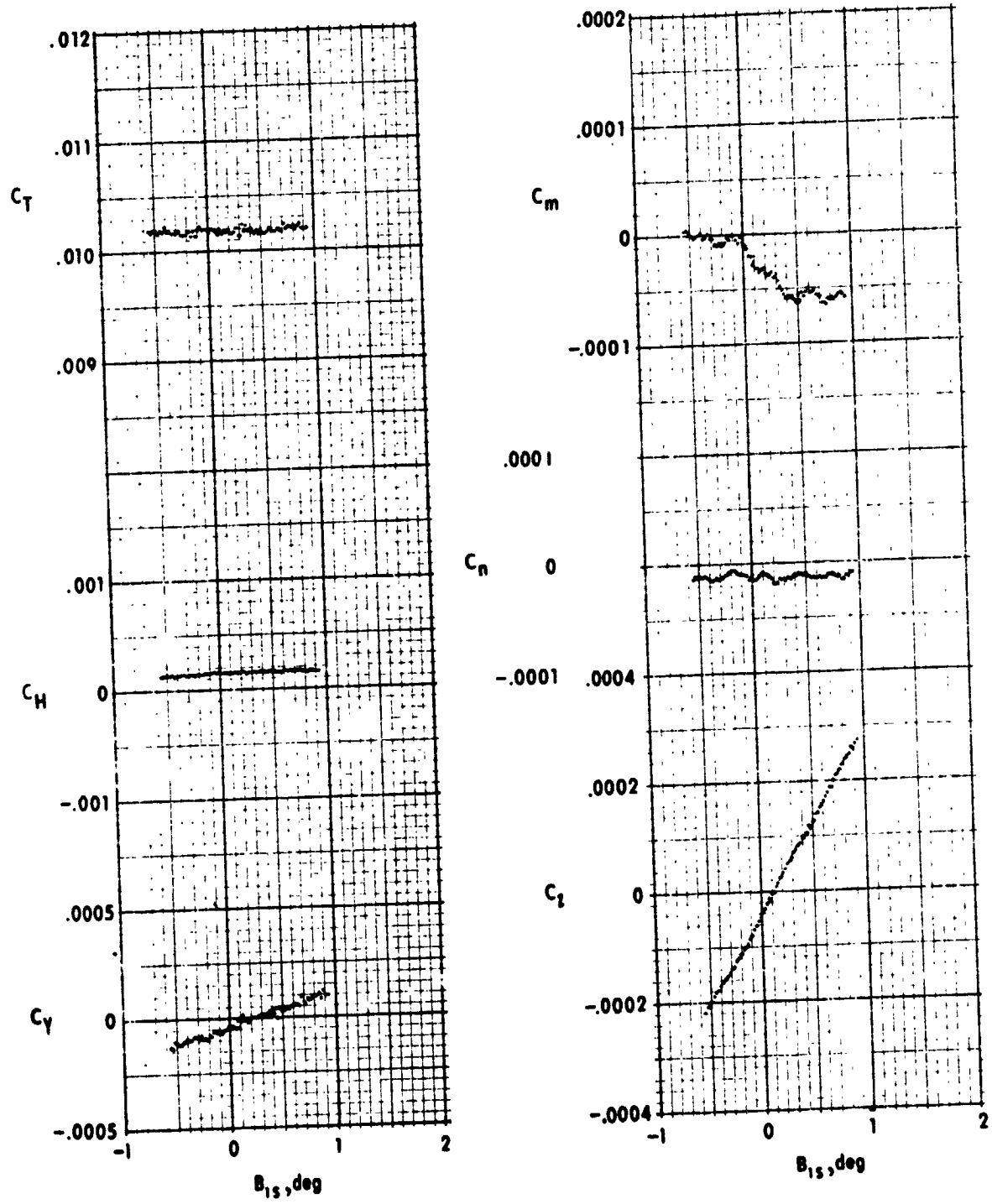

(b) $\mu \approx 0.1$, flight idle thrust, run 62

Figure 11. - Continued.

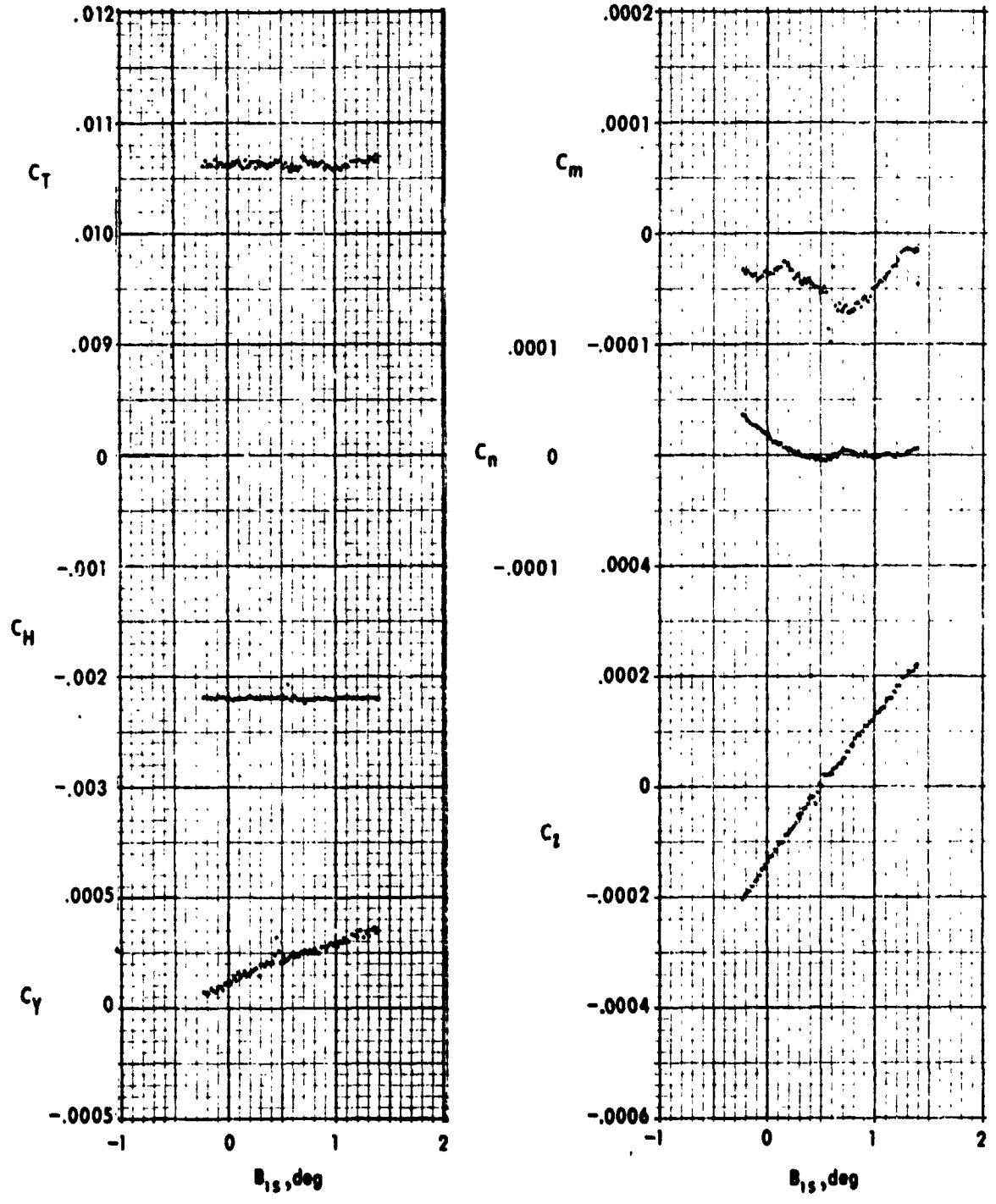

(c) $\mu \approx 0.1$, trim thrust, run 39

Figure 11. - Continued.

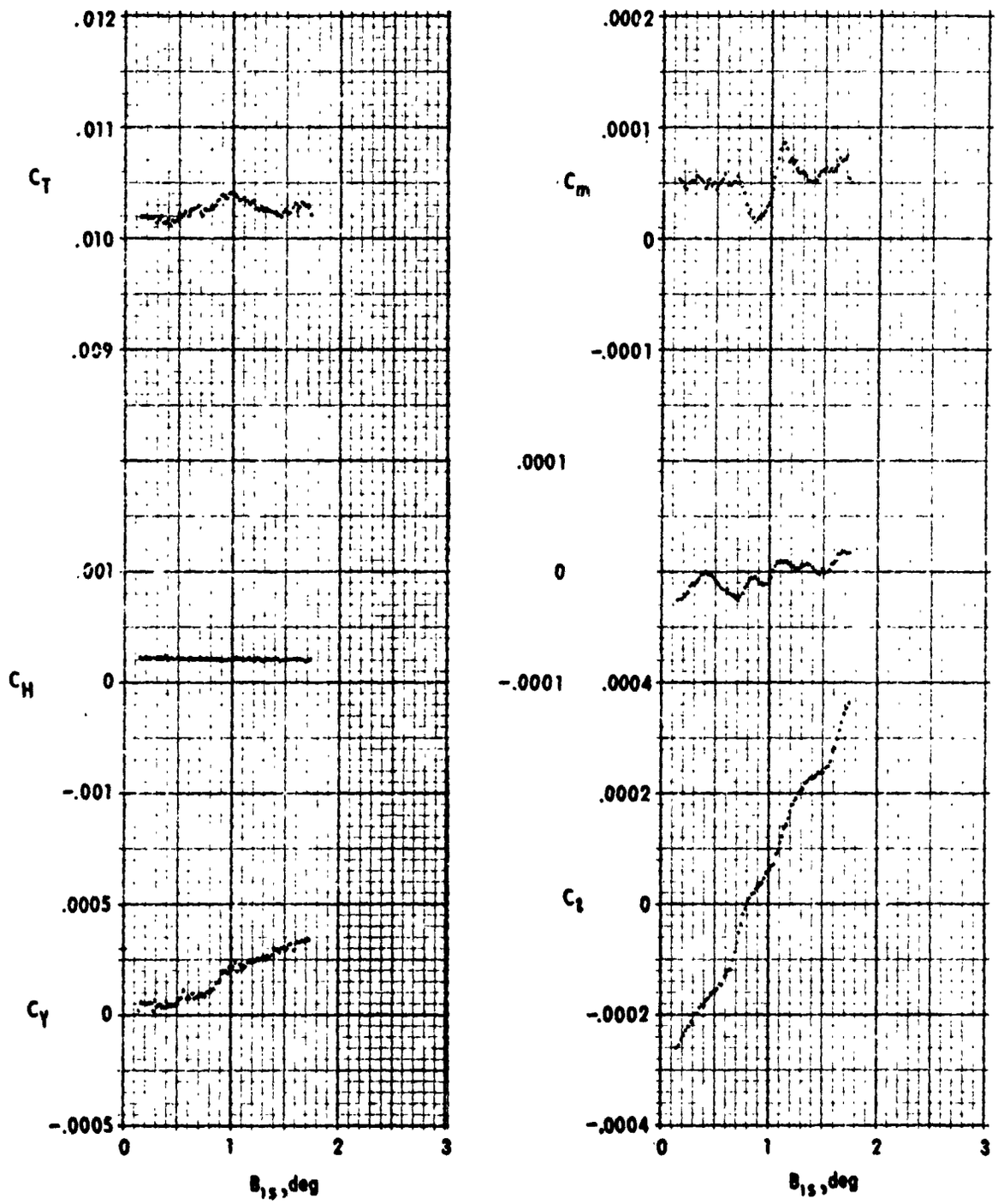

(d) $\mu \approx 0.2$, trim thrust, run 52

Figure 11. - Continued.

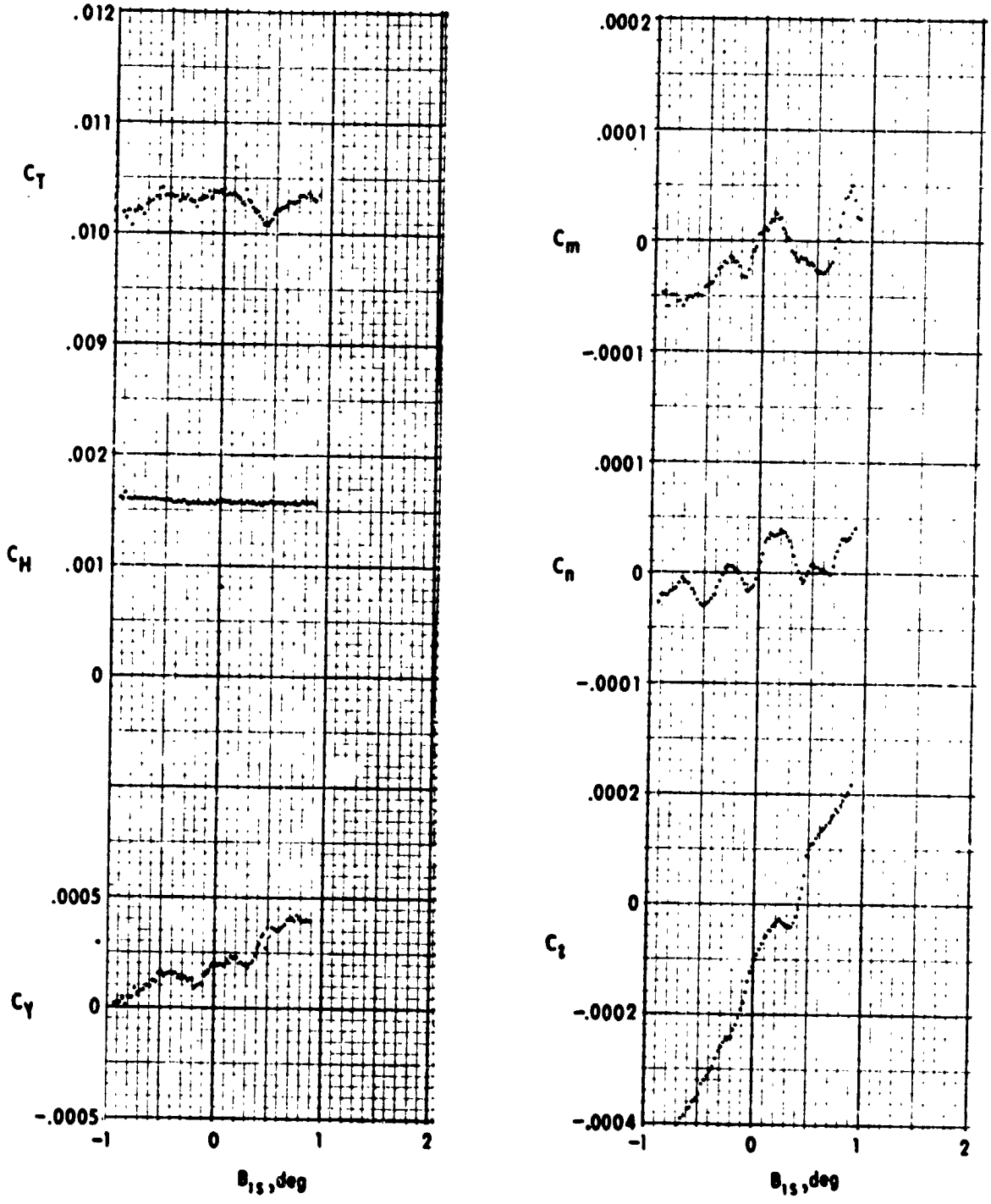

(e) $\mu \approx 0.3$, flight idle thrust, run 77

Figure 11. - Continued.

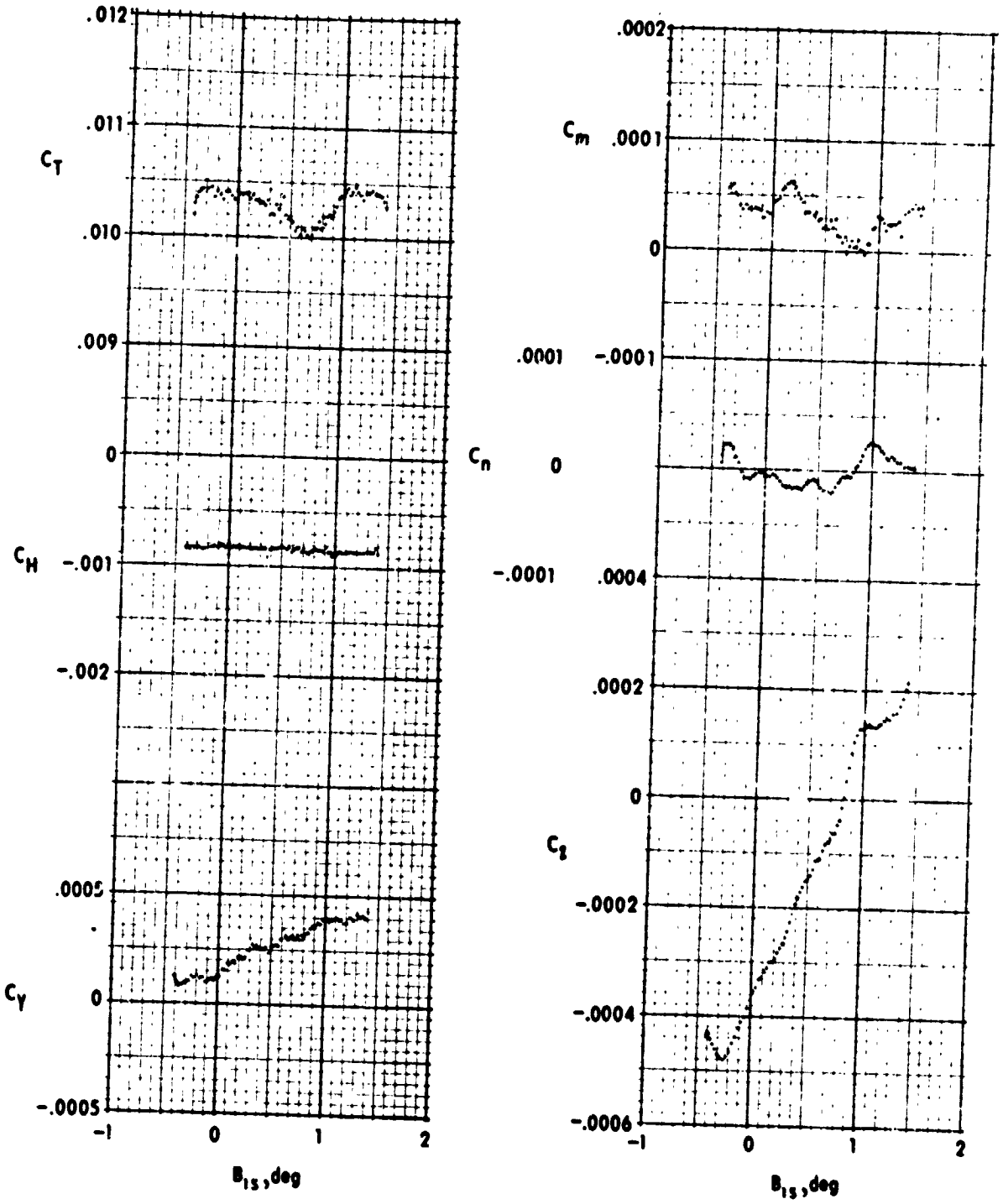

(f) $\mu \approx 0.3$, trim thrust, run 87

Figure 11. - Concluded.

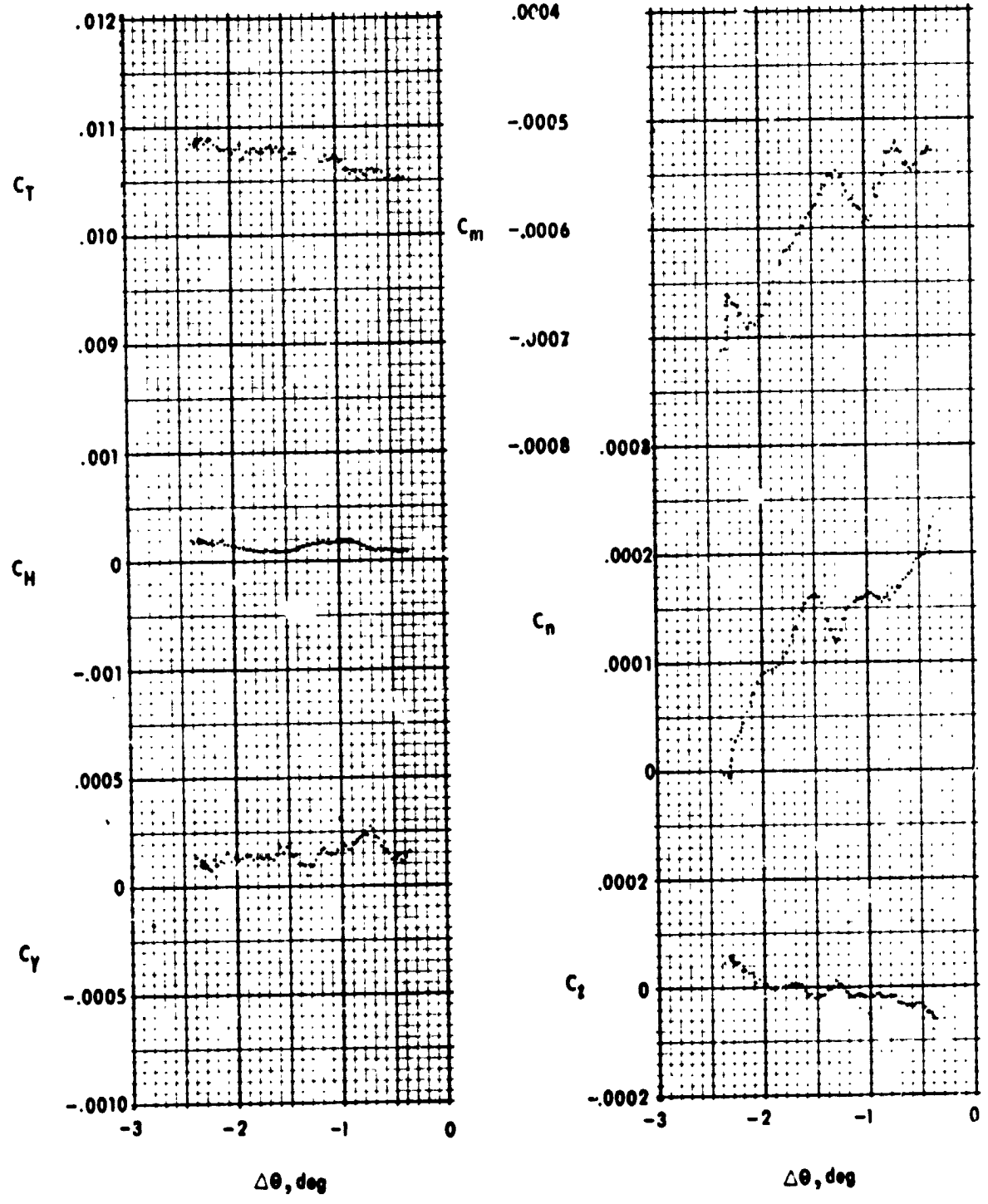

(a) $\mu \approx 0$, no thrust, run 231

Figure 12. - Variation of the airframe forces and moments with rotor differential collective pitch.

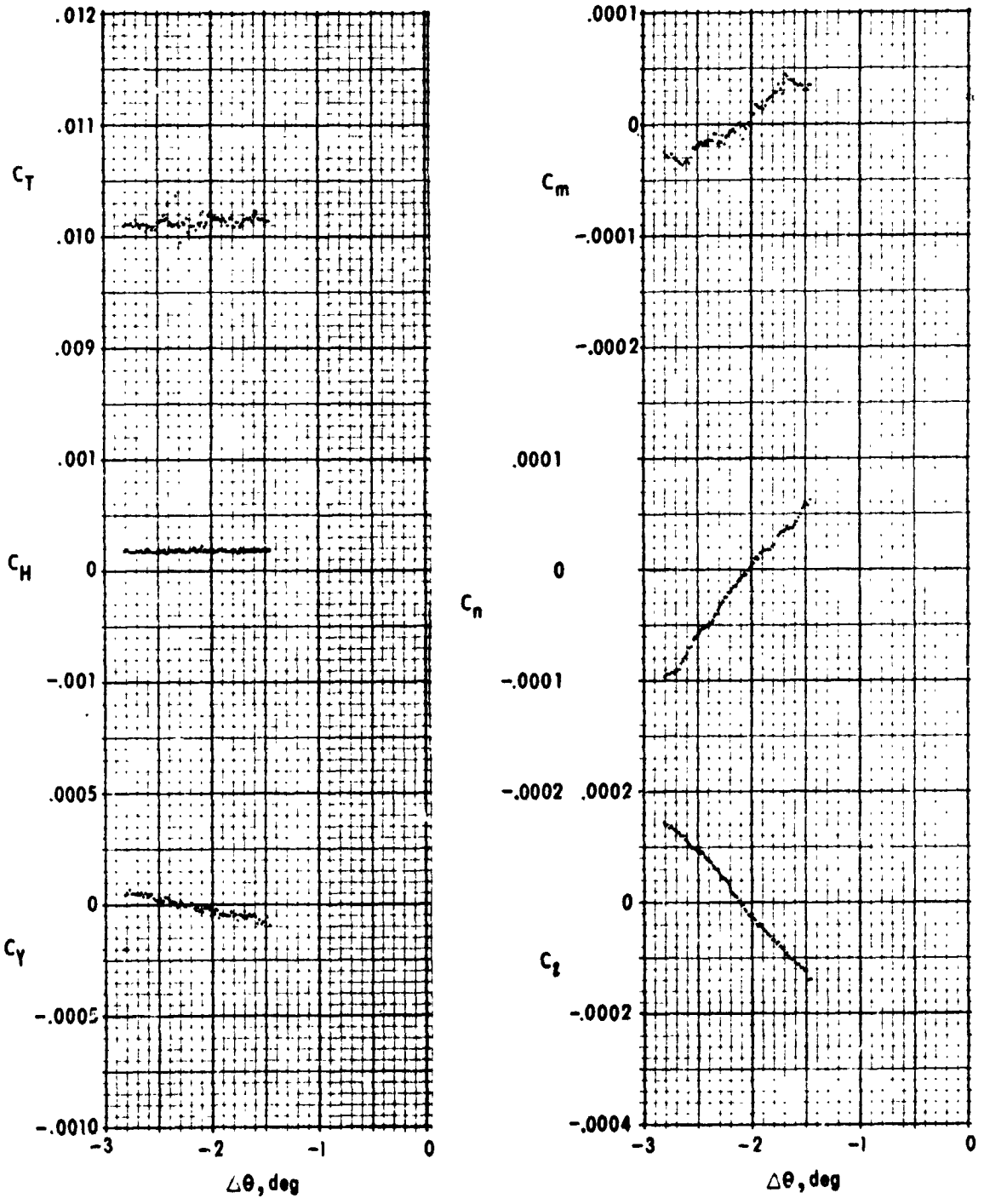

(b) $\mu \simeq 0.1$, flight idle thrust, run 64

Figure 12. - Continued.

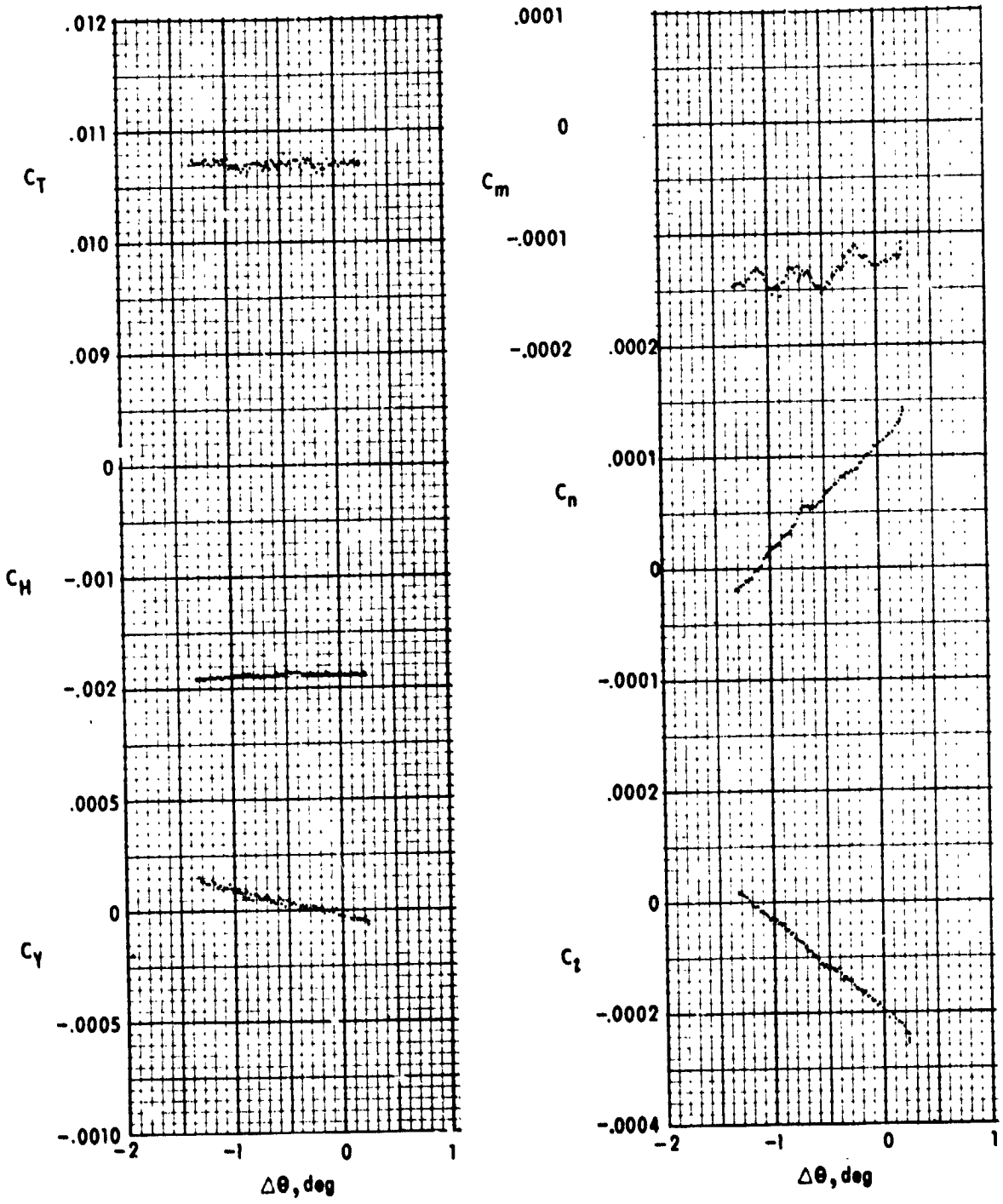

(c) $\mu \simeq 0.1$, trim thrust, run 42

Figure 12. - Continued.

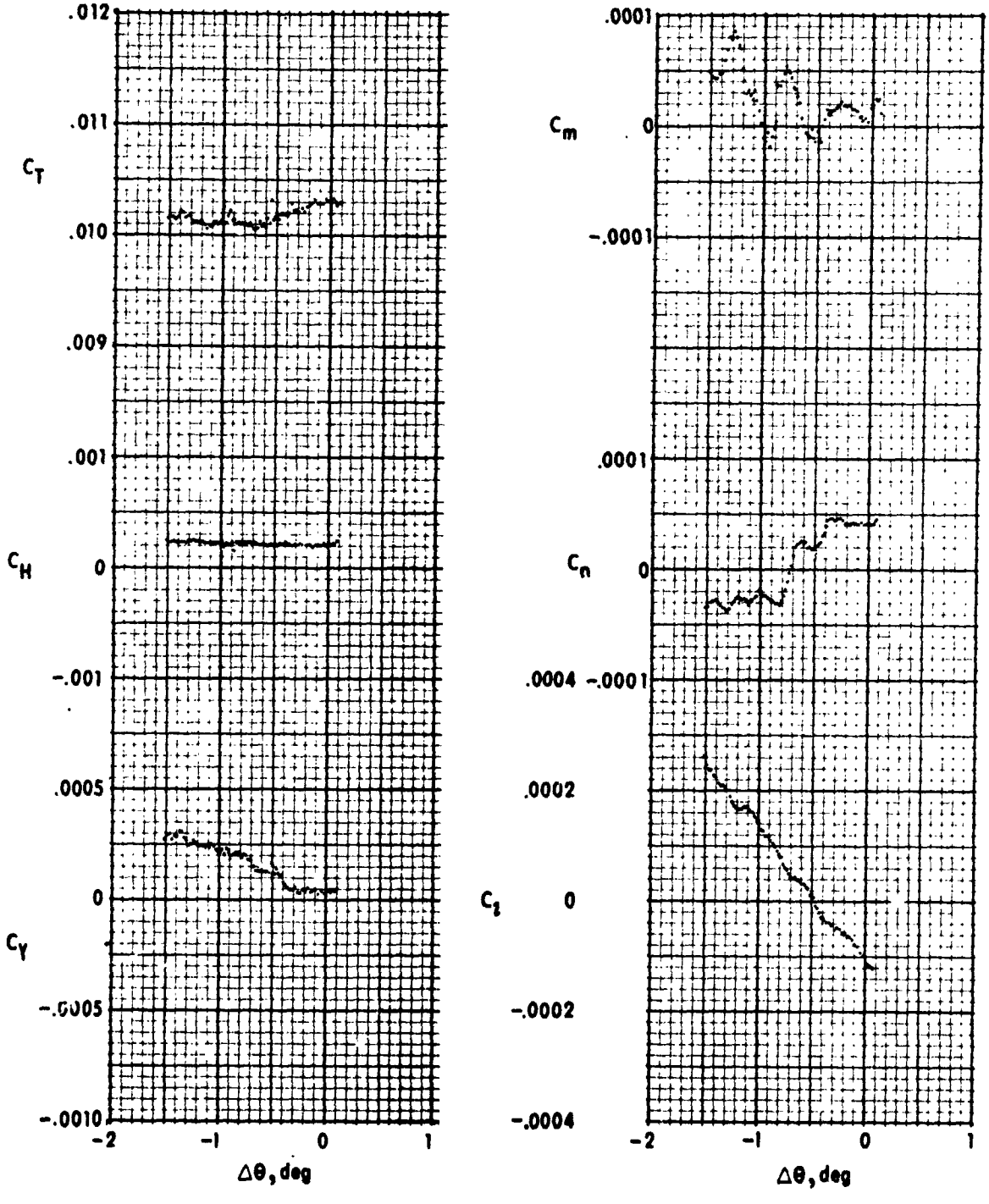

(d) $\mu \simeq 0.2$, trim thrust, run 54

Figure 12. - Concluded.

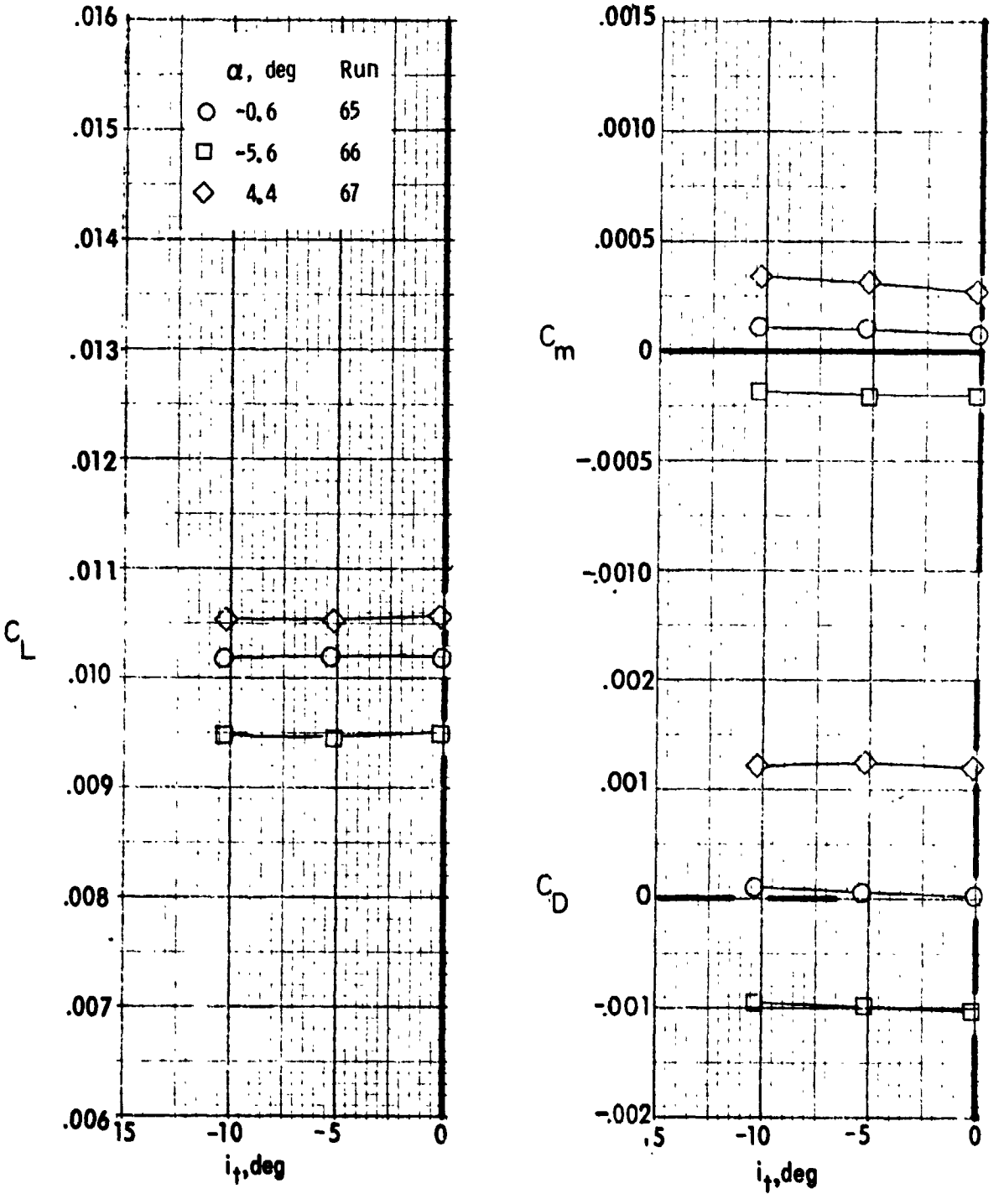

(a) $\mu \approx 0.1$, flight idle thrust

Figure 13. - Variation of airframe longitudinal aerodynamic characteristics with tail incidence

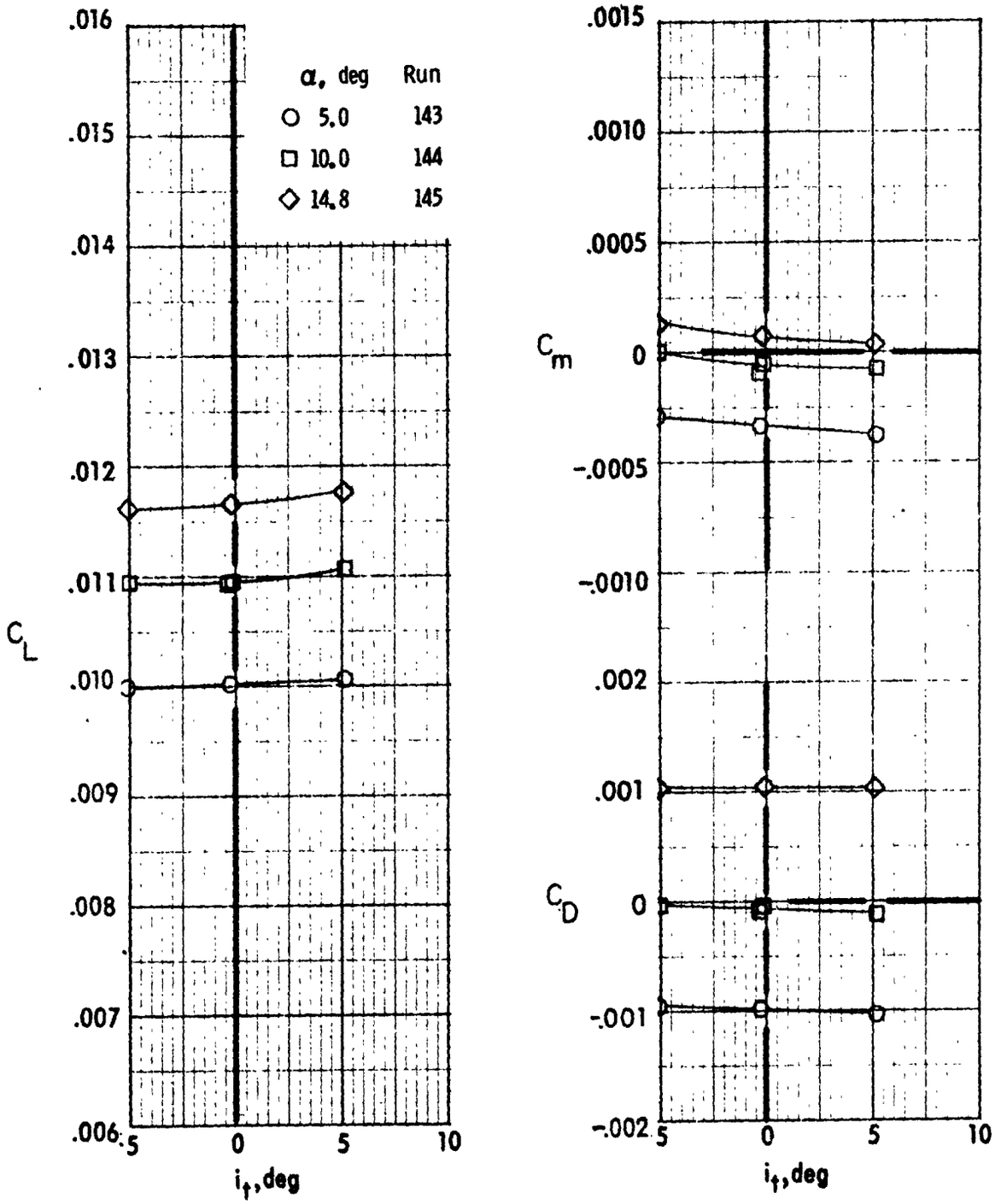

(b) $\mu \approx 0.1$, trim thrust

Figure 13. - Continued.

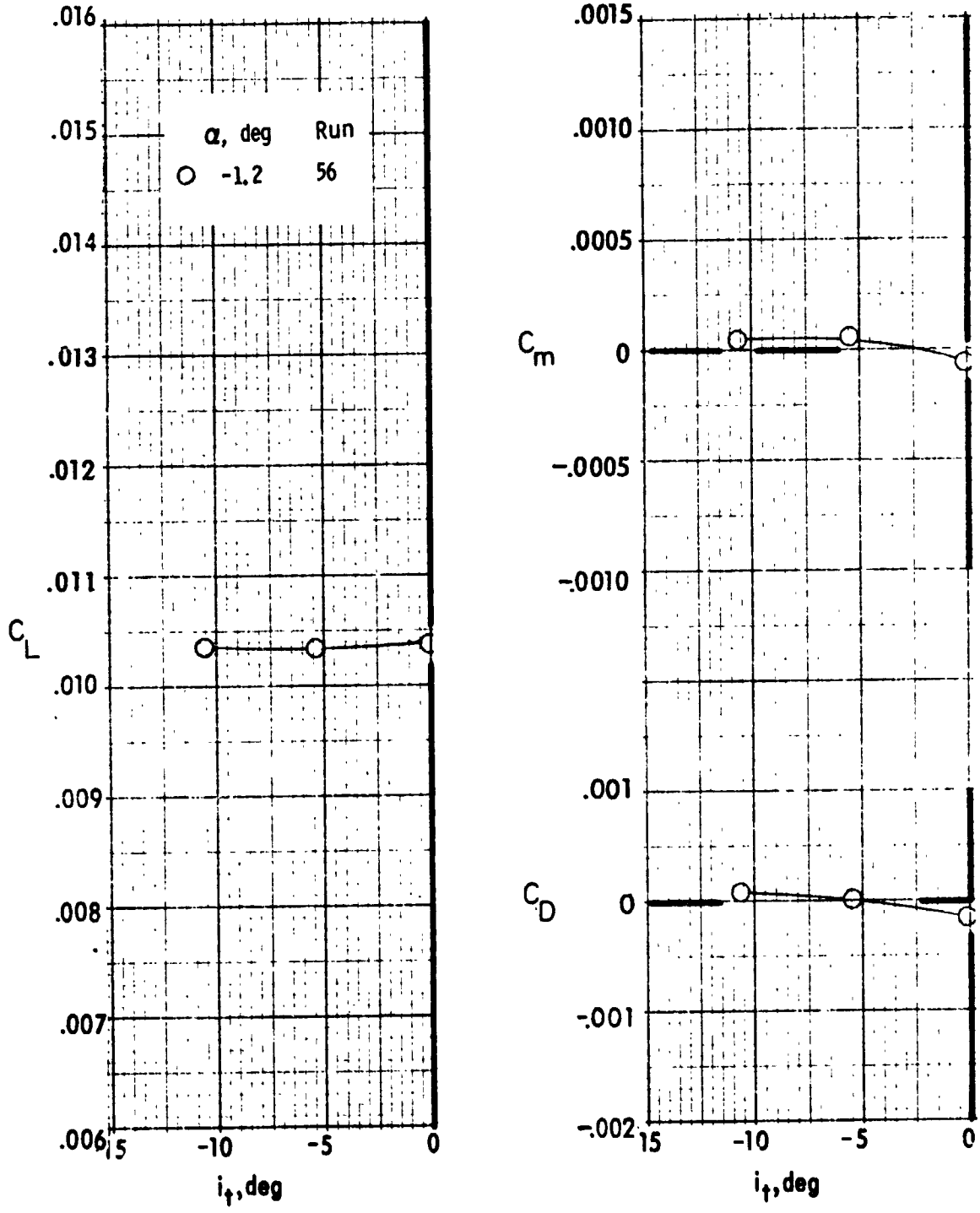

(c) $\mu \approx 0.2$, trim thrust

Figure 13. - Continued.

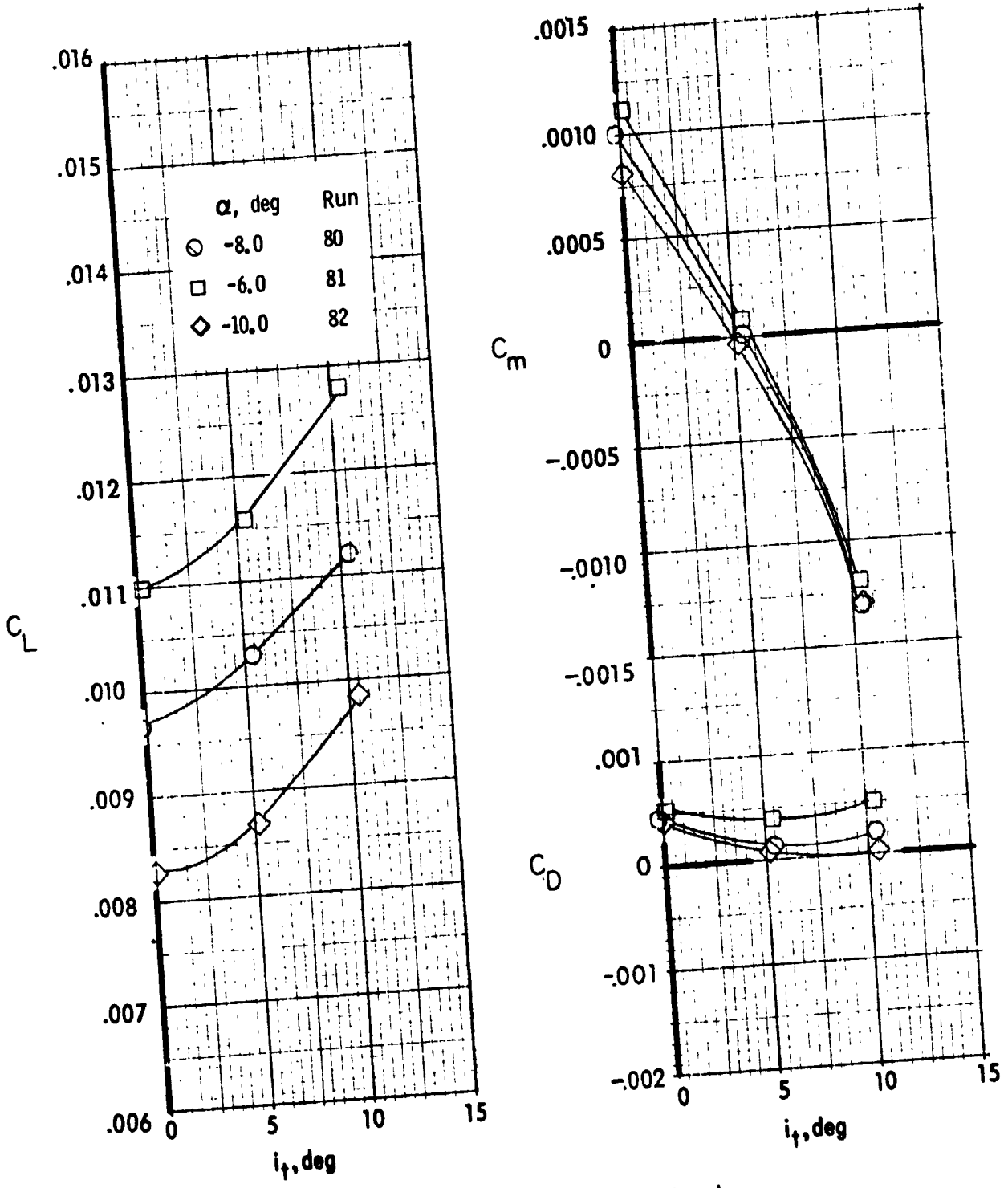

(d) $\mu \approx 0.3$, flight idle thrust

Figure 13. - Continued.

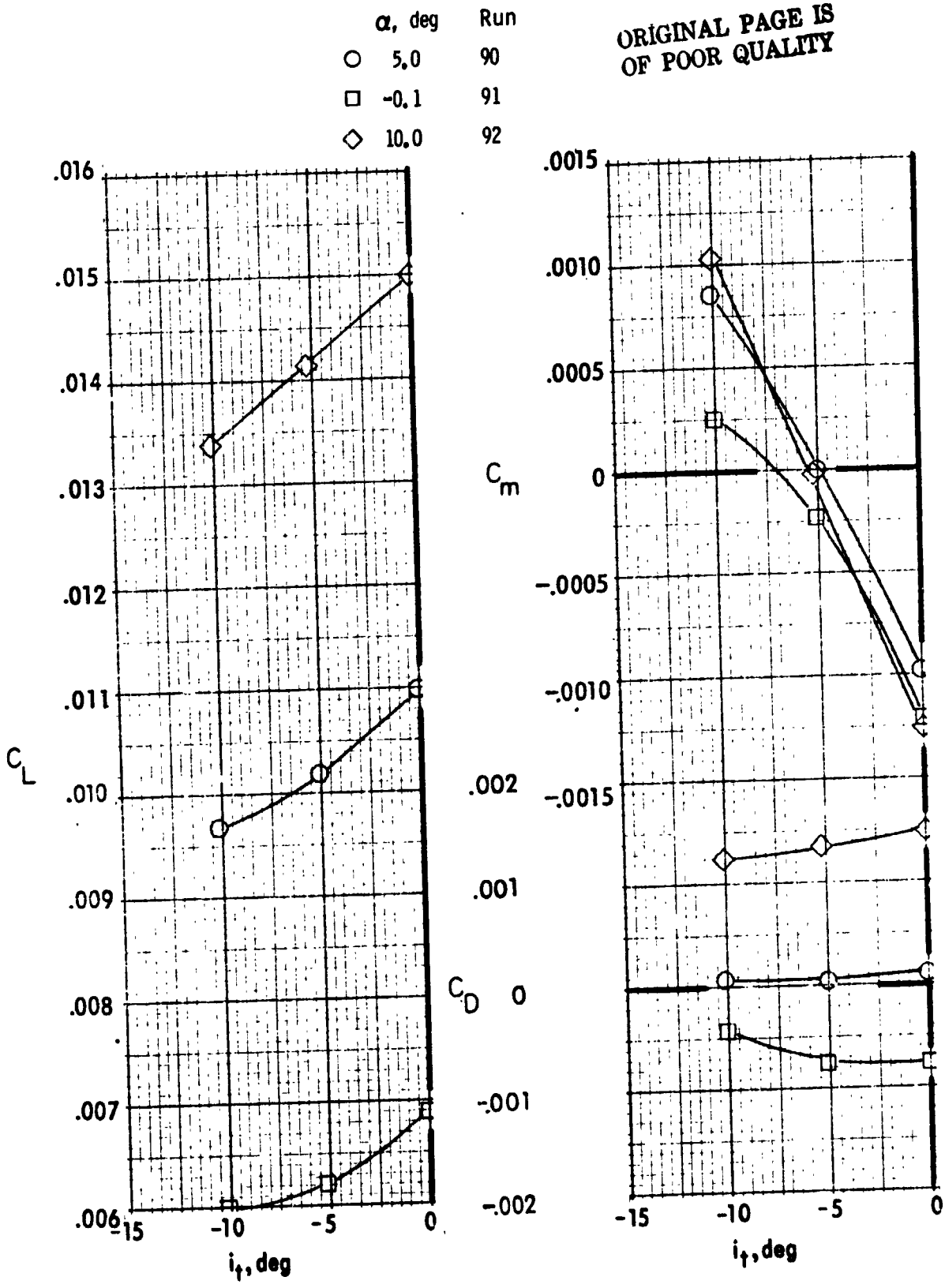

(e) $\mu \approx 0.3$, trim thrust

Figure 13. - Concluded.

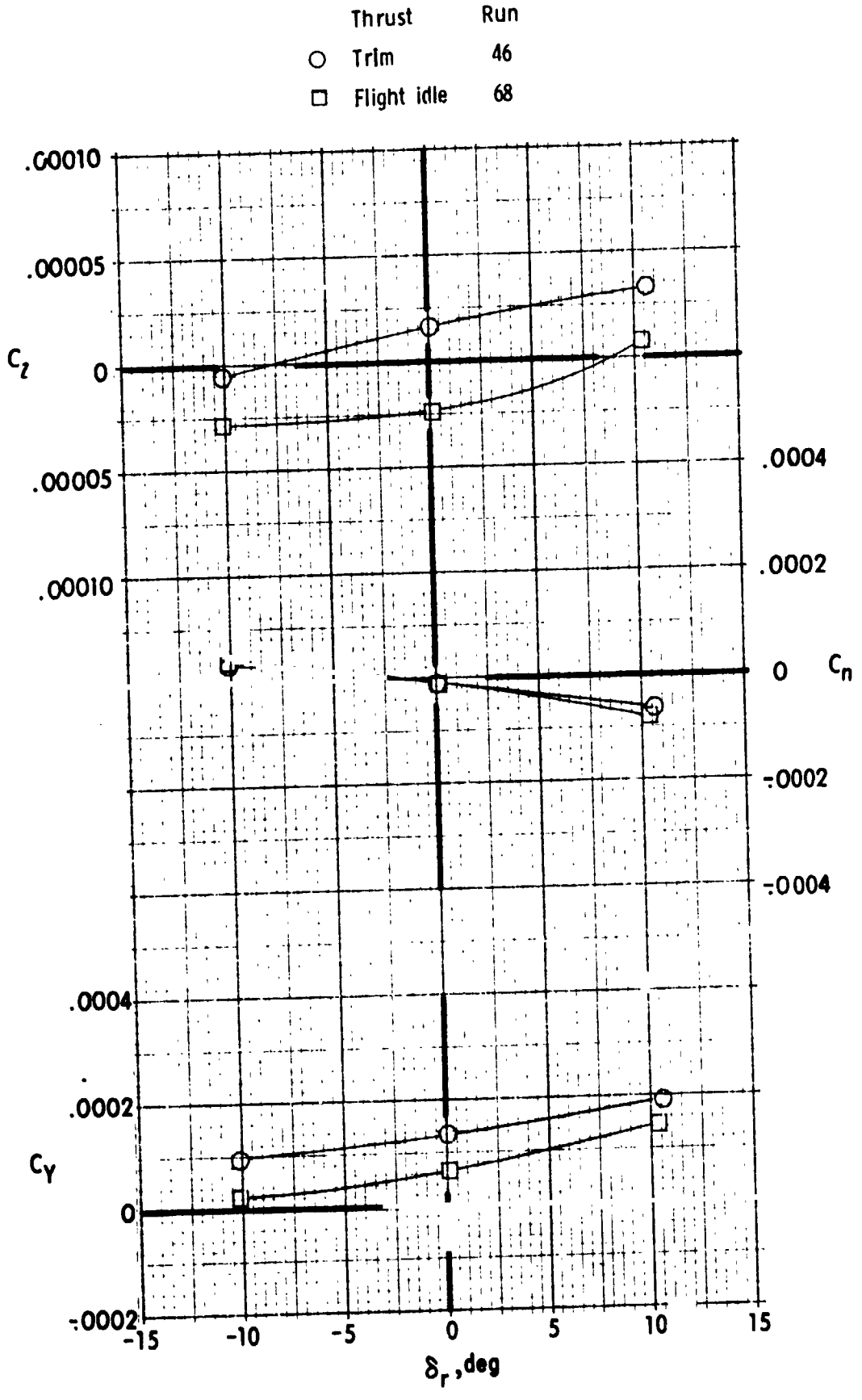

(a) $\mu \approx 0.1$

Figure 14. - Variation of airframe lateral aerodynamic characteristics with rudder deflection.

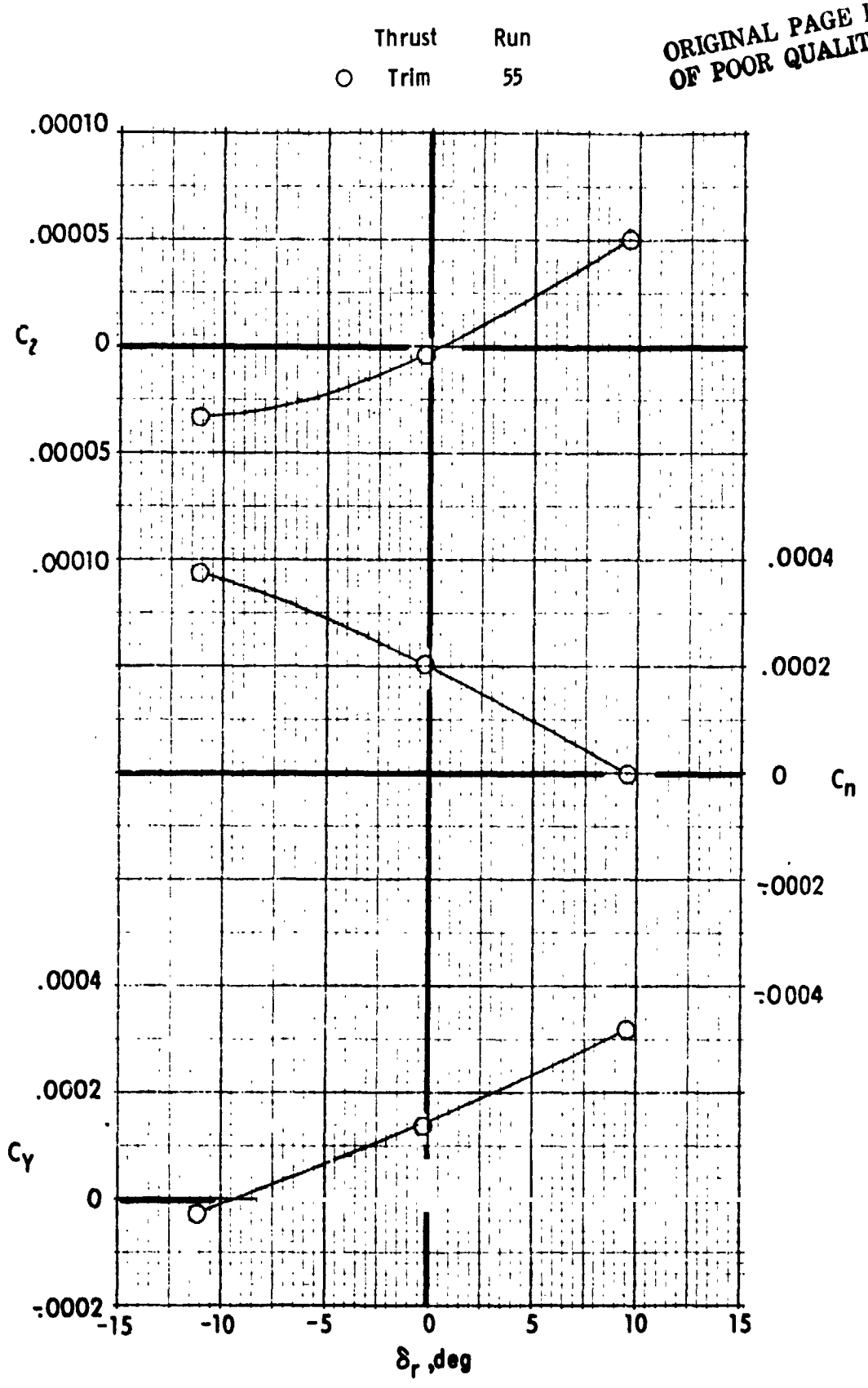

(b) $\mu \approx 0.2$

Figure 14. - Continued.

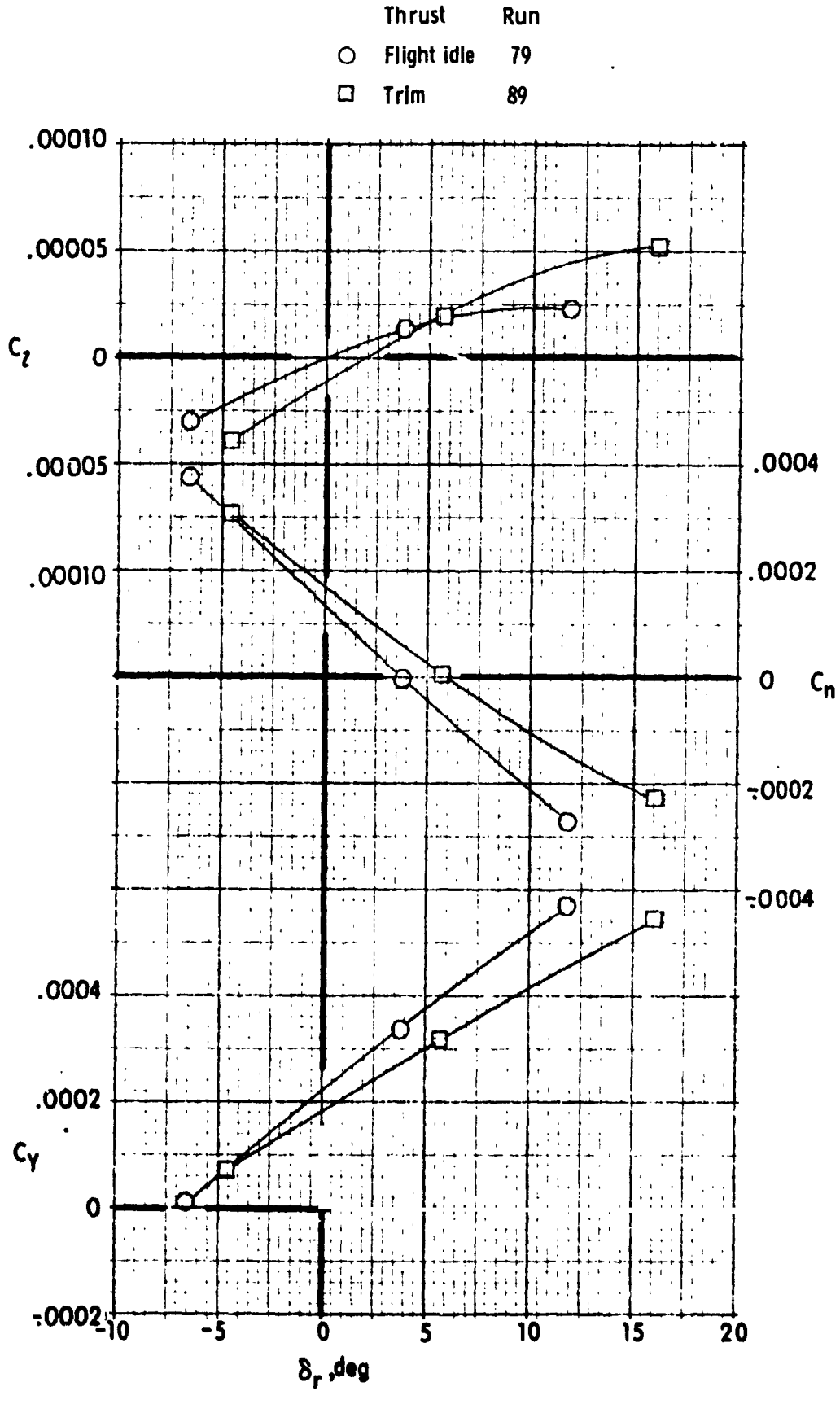

(c) $\mu \approx 0.3$

Figure 14. - Concluded.

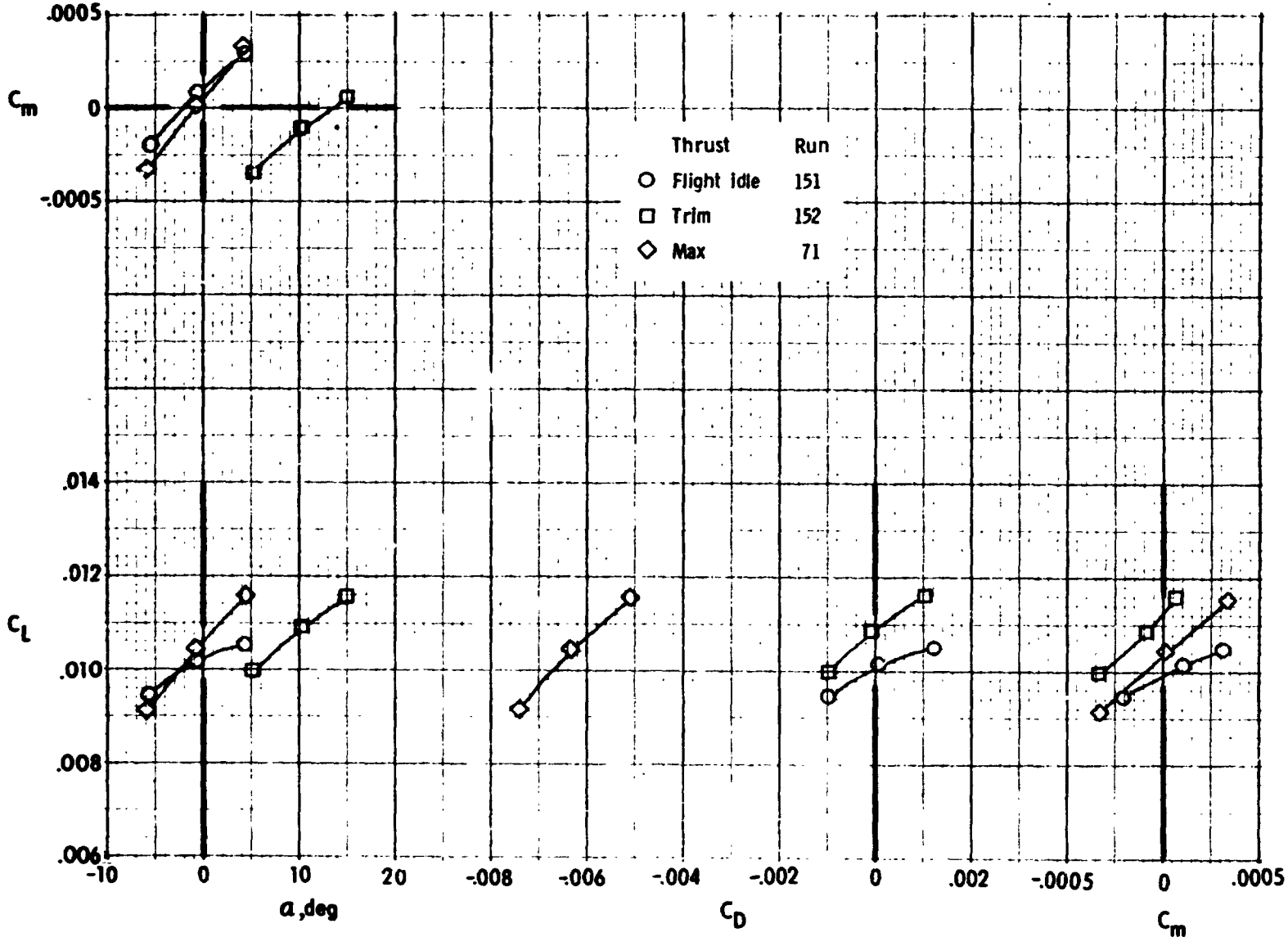

(a) $\mu \approx 0.1$

Figure 15. - Effect of auxiliary engine thrust level on the longitudinal aerodynamic characteristics.

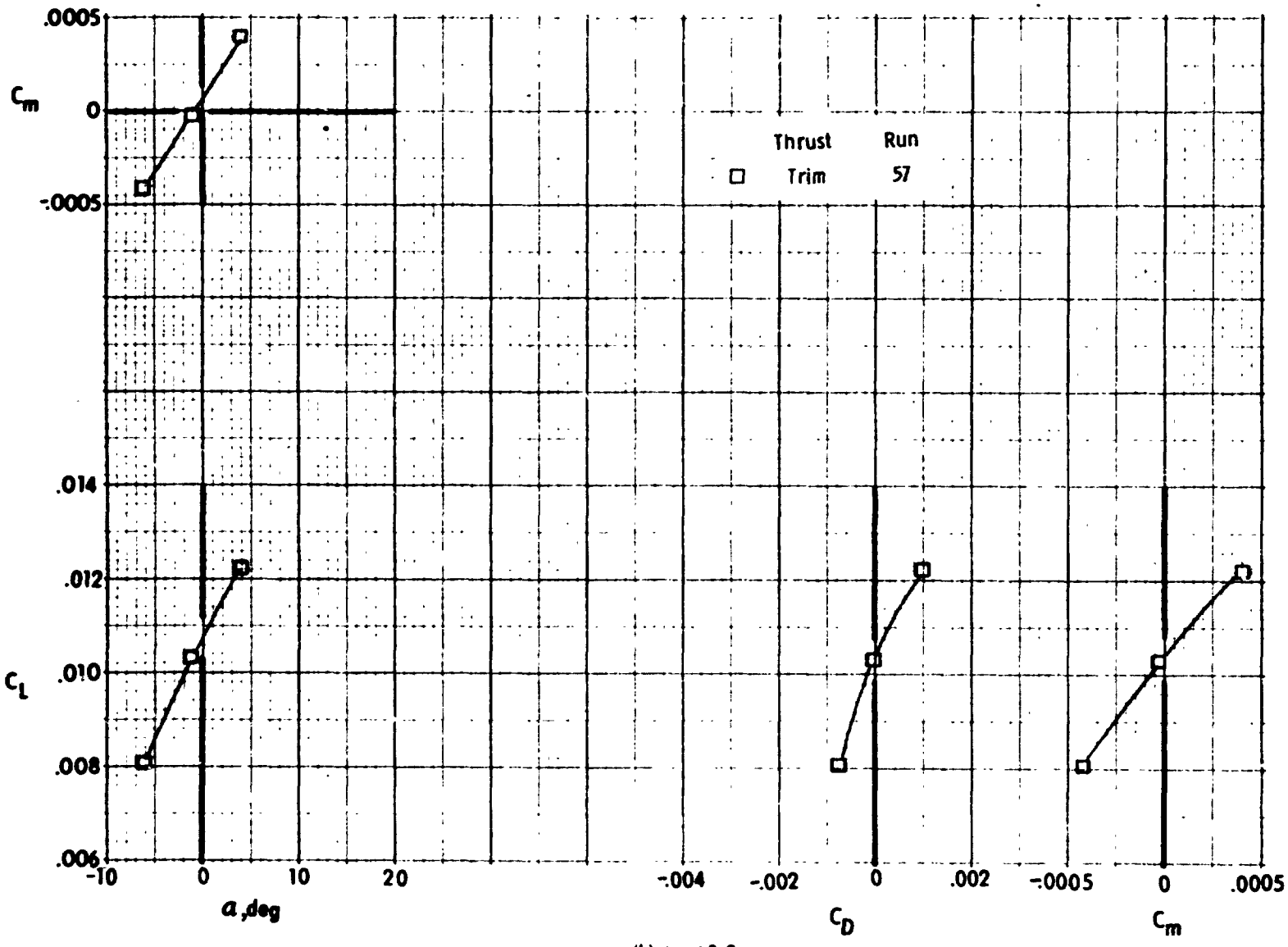

(b) $i_t = 0.2$

Figure 15. - Continued.

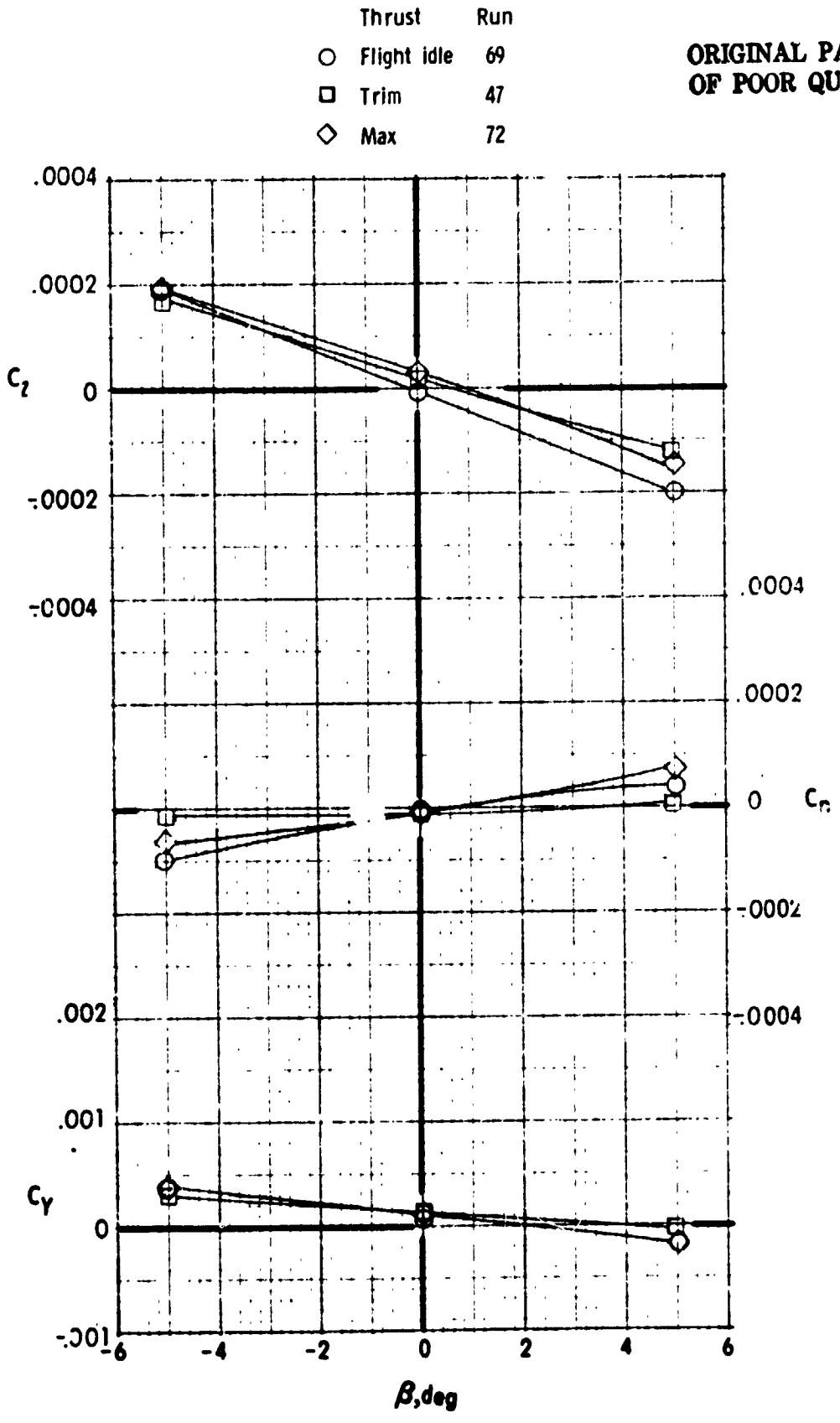

(a) $\mu \approx 0.1$

Figure 16. - Effect of auxiliary engine thrust level on the lateral aerodynamic characteristics.

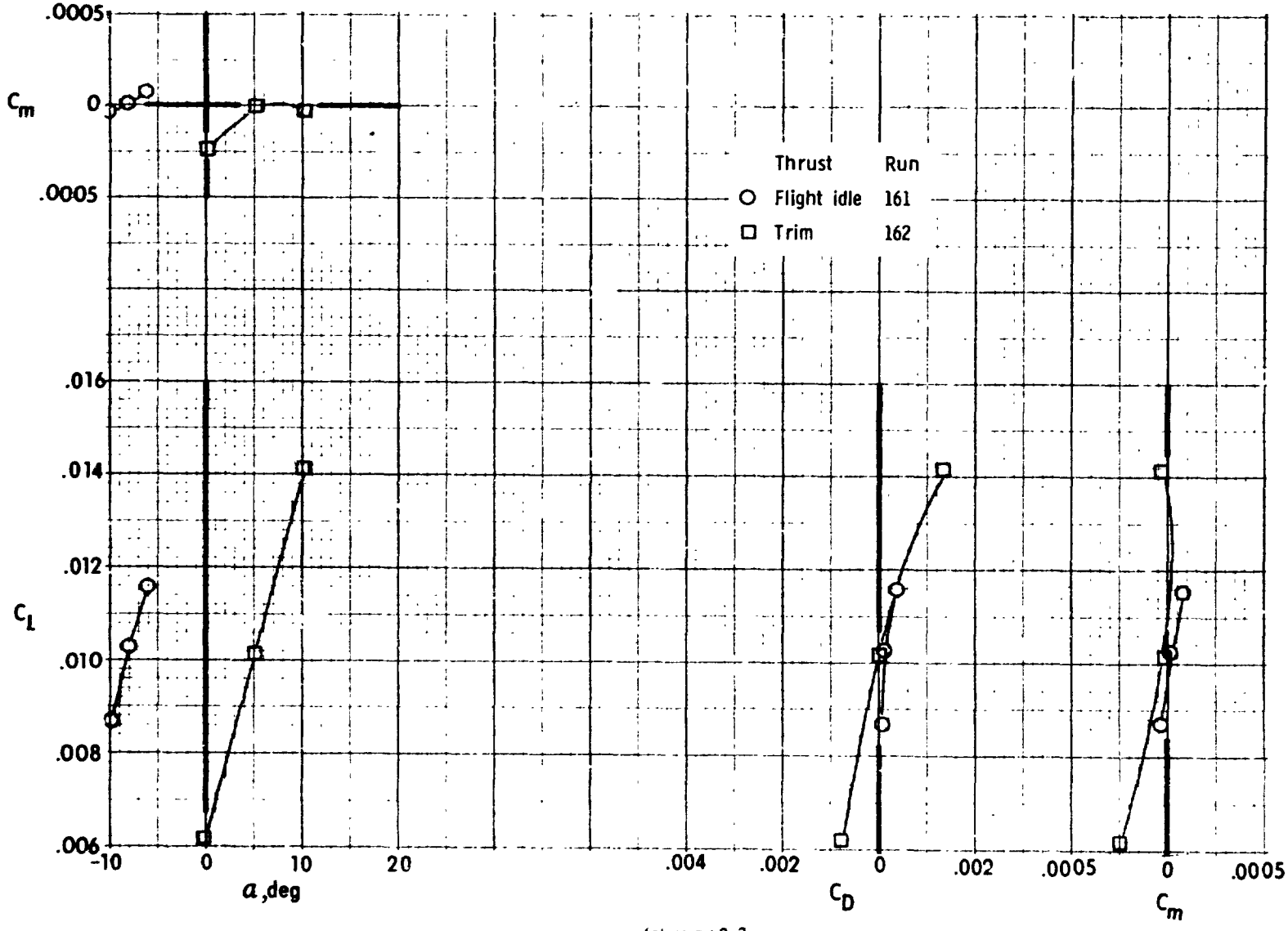

(c) $\mu \approx 0.3$

Figure 15. - Concluded.

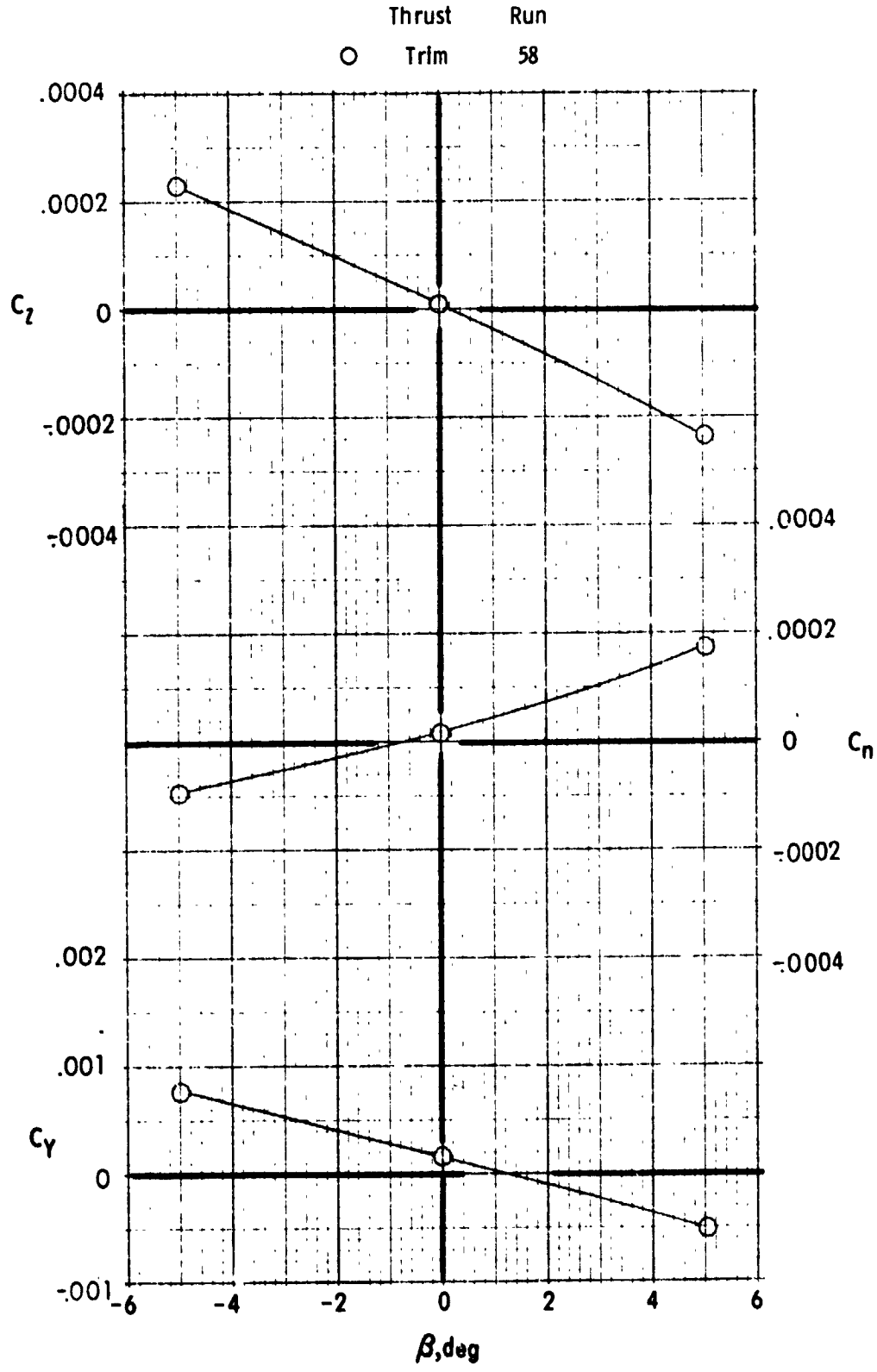

(b) $\mu \approx 0.2$

Figure 16. - Continued.

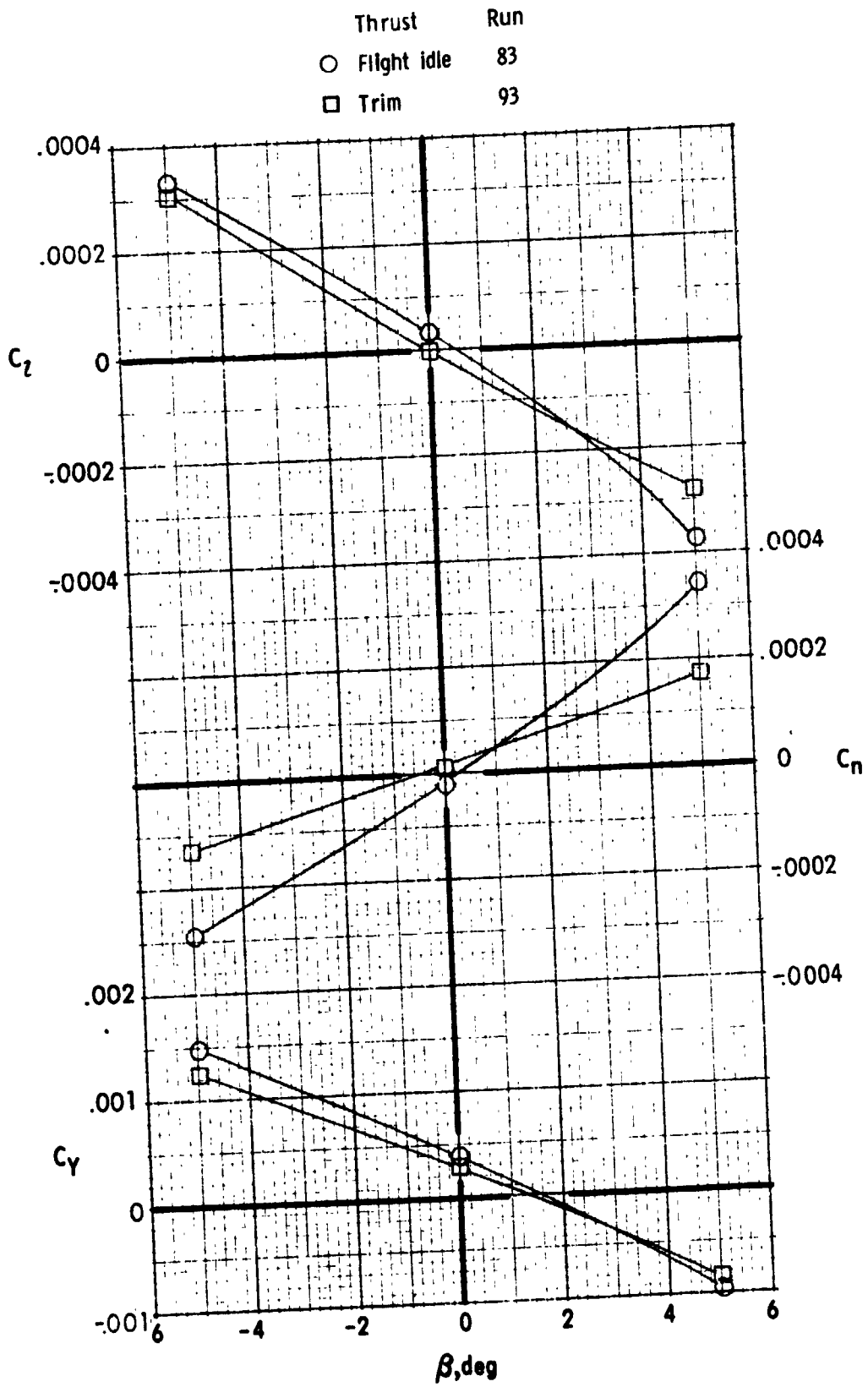

(c) $\mu \approx 0.3$

Figure 16. - Concluded.

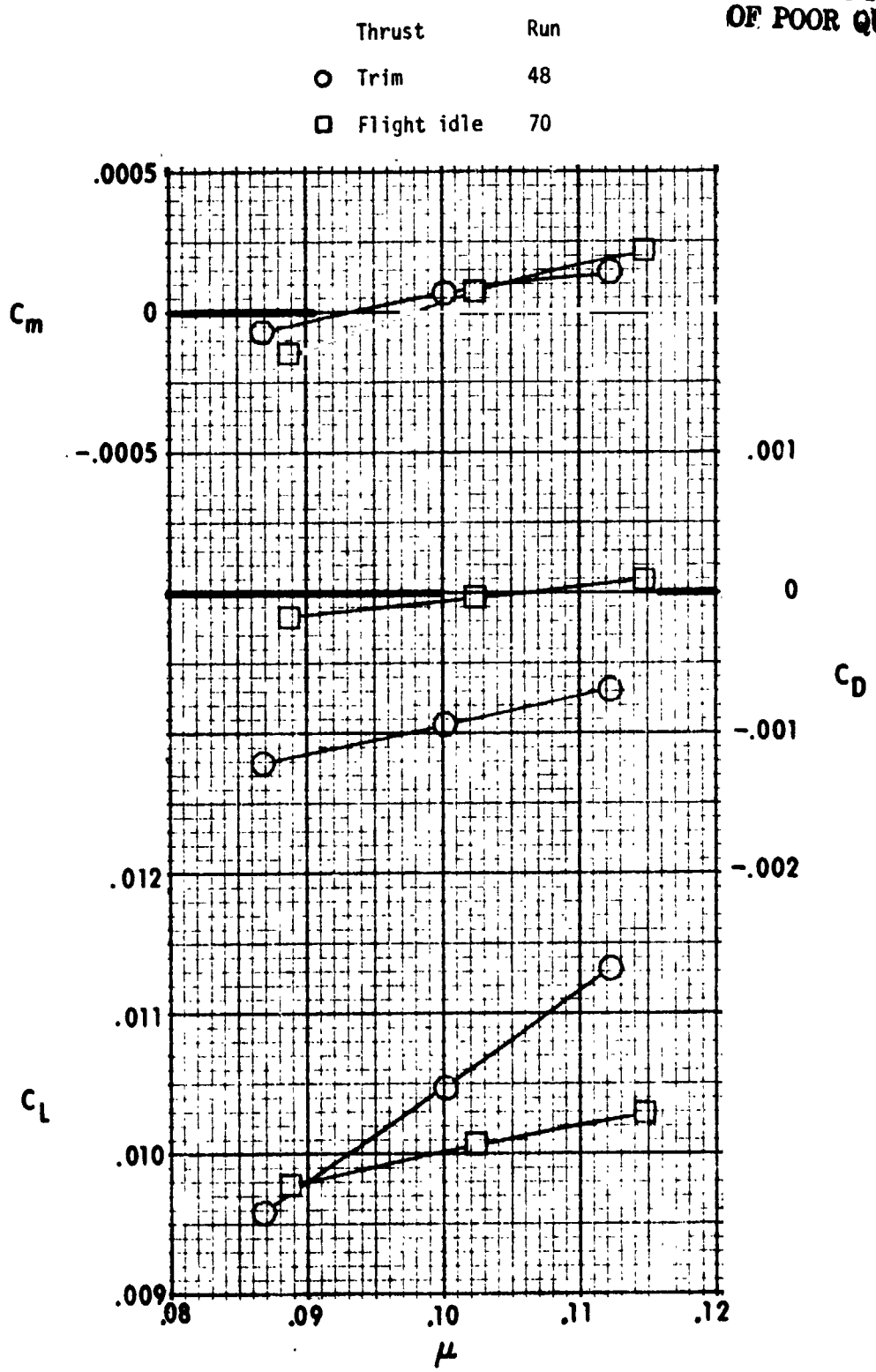

(a) $\mu \approx 0.1$

Figure 17. - Variation of the airframe longitudinal aerodynamic characteristics with advance ratio.

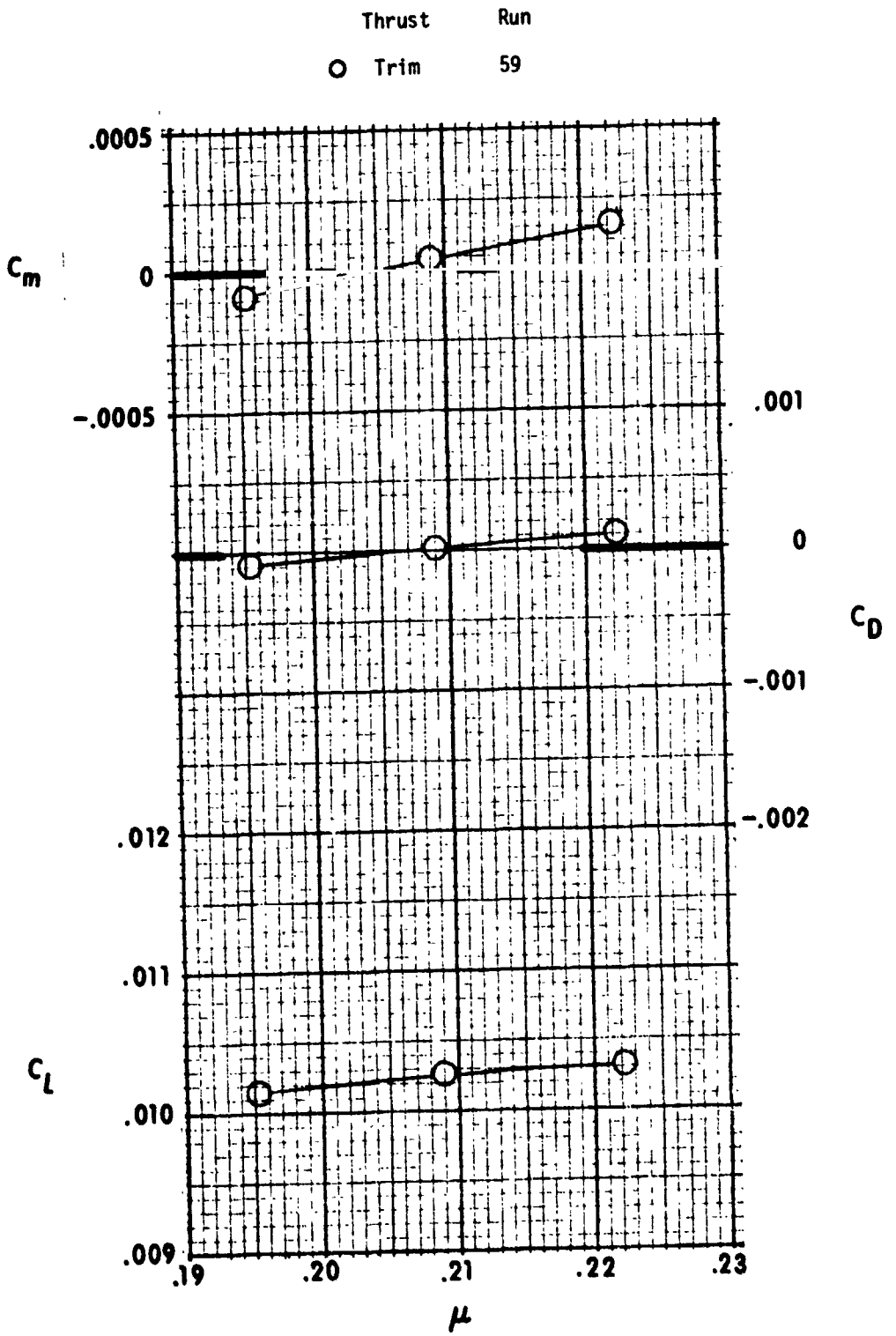

(b) $\mu \approx 0.2$

Figure 17. - Continued.

Thrust	Run
○ Flight idle	84
□ Trim	94

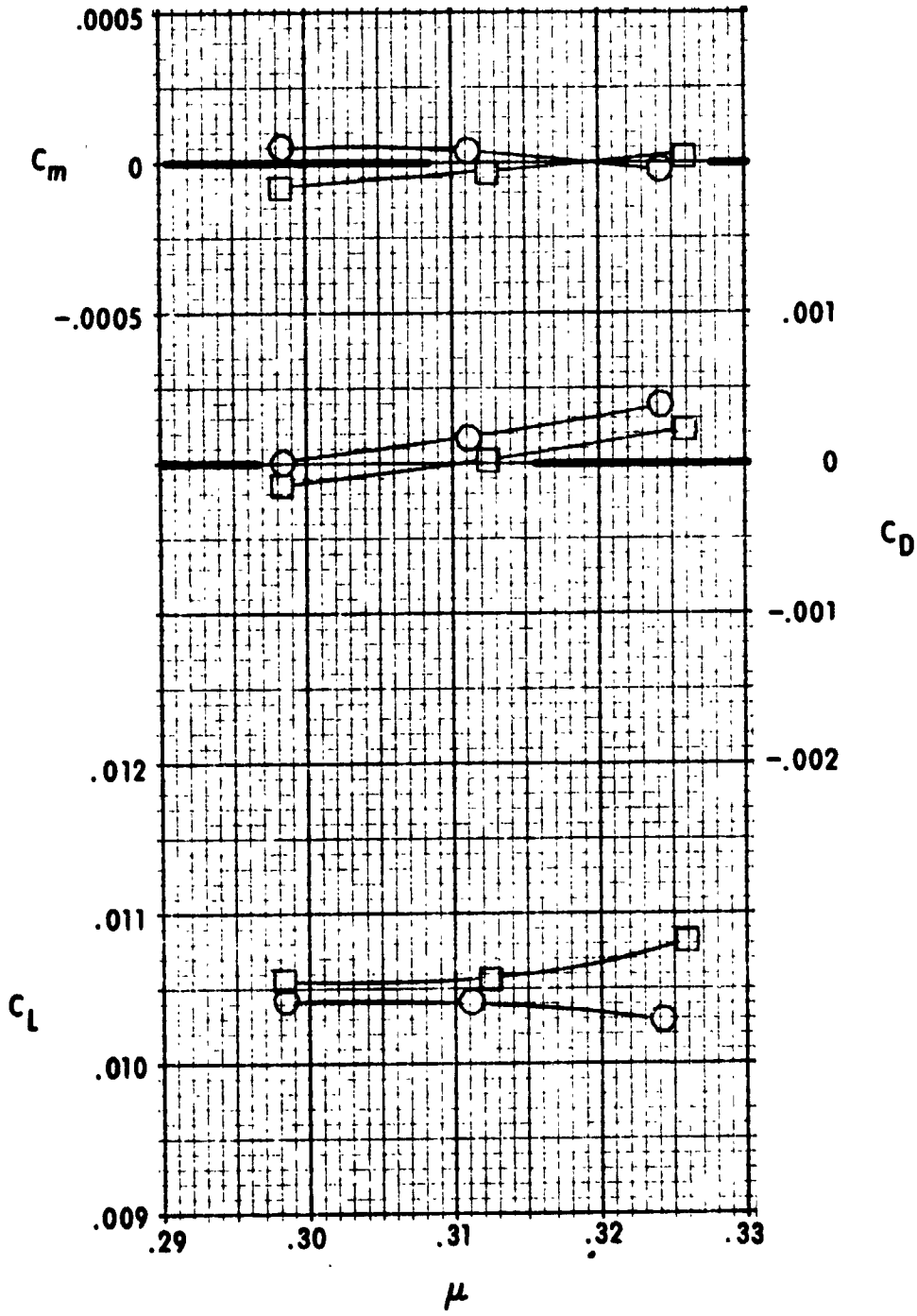

(c) $\mu \approx 0.3$

Figure 17. - Concluded.

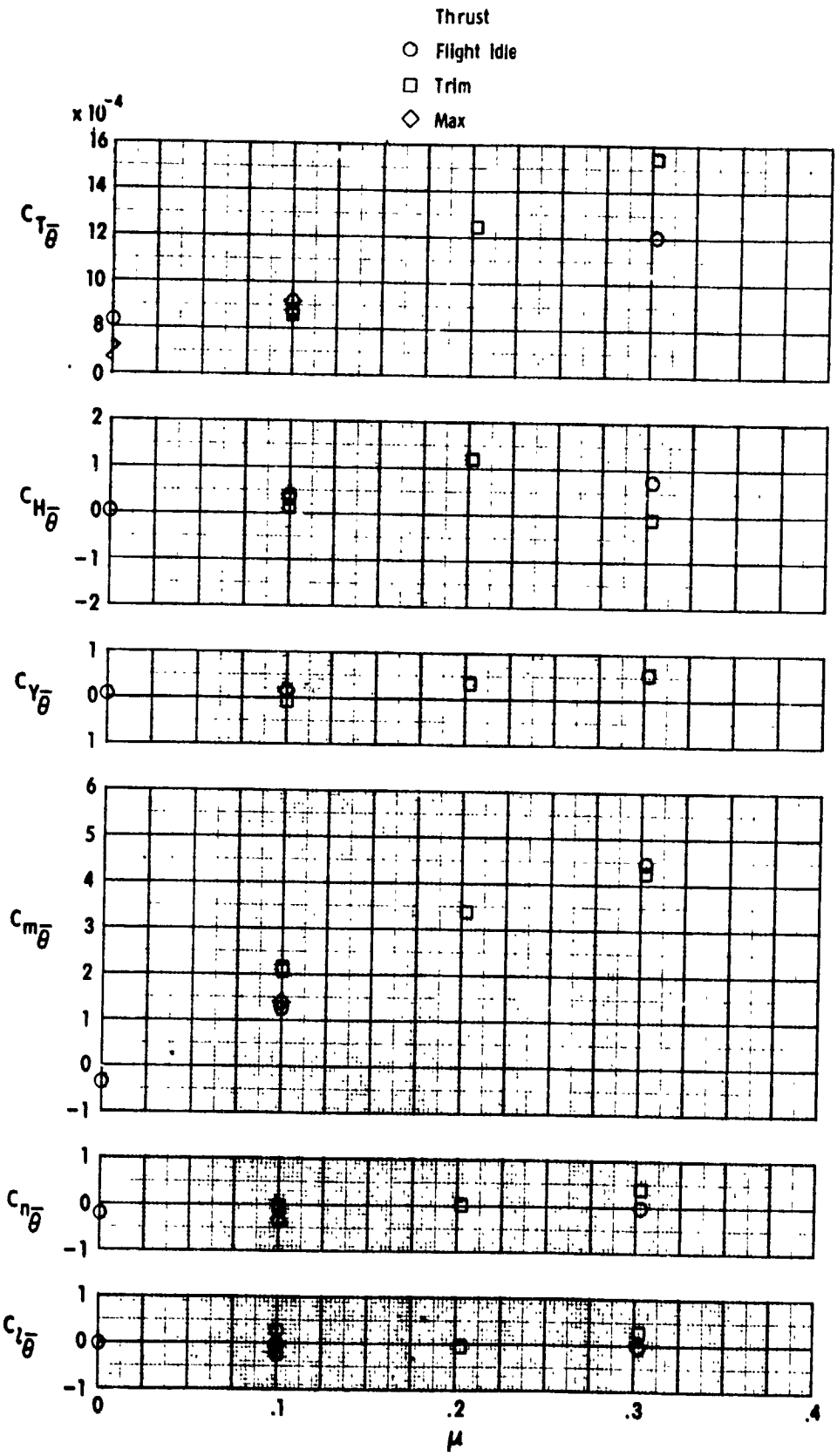

Figure 18. - Variation of the rotor collective pitch control power with advance ratio.

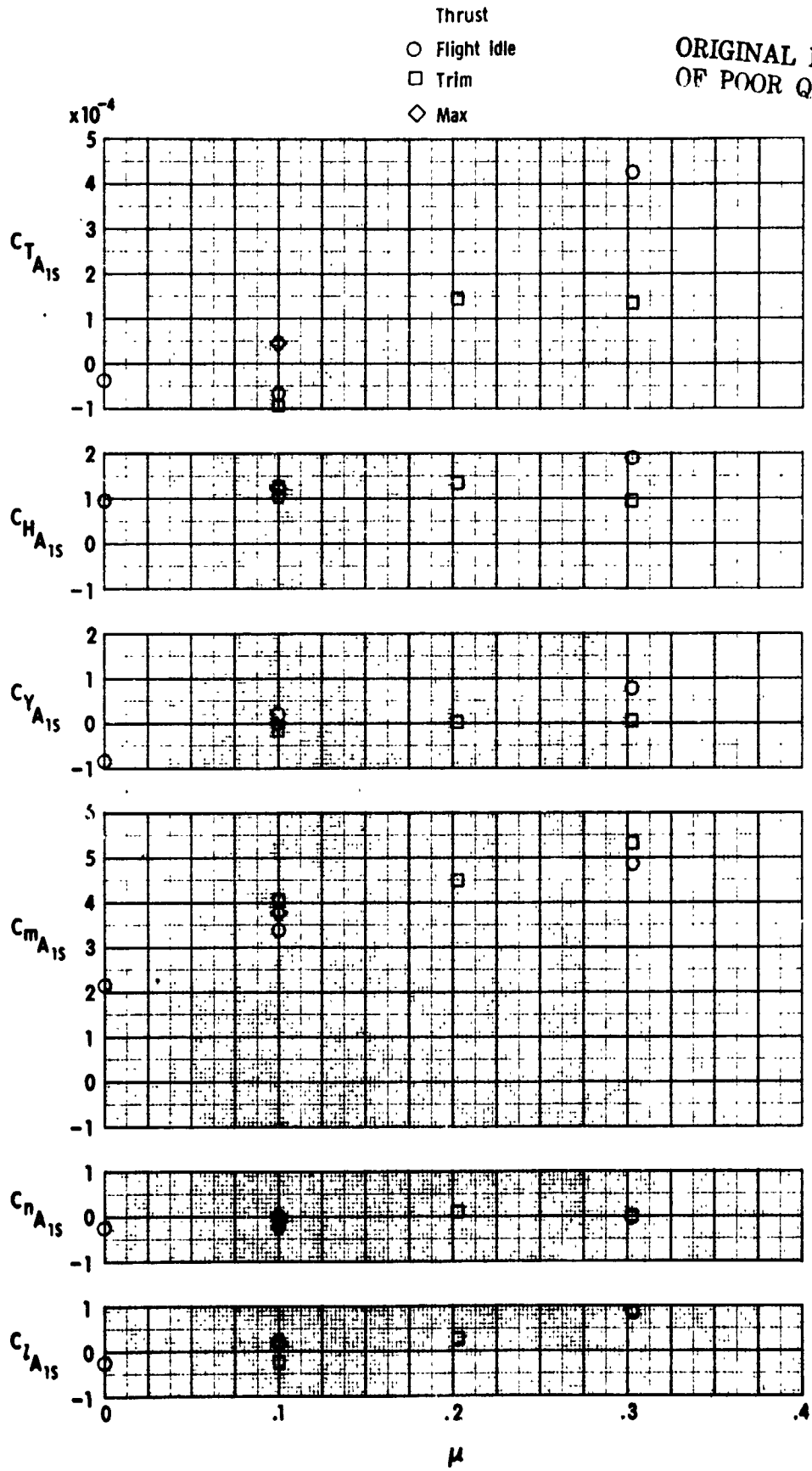

Figure 19. - Variation of rotor longitudinal cyclic pitch control power with advance ratio.

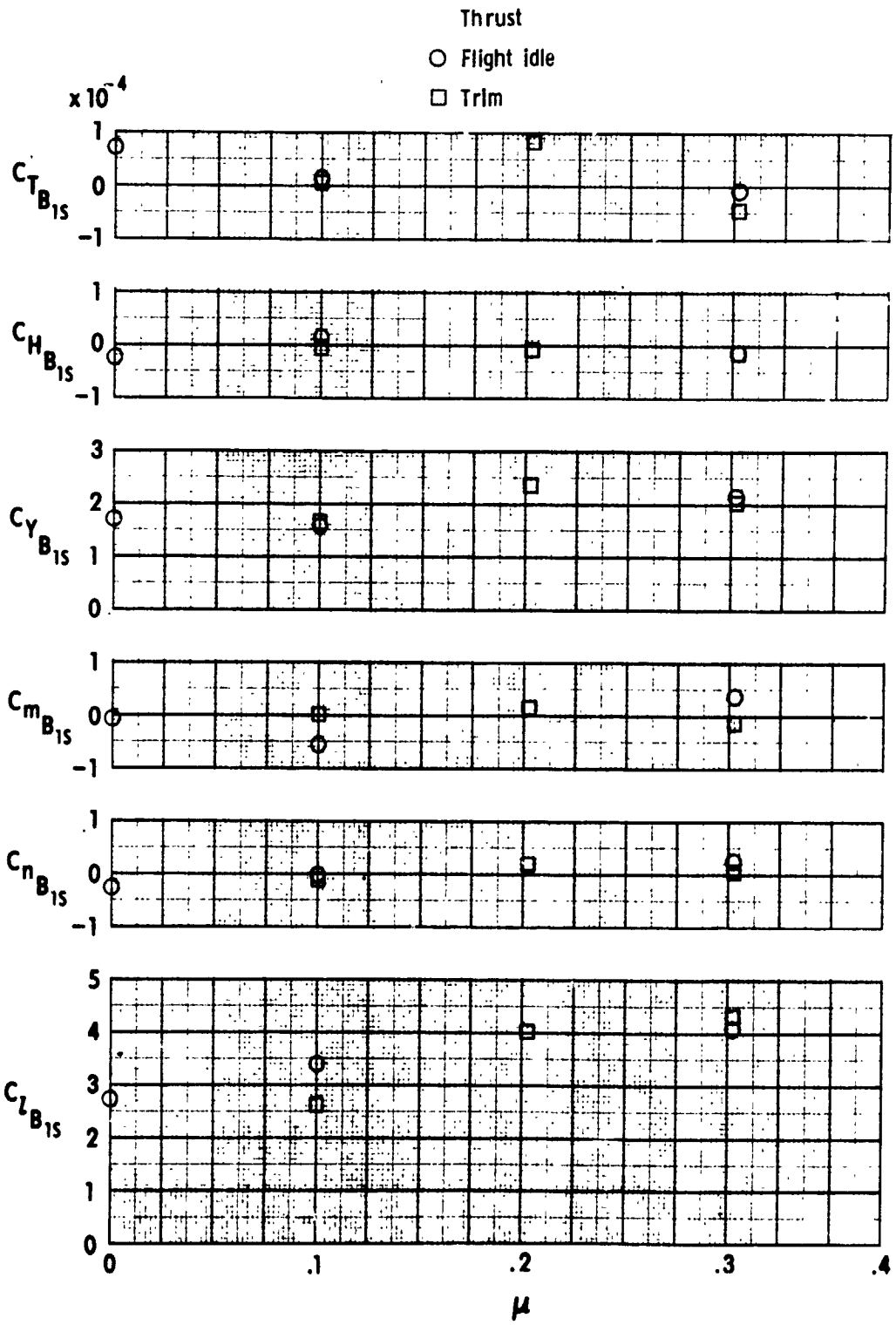

Figure 20. - Variation of rotor, lateral cyclic pitch control power with advance ratio.

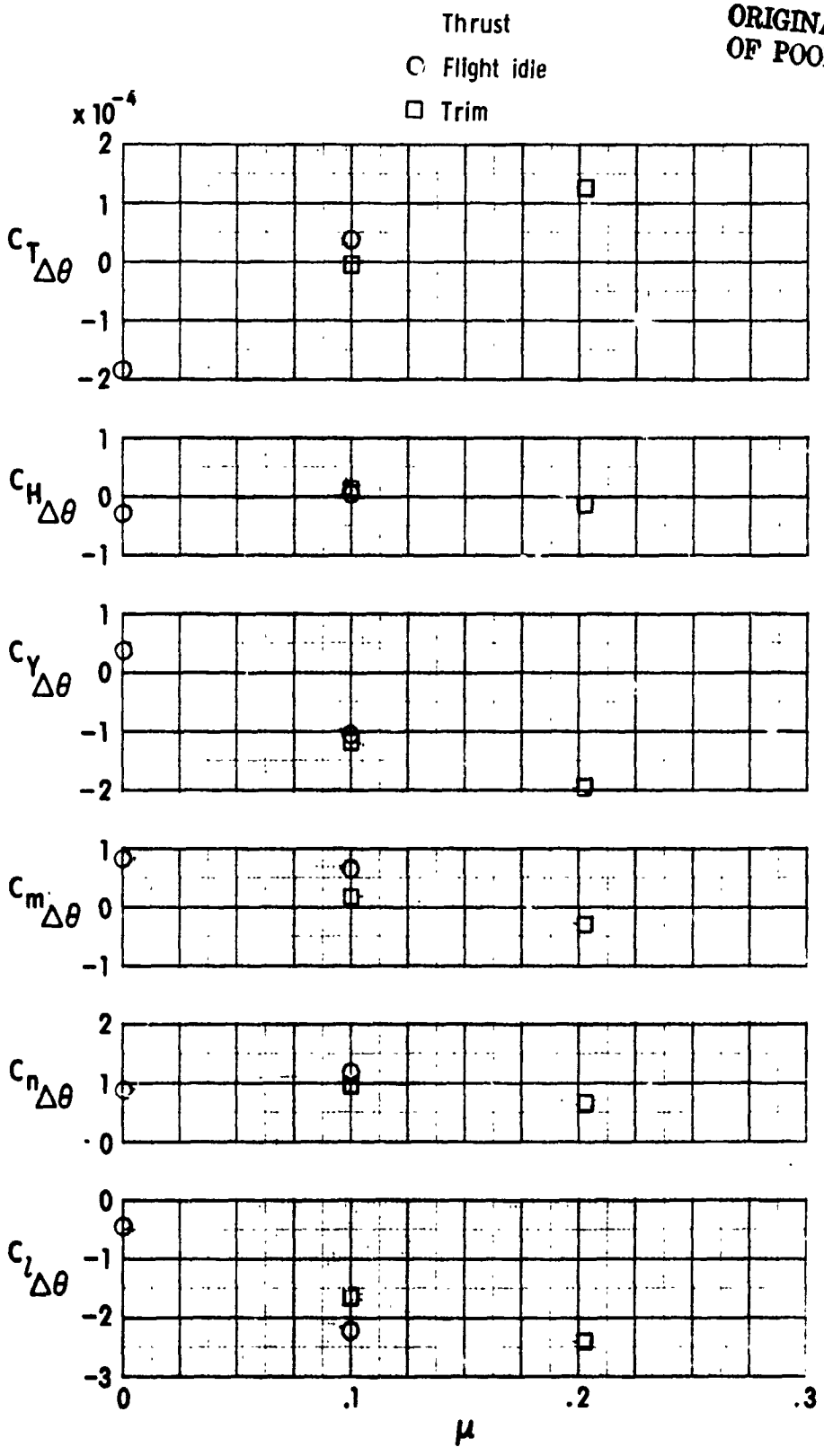

Figure 21. - Variation of rotor differential collective pitch control power with advance ratio.

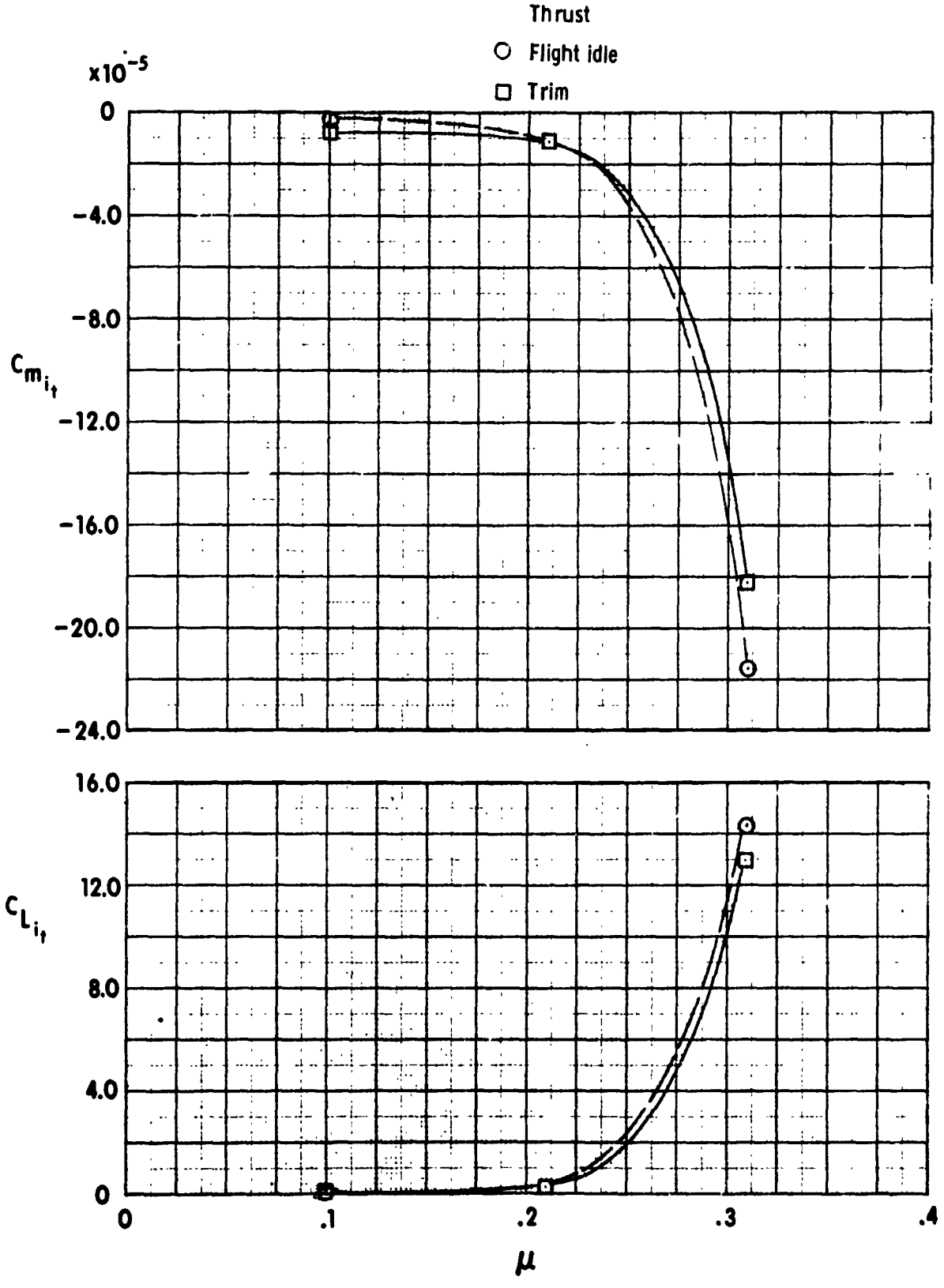

Figure 22. - Variation of horizontal tail control power with advance ratio.

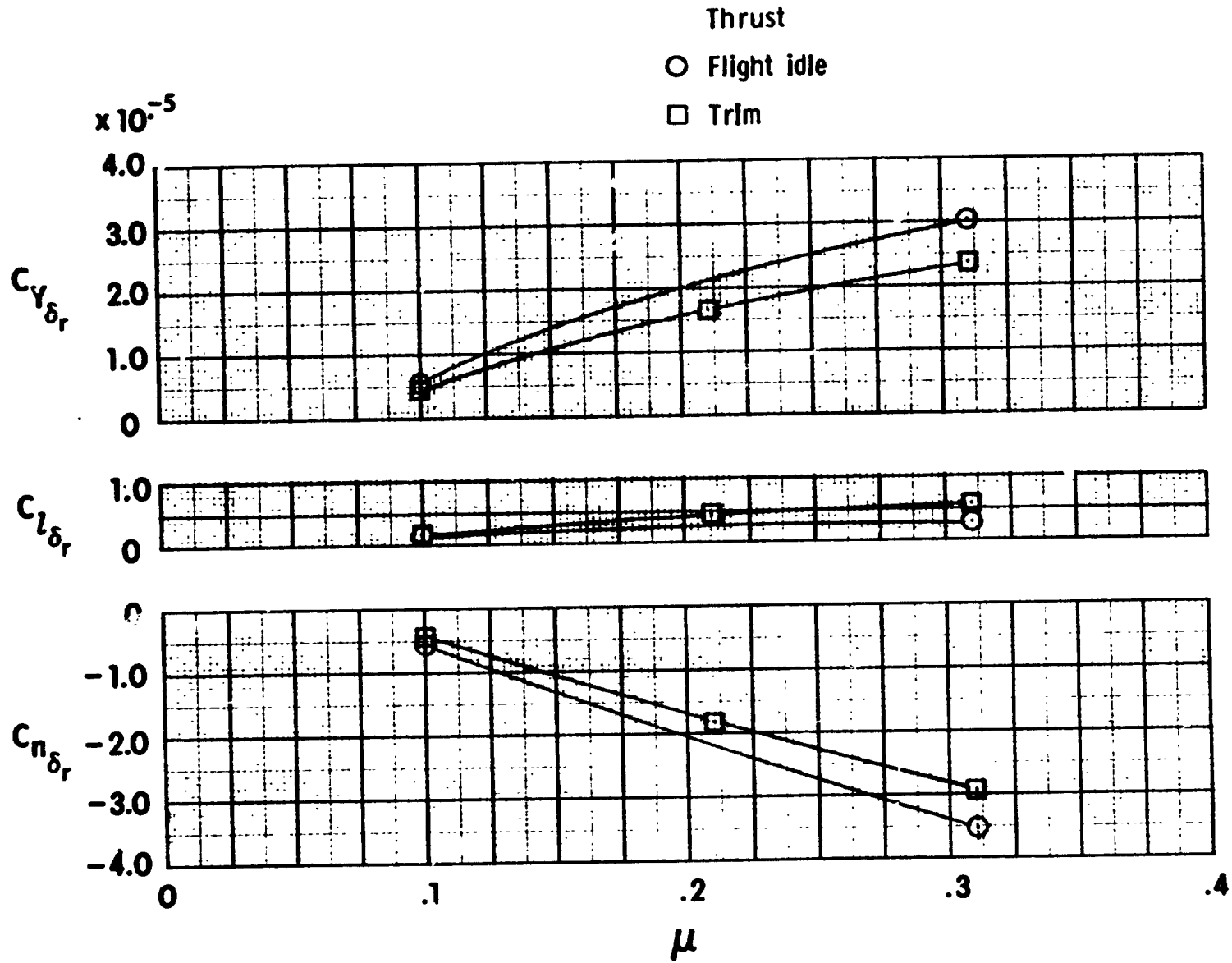

Figure 23. - Variation of rudder control power with advance ratio.

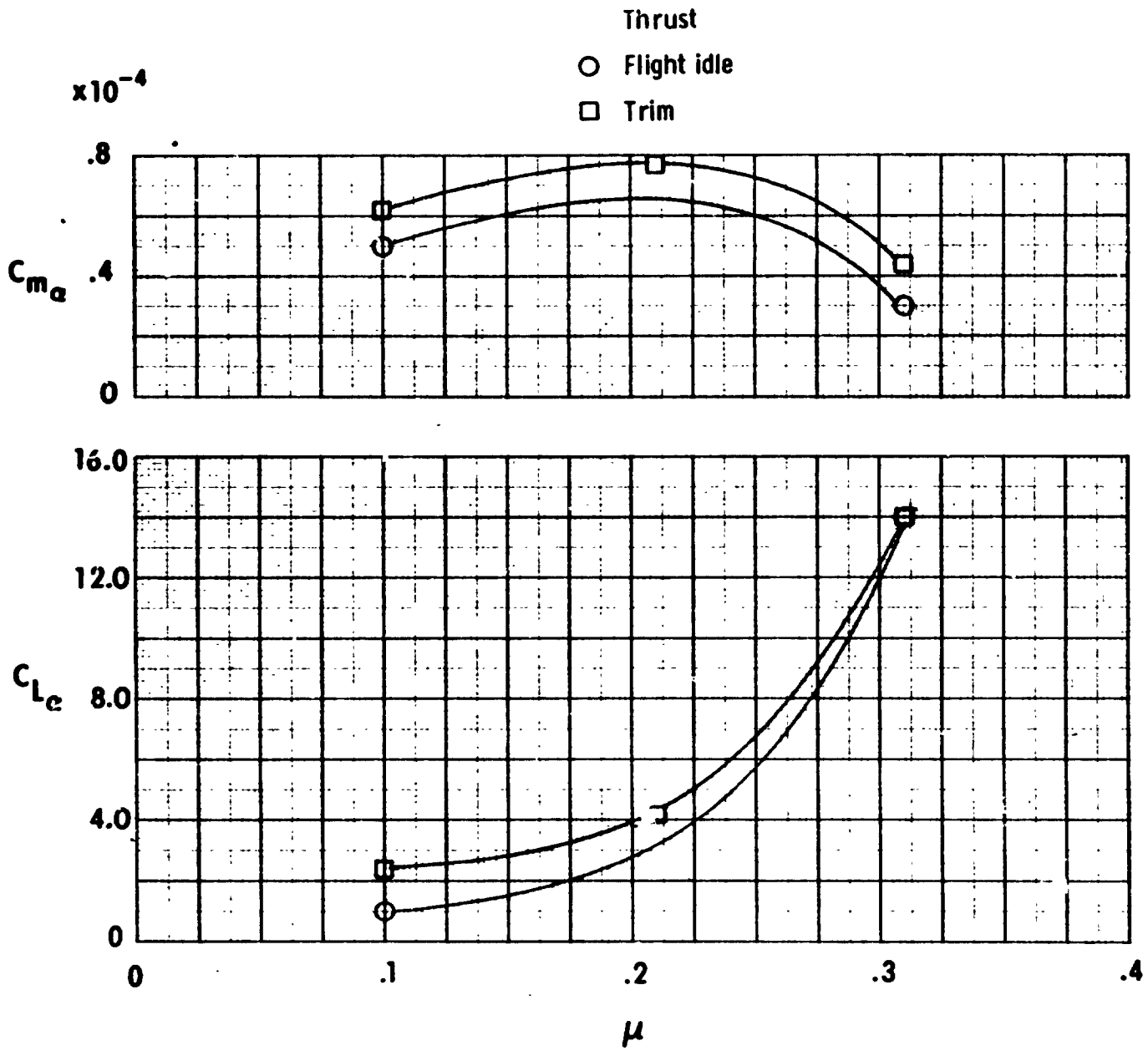

Figure 24. - Variation of longitudinal stability derivatives with advance ratio.

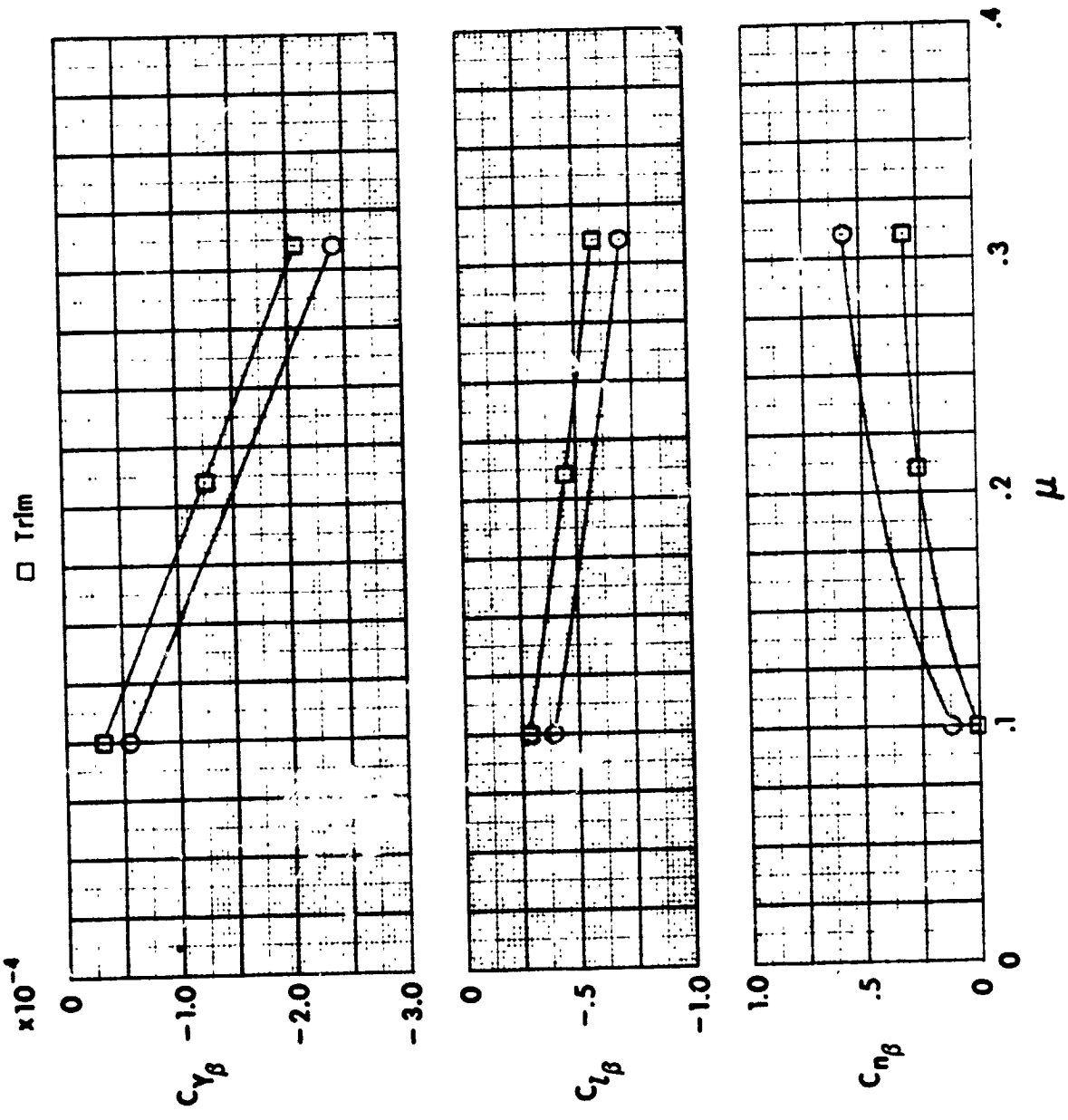

Figure 25. - Variation of lateral-directional stability derivatives with advance ratio.

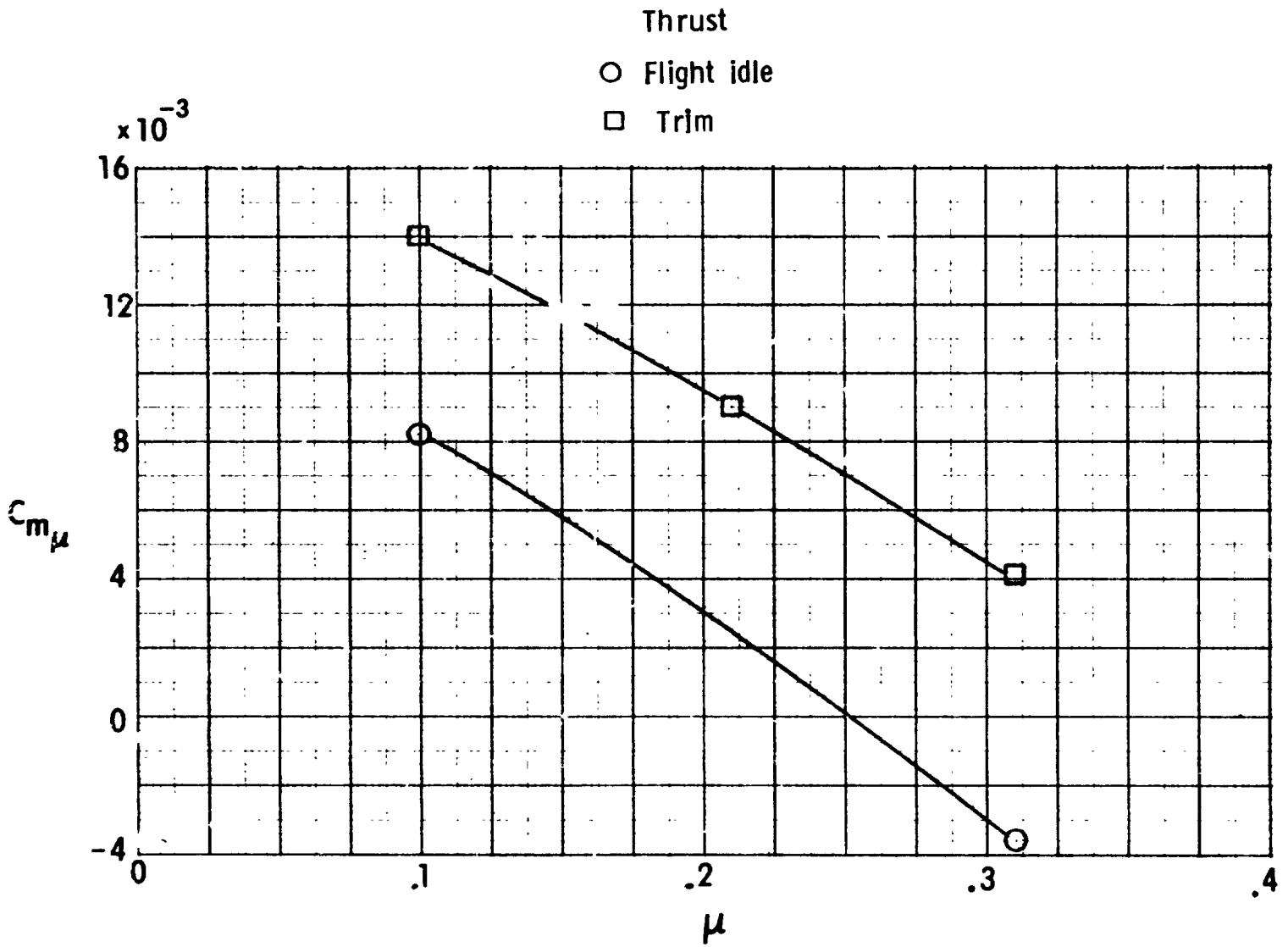

Figure 26. - Variation of speed stability with advance ratio.

1 Report No	2 Government Accession No.	3. Recipient's Catalog No
NASA TM 78705		

4 Title and Subtitle	5 Report Date
AERODYNAMIC CHARACTERISTICS OF A COUNTER-ROTATING, COAXIAL, HINGELESS ROTOR HELICOPTER MODEL WITH AUXILIARY PROPULSION	May 1978
	6. Performing Organization Code
7. Author(s)	8. Performing Organization Report No
Arthur E. Phelps and Raymond E. Mineck	
9 Performing Organization Name and Address	10. Work Unit No.
Structures Laboratory USARTL (AVRADCOM) NASA Langley Research Center Hampton, VA 23665	505-10-23-05
	11. Contract or Grant No
	13 Type of Report and Period Covered
12 Sponsoring Agency Name and Address National Aeronautics and Space Administration Washington, DC 20546 and U.S. Army Aviation R&D Command, St. Louis, MO 63166	Technical Memorandum
	14. Sponsoring Agency Code

15. Supplementary Notes

16. Abstract

A wind-tunnel investigation was conducted in the Langley V/STOL tunnel to determine the aerodynamic characteristics of a coaxial, counter-rotating helicopter model with auxiliary jet propulsion. The model was tested at advance ratios from 0 to 0.3 with and without auxiliary jet engine thrust. At each advance ratio and engine thrust, both the control power and the aircraft stability were measured.

The results indicate that there is a cross-coupling for collective pitch and longitudinal cyclic pitch inputs. The control power for these inputs increases with advance ratio. There is also a cross-coupling for differential collective pitch inputs. The airframe is longitudinally unstable, but the instability is less at the highest advance ratio tested. The airframe shows both positive effective dihedral and positive directional stability.

17 Key Words (Suggested by Author(s))	18 Distribution Statement
Coaxial rotors Helicopters Auxiliary propulsion	Unclassified - Unlimited Subject Category 02

19 Security Classif (of this report)	20. Security Classif. (of this page)	21. No of Pages	22 Price
Unclassified	Unclassified	83	$5.00

For sale by the National Technical Information Service, Springfield, Virginia 22151